INVESTIGATION OF PISTON GEOMETRY IN RAPID COMPRESSION MACHINES AND SAMPLING METHODS FOR INTERNAL COMBUSTION ENGINES

A DISSERTATION
SUBMITTED TO THE FACULTY OF
UNIVERSITY OF MINNESOTA
BY

DERECK KESHAAN DASRATH

IN PARTIAL FULFILLMENT OF THE REQUIREMENTS
FOR THE DEGREE OF
DOCTOR OF PHILOSOPHY

WILLIAM F. NORTHROP

JULY, 2019

Acknowledgments

I would like to express my deepest gratitude to my advisor Dr. William Northrop for his guidance throughout my graduate career. His energetic nature coupled with his patience, intelligence, and drive for research gave me the motivation to overcome any obstacle that arose over the years. He provided an environment for students to flourish at the Thomas E. Murphy Engine Research Laboratory. I would also like to thank Dr. Zongxuan Sun for his insight and direction, Dr. David Kittelson, and Dr. Jonathan Chaplin for their support on my doctoral committee.

I am especially thankful to Abhinav Tripathi for his partnership in research along with my colleagues, Dr. Wei Zhang, Dr. Andrew Kotz, Noah Bock, Seamus Kane, Ying Lin, and Dr. Xuesong Li. I would like to acknowledge Darrick Zarling for his help whenever required. I would like to recognize the National Science Foundation for funding my graduate studies.

Finally, I am especially grateful to my friends, family, and Kayla Dharampaul for their endless support during this journey.

Dedication

I dedicate this dissertation to my parents, Neal and Kamini Dasrath.

Abstract

There is a growing effort to reduce carbon dioxide (CO_2) emissions produced by internal combustion (IC) engines as an effort to curb anthropogenic climate change. The transportation sector accounts for 28% of anthropogenic CO_2, motivating fundamental combustion research to understand and develop more efficient advanced combustion modes. Study of ignition delay time, autoignition pressure and temperature, the chemistry of fuel mixtures, and speciation of combustion products provide important insights into phenomena like pre-ignition (knock) and pollutants (CO_2, oxides of nitrogen, soot, etc.) from modern-day IC engines. This body of work investigates novel speciation methods for studying combustion products from IC engines and unique piston geometries for rapid compression machines (RCMs).

Quantifying combustion products is an important step in creating accurate numerical models for engine combustion. Many groups have used various instruments in conjunction to characterize a range of combustion generated hydrocarbons but few have used instruments in tandem to improve speciation methods during unconventional combustion modes and address the issues associated with off-line speciation. The first part of this thesis presents an investigation that quantified light unburned hydrocarbons (UHC) using a combination of Fourier transform infrared (FT-IR) spectroscopy and gas chromatography-mass spectroscopy (GC-MS). A light-duty diesel engine is used to generate hydrocarbons at various exhaust gas recirculation (EGR) levels and partially premixed low-temperature combustion (LTC) modes. Exhaust samples are extracted with a novel fixed-volume sampling system and sent into a gas chromatograph (GC) while minimizing unknown dilution, light unburned hydrocarbons (LHC) losses, and removing

heavy unburned hydrocarbons (HHC). Along with the wide range of LHCs quantified in this study, focus is directed towards the problem of misidentification of propane by the FT-IR during LTC modes. In the region commonly identified as the absorption spectra of propane (2700 and 3100 cm^{-1}), analysis of the FT-IR spectra indicates absorption band interference caused by components found in unburnt diesel fuel. One of the primary findings of this work is that GC-MS can aid in FT-IR spectral analysis to further refine FT-IR methods for real-time measurement of unconventional combustion mode exhaust species.

Rapid compression machines (RCMs) and rapid compression and expansion machines (RCEMs) are apparatuses that have the ability to operate at engine-relevant conditions to study fuel autoignition and pollutant formation. These machines are currently limited for use in speciation studies due to thermal and mixture inhomogeneities caused by heat transfer and gas motion during compression. Studies have shown the disadvantages of using common flat and enlarged piston crevice designs for sampling reaction chamber gases during and after combustion. For instance, computer fluid dynamics (CFD) simulations performed by numerous groups, including collaborators on this work, have confirmed that unburnt fuel mixture emerges from the enlarged crevice after compression then subsequently mixes with reaction chamber gases during RCM and RCEM operation. This disadvantage renders whole-cylinder sampling techniques inaccurate for quantifying combustion products and reduces the relevance of RCMs and RCEMs for comparison with IC engines. Complex fast-sampling systems are implemented by a number of research groups to extract small quantities of gas from the center of the chamber before mixing occurs. Drawbacks with this approach include small sample volumes, local composition

non-uniformities, and non-uniform progression of chemical kinetics during sampling. Experimental and computational studies emphasize the importance of piston design for the formation of a well-mixed, homogeneous core gas inside RCM and RCEM reaction chambers.

In the second part of this thesis, a novel piston containing a bowl-like geometry similar to those used in diesel engines is implemented to overcome thermal and compositional non-uniformities within RCMs/RCEMs. By eliminating the enlarged crevice and introducing squish flow with the bowl piston, CFD studies show increased thermal uniformity for both RCM and RCEM trajectories. Experiments to characterize piston performance includes flat, enlarged crevice, and bowl piston profiles and four fuel mixtures using the University of Minnesota – Twin Cities controlled trajectory RCEM (CT-RCEM). Heat release analysis (HRA) indicates greater combustion efficiencies when using the bowl piston opposed to the standard flat and enlarged creviced pistons. This is indicative of smaller fractions of unburnt fuel left in the combustion chamber after combustion, ideal for dump sampling and the differentiation of unburnt fuel from combustion products during speciation. Ignition analysis for the bowl piston derived stronger ignition characteristics than the enlarged crevice and flat piston designs. As a result of stronger ignition and better uniform burning, the amount of fuel converted to products of combustion is increased.

Table of Contents

List of Figures

List of Tables

Nomenclature

AFR	Air-Fuel Ratio
AHC	Aromatic Hydrocarbons
BSB	Background Subtraction
CDC	Conventional Diesel Combustion
CFD	Computer Fluid Dynamics
CI	Compression Ignition
CT-RCEM	Controlled Trajectory – Rapid Compression Expansion Machine
DBTDC	Degrees Before Top Dead Center
DOC	Diesel Oxidation Catalyst
DPF	Diesel Particulate Filter
EES	Engineering Equation Solver
EI	Emissions Index
EGR	Exhaust Gas Recirculation
EM	Electron Multiplier
EOC	End of Compression
ELTC	Early Low-Temperature Combustion
FID	Flame Ionization Detector
FT-IR	Fourier Transform Infrared
GC-MS	Gas Chromatography-Mass Spectroscopy
GHG	Greenhouse Gases
HC	Hydrocarbon
HCCI	Homogenous Charge Compression Ignition

HED	High Energy Conversion Diode
HRA	Heat Release Analysis
HRR	Heat Release Rate
IC	Internal Combustion
ITHR	Intermediate Temperature Heat Release
LHC	Light Hydrocarbons
LHV	Lower Heating Value
LPG	Liquefied Petroleum Gases
LPM	Liters per Minute
LTC	Low Temperature Combustion
LVDT	Linear Variable Differential Transformer
MS	Mass Spectrometer
NDIR	Nondispersive Infrared
NTC	Negative Temperature Coefficient
OEM	Original Equipment Manufacturer
PFR	Plug Flow Reactor
PLOT	Porous Layer Open Tubular
PM	Particle Matter
RCM	Rapid Compression Machine
RCEM	Rapid Compression Expansion Machine
RF	Radio Frequency
ROHR	Rate of Heat Release
SPCCI	Spark Controlled Compression Ignition

STP	Standard Temperature and Pressure
SVHC	Semi-Volatile Hydrocarbons
SWACER	Shock Wave Amplification by Coherent Energy Release
TCD	Thermal Conductivity Detector
TDC	Top Dead Center
THC	Total Hydrocarbons
TIC	Total Ion Chromatogram
UHC	Unburned Hydrocarbons
USLD	Ultra-low Sulfur Diesel
VGT	Variable Geometry Turbocharger
VSA	Variable Swirl Actuation

CHAPTER 1 Introduction

1.1 Motivation

Despite increasing public and regulatory interest in electric vehicles, it is widely accepted that internal combustion (IC) engines will continue to dominate in the vehicle fleet for the next several decades [1]. For over a century, IC engines have enabled the growth of industrialized society by providing useful work. As long as engines have been around, researchers have been studying ways to increase engine thermal efficiency, power-to-weight ratio, and decrease harmful emissions. Oxides of nitrogen (NO_X), hydrocarbons (HC), and nanoscale particulate matter (PM) emitted from IC engines are not only harmful to the environment but also pose a high risk to human health [2]. Additionally, heat-trapping "greenhouse" gases (GHG) like carbon dioxide (CO_2), methane, and nitrous oxide (N_2O) emissions from combustion engines are directly linked to anthropogenic climate change [3]. Growing evidence of anthropogenic climate change is motivating society to reduce these human-driven emissions that are affecting every individual and living organism on this planet.

Stringent regulations introduced around the world to limit harmful emissions have led researchers and original equipment manufacturers (OEMs) to focus efforts on developing new low-carbon fuels and advanced engines that are both highly efficient and clean [4], [5]. Some research has focused on novel advanced combustion concepts that have the potential to achieve these objectives. For example, Mazda's innovative Skyactiv-X spark-controlled compression ignition (SPCCI) engine achieves increased thermal efficiency of homogeneous charge compression ignition (HCCI) engine operation and couples it with spark ignition to increase fuel economy and overcome ignition timing issues

that has previously stymied real-world implementation of HCCI. The SPCCI concept was achievable only through decades of research in HCCI and spark-assisted gasoline concepts as reviewed in [6]. As partially premixed combustion modes like HCCI and SPCCI are largely controlled by autoignition chemistry and less by flame propagation from an ignition source, it is crucial to study hydrocarbon combustion chemistry influenced by, and isolated from, thermal stratification and in-cylinder flow dynamics.

Understanding combustion chemistry requires development of detailed kinetic mechanisms made up of many elementary reactions derived from experimental data collected over a wide range of temperature, pressure and mixture fraction. These mechanisms are used to feed detailed engine and combustion models, and to predict kinetics in conditions where experimental data has not been generated. As novel combustion modes and engine designs are conceived, it is essential to experimentally explore new regimes of combustion chemistry not derivable from existing mechanisms. Low temperature combustion and cool flame behavior [7] are examples of combustion modes in advanced engines that result from chemical pathways not possible to extrapolate from high temperature reaction sets.

Mechanism development requires using a variety of combustion apparatuses to generate a wide range of physical conditions. Experimental data, including detailed engine-out emissions concentrations, from IC engines are typically used to validate kinetic mechanisms used in models and give insight into the development of detailed chemical kinetics. Although experimental data from practical combustion facilities are relevant, influences from in-cylinder fluid motion, varying mixture fraction, and thermal stratification prohibit the derivation of elementary reactions mechanisms. For example,

swirl and tumble-generated turbulence induced by port, valve, and squish flows introduce complex interactions with chemical reactions making it difficult to deconvolute quality kinetics from engine experimental data.

To isolate combustion chemistry under engine-relevant thermodynamic conditions, standardized combustion apparati are used to provide uniform mixing, low spatial thermal gradients, and negligible fluid mechanics effects. Devices used by researchers include turbulent flow reactors, jet-stirred reactors, shock tubes, rapid compression machines (RCMs) and rapid compression expansion machines (RCEMs) [8]. Data from all these devices provide combustion information over a wide range of temperatures, pressures, time scales, and diagnostic techniques for the development of accurate and detailed chemical kinetic mechanisms.

This work investigates two methods for improving the understanding of combustion chemistry in advanced engine combustion modes. The first is an improved speciation method for internal combustion engines that enhances the understanding of unburned hydrocarbon concentrations by blending Fourier Transform Infrared (FT-IR) with gas chromatography-mass spectrometry (GC-MS) techniques. Secondly, novel piston designs were examined experimentally to improve autoignition strength, avoid thermal stratification, and eliminate adverse fluid mechanics effects in RCMs/RCEMs. Taken together, the research presented will help develop a better mechanistic understanding of hydrocarbon combustion chemistry to feed further improvements in IC engine efficiency and emissions in the decades to come.

1.2 Research Objectives

The first objective of this work was to understand how GC-MS can be used to improve FT-IR hydrocarbon speciation from IC engines. Hydrocarbon speciation is an important diagnostic technique used to characterize the combustion performance of fuels and engine modes. It is also an essential method in tuning common engine design and operational parameters such as combustion chamber geometry, valve timing, fuel injection and spark timing, as well as percentage of exhaust gas recirculation (EGR).

Due to its ease of operation, FT-IR is the most common speciation instrument used by OEMs and research institutions to measure hydrocarbons from engine exhaust in real-time. Recipes loaded onto an FT-IR contain predetermined sets of calibrated compounds developed for specific engine modes that identify and quantify compounds. This is done by fitting specific absorption bands in a particular wavenumber region for a given compound. Difficulties arise in the identification and quantification of compounds when conventional FT-IR recipes are used during unconventional engine modes like low temperature combustion (LTC). Most commonly is the false identification and incorrect quantification of compounds from absorption bands of "unexpected" compounds interfering in wavenumber regions where calibrated compounds absorb.

GC-MS is considered the gold standard when identifying and quantifying compounds are concerned. Its ability to separate compounds via gas chromatography and quantify compounds based on their mass-to-charge ratio allow for highly accurate measurements over a vast range of compounds. The downfall of this technique is its off-line operation. Engine exhaust speciation using GC-MS has typically been difficult and significantly inaccurate since exhaust gas requires being captured, moved, and then

introduced into the instrument. This process has normally been known to introduce error by unknown dilution, chemical instability/reactivity, and contamination.

The second objective of this research is focused on the development and validation of a combustion piston geometry that simultaneously improves the thermal uniformity and autoignition strength of a fuel mixture during RCM and RCEM operation. Difficulty with using flat and creviced piston geometries have been a persistent problem for RCM/RCEM studies that require the complete conversion of fuel mixture to products of combustion. In particular, combustion product speciation by extracting the contents of an entire combustion chamber. This method is commonly referred to as “dump” sampling and can eliminate the challenges associated with fast-sampling systems such as small sample volumes, local composition non-uniformities, and non-uniform progression of chemical kinetics during sampling.

Computer fluid dynamics (CFD) simulations performed by numerous research groups have confirmed RCM operation with flat piston geometries produce vortices by shearing cool boundary layer gases from combustion chamber walls during compression. Consequently, these vortices create thermal inhomogeneities throughout the reaction chamber and cause non-uniform progression of chemical kinetics. Similar studies have confirmed fuel mixture stored in the enlarged volume on the periphery of the creviced piston is not likely to ignite due to cooling effects. The same volume of unburnt gas is also known to emerge and mix with combustion gases after compression and during expansion for RCM and RCEM trajectories, respectively. Intuitively, the environment these pistons create is less than ideal for the complete conversion of unburnt fuel and is not well suited for complete cylinder speciation studies. The research presented here investigates the

performance of a non-conventional bowl piston designed for increasing the conversion efficiency and ignition mode of fuel mixtures in RCMs/RCEMs.

CHAPTER 2 Background

2.1 IC Engine Hydrocarbon Speciation

To develop cleaner and more efficient engines, a more detailed understanding of combustion processes is required. An effective way to diagnose engine combustion is to measure the detailed hydrocarbon species concentrations found in the exhaust. Common emissions analyzers mostly measure gases like carbon oxides, oxygen, and total hydrocarbons. These analyzers, while providing global data to calculate engine combustion efficiency and stoichiometry, do not allow for more detailed examination of hydrocarbon combustion chemistry.

Fourier Transform Infrared (FT-IR) analyzers provide more information than commonly available engine exhaust analyzers as they can provide speciation information including unburned hydrocarbons (UHC) species concentration from engine exhaust in real-time. Unlike other methods like mass spectrometers and thermal conductivity detectors (TCD), FT-IR can simultaneously speciate a predetermined set of calibrated compounds. FT-IR analysis methods identify and quantify compounds by fitting specific absorption bands in a particular wavenumber region for a given compound. However, selecting interference free bands when measuring complex gas mixtures at low resolution can lead to significant inaccuracies [9]. Today's modern FT-IR analyzers can operate at high resolution (0.5 cm^{-1}), and modern computing power has made FT-IR spectral fitting and data reporting reasonably fast at up to 5 Hz. However, absorption band interference can be difficult to account for without knowing what comprises the sampling spectra. This key issue remains when accounting for "unexpected" compounds when using FT-IR, which

may arise in the exhaust from unconventional combustion strategies and/or alternative fuels [10].

Total hydrocarbons (THC) in engine exhaust are traditionally measured with an on-line flame ionization detector (FID), which counts carbon molecules by measuring ions produced when organic compounds pass through a hydrogen flame. Previous work by Northrop et al. [11] has shown that FT-IR underreported total THC concentration at light-load LTC conditions as compared to an FID, showing that THC and FT-IR measurements may not be comparable for engine conditions containing high THC emissions. Indeed, it is well known that these two methods do not directly compare when measuring THC from conventional combustion exhaust. FIDs suffer from reduced signal response depending on the molecular composition of the HC species, especially for oxygenated hydrocarbons where oxygen changes the process of ion formation [12]. Although FT-IR does not suffer from differential hydrocarbon response like FID, it can only quantify the hydrocarbons included in the method evaluation for a given fuel and combustion strategy and may miss some species not included in the method.

Previous work has sought to use the combination of FID and FT-IR to better understand UHC emissions from advanced combustion modes. For example, Koci et al. [13] conducted a detailed investigation of UHCs in a highly-dilute LTC regime that included nondispersive infrared (NDIR), FID, chemiluminescence, and smoke analyzers capable of measuring CO, CO_2, O_2, THC, NO_X, as well as particulate matter. In addition, a wide spectrum FT-IR was used to identify several hydrocarbons in the C_1 - C_{12} range. A comparison between THC as measured by FID and FT-IR showed a correlation, except at

extremely early and late injection times where HC species (< C_6) had a decreased FT-IR response compared to FID.

UHC speciation can also be accomplished off-line by analyzing collected samples using gas chromatography (GC). For example, Han et al. [14] used GC with FID to perform a thorough investigation of the species formed under several different LTC conditions. Tedlar® bags were used to collect hydrocarbons (C_1 - C_8) and Tenax® traps for semi-volatile hydrocarbons (SVHC) (> C_8). Two GC instruments with FID and thermal conductivity detectors were used: one for HCs and the other for the SVHCs. In total, over 210 exhaust hydrocarbon species were detected, and 70% of total carbon mass was identified. Known concentrations of propane were added to each Tedlar® bag as an internal standard before GC-FID analysis. With the absence of a mass spectrum, use of the propane as an internal standard helped with peak identification and quantification. The GC-FID results were validated by comparing overall UHC concentration with THC measurements from an FID.

With the capability to identify any compound based on its mass spectrum, GC-MS is a powerful tool when the identity of exhaust species is ambiguous. More broadly, it is also one of the most accurate techniques used for quantitative concentration measurements for gases. Because GC is an off-line analysis method, transferring a gas sample from the point of extraction to the point of injection increases the chances for compound loss and contamination, thereby compromising repeatability, accurate identification, and quantification. Examples of losses include, but are not limited to, condensation in unheated sample lines, chemical instability/reactivity, and dilution with partially evacuated or unpurged storage reservoirs and lines. Carefully designing a gas sample system is crucial

to mitigate such sources of potential loss, to identify sources of dilution, and to increase measurement repeatability for this type of gas analysis.

Though many studies have used a single method for speciating UHCs, few have combined methods to qualitatively and quantitatively compare their accuracy [15]. In one study, Dagaut et al. combined FT-IR and GC-TCD/FID to analyze combustion processes in a jet-stirred reactor [16]. Low pressure samples were collected by a sonic quartz probe sampling into 1-liter Pyrex bulbs initially at ~40 mbar. The results showed that the independent methods were in very good agreement for methane, CO, and CO_2.

2.2 Low Temperature Combustion

Low-temperature combustion (LTC) is a well-known approach for preventing in-cylinder soot and NO_X formation in diesel engines. It is achieved by extending ignition delay through increasing injection pressure to augment mixing and by adding high levels of exhaust gas recirculation (EGR) [17]–[21]. Extended ignition delay results in primarily premixed combustion and increased dilution lowers combustion temperatures. LTC can be attained with either early or late injection strategies. Early LTC (ELTC) injects fuel 20 to 30 crank angle degrees before top dead center (DBTDC) during the compression stroke, while late LTC (LLTC) injects fuel 0.5 to 9 DBTDC. Both methods allow for high levels of mixing and smokeless combustion [22], [23].

While soot and NO_X are essentially eliminated during LTC modes, UHC emissions increase. Intermediate hydrocarbon species from combustion such as methane, ethane, propylene, formaldehyde, acetaldehyde, and others cannot be fully oxidized due to low combustion temperatures, resulting in increased UHC emissions [24]–[26]. Other sources of UHC emissions include fuel impinging on the piston bowl and incomplete combustion

in over-lean regions of the cylinder. In practice, UHCs from conventional diesel combustion (CDC) are oxidized in a diesel oxidation catalyst (DOC) that typically require exhaust temperatures to be greater than 250 °C for complete conversion. In LTC, exhaust temperatures are often lower than the required limits for conversion efficiencies found during CDC, preventing their oxidation in a DOC. Further, CO and unsaturated hydrocarbons are known to reversibly poison DOCs at the high concentrations found in LTC exhaust [26]. Since certain species are more likely to deactivate DOCs than others, it is advantageous to understand the individual species that make up the overall UHC in diesel LTC.

2.3 Fuels

Emerging needs and further opportunities for cleaner burning, high efficiency fuels continue to drive exploration into autoignition and pollutant formation chemistry. In this study, three fuels were selected to characterize various piston designs for use in RCMs and RCEMs while developing additional knowledge of their autoignition chemistry. They were also chosen based on their well-known chemical kinetics and mechanisms that aid in accurate numerical modeling studies.

2.3.1 Dimethyl ether

Dimethyl ether (DME), chemical formula CH_3OCH_3 is a transparent gas at ambient conditions. It is the simplest ether and also has properties similar to liquefied petroleum gases (LPG) like propane and butane. Due to its high cetane number (55-60) and low particulate, soot, CO, and NO_x emissions, DME could be a clean alternative to diesel fuels and ideal for use in CI engines [27], [28]. Modeling results conducted by Good et al. have shown the tropospheric lifetime of DME is 5.1 days and concluded it is environmentally

benign [29], [30]. DME is usually produced from carbonaceous energy sources such as coal, natural gas, crude oil, and biomass [31].

Autoignition studies at engine-relevant conditions is important to understand the ignition kinetics of DME for use as a modern-day fuel alternative. Previous studies have shown combustion product concentrations from DME combustion, such as, smoke and PM to be lower than those from diesel fuel combustion [32], [33]. DME and DME blends have been studied with shock tubes [34]–[40], but very few at elevated pressures and low-to-intermediate temperatures. Mittal et al. conducted RCM experiments to fill the void of high pressure, low-temperature DME/oxidizer combustion to validate and refine kinetic models for DME oxidation [31]. In recent years, DME fuel blend experiments have increased in the prospect of cleaner burning, higher thermal efficiency engines [37], [41], [42].

2.3.2 n-Butane

n-Butane, C_4H_{10}, is a single component fuel with relatively well-known kinetics and is an important component in fuels such as LPG and petroleum. It is also used as a blending agent to improve the vaporization characteristics of gasoline for use in low-temperature environments [43]. Early studies noticed that small changes in the volume fraction of butane in natural gas had a significant influence on its ignition properties [44]–[46]. Such work highlights the significance of autoignition studies of butane for the development and optimization of IC engines and modern fuels.

Substantial work has been conducted over the years to understand the autoignition properties of butane isomers with parameters such as temperature, pressure, and fuel loading. Early autoignition studies done by Carlier et al. were conducted at low pressures using a flame burner and at higher pressures using an RCM for a *n*-$C_4H_{10}/O_2/N_2$/Ar mixture

[47]. Experimental results were compared to a butane-oxidation model by Pitz et al., which found the model to be more reactive than the experiments and incorrectly predicted the temperature at the start of the NTC region and its duration [48].

A recent study by Gersen et al. measured ignition delay times for both *n*-butane and *iso*-butane that show both isomers exhibit two-stage ignition and an NTC region at low temperatures (680 - 825 K). Increasing the pressure from 15 bar to 30 bar resulted in a decrease in the amplitude of the NTC regions and shortened ignition delay by a factor of 3 for both butane isomers [49]. Similarly, Healy et al. used a RCM and shock tube to study *n*-butane/air and *iso*-butane/air mixtures covering a wide range of pressures and temperatures [50], [51]. With updated kinetic models from collected ignition delay time data, the authors found *n*-butane to be more reactive than *iso*-butane with greater divergence in reactivity at lower temperatures and higher equivalence ratios. Over the years, a number of other butane and butane blended mixtures have been studied extensively using RCMs, shock tubes, and burners to validate and improve kinetic models [52]–[59].

2.3.3 Ethanol

As the transportation sector continues to grow, the need for cleaner and more efficient alternative fuels is vital for replacing the dependence on fossil fuels [60]. Significant attention has been given to ethanol since it is made from a renewable source of energy and can be used as a neat fuel, fuel extender, and octane number enhancer [61]. The primary source of ethanol is made through a fermentation process using glucose derived from sugars and starches.

Ethanol being the simplest alcohol, after methanol, has been extensively studied using a wide range of instruments such as flow and jet reactors [35], [61]–[64], laminar

burning flames [65]–[69], and shock tubes [70]–[74]. However, ethanol pyrolysis experiments at low-to-intermediate temperatures at engine relevant pressures are meager. For engine developers, a validated chemical kinetic mechanism is vital for modeling neat and blended ethanol combustion.

Early studies by Lee et al. reported ignition delays for stoichiometric ethanol, nitrogen, and argon mixture at five temperatures [75]. They found ethanol displayed similar autoignition characteristics to methanol but with a lower activation energy of 130 kJ/mol. The activation energy matched previous shock tube results although the ignition delay was higher by a factor of three. A more in-depth study of ethanol was conducted by Lee et al. where measured ignition delays were used to develop an updated kinetic mechanism for ethanol combustion [76]. This followed the work done by Mittal et al. who looked at the autoignition of ethanol over a range of stoichiometry and temperatures [77]. Results were used to update their model's kinetic reaction rates for hydroperoxyl radicals, specifically $C_2H_5OH + H\dot{O}_2$, which considerably improved predictions. Recent studies have been conducted to further investigate ethanol combustion using gas sampling and gas chromatography techniques to identify and quantify intermediate species formed during the ignition delay period [78].

Currently, there is an initiative in the RCM and RCEM community to identify facility-to-facility differences [79]. Ethanol was chosen as the model fuel because it does not exhibit NTC behavior, the reaction kinetics are well understood, and its reactivity range makes it combustible in most RCM/RCEMs.

2.4 Reactors for Studying Chemical Kinetics of Pre-Mixed Combustion

Chemical kinetics is the study of reaction rates of chemical processes and their dependence on environmental conditions. The progression of chemical reactions in engines is complex and depends on a large number of variables such as temperature, pressure, and air-fuel ratio (AFR). The detailed study of rates and mechanisms of combustion reactions is important for investigating the formation of combustion products during the evolution of chemical kinetics. Investigation is required to understand the formation and reduction of combustion products such as CO_2, NO_x, and soot for specific combustion modes. For modeling purposes, detailed kinetic mechanisms also need experiments over a wide range of temperatures, pressures, and mixture compositions for validation. For these reasons, facilities such as flow reactors, jet stirred reactors, shock tubes, RCMs and RCEMs are used to create a range of desired experimental environmental conditions.

2.4.1 Turbulent Flow Reactors

Turbulent flow reactors, commonly referred to as plug flow reactors (PFA), constantly flows premixed fuel mixture down a tube at a uniform temperature and pressure [80]. Being heavily diluted by an inert gas, the fuel mixture flow rate is high, which in turn, constitutes a large reaction zone. This method of combustion generates negligible axial temperature and concentration gradients allowing for accurate measurement of gas temperature and sampling of combustion species [81]. With a PFA, detailed measurements of chemical kinetics are possible but only for slow, highly dilute reactions. Slow ignition studies are of interest due to gas-turbine operating conditions with extended test times beyond 500 ms.

2.4.2 Jet Stirred Reactors

Jet stirred reactors provide very fast reactions with small dilution ratios. Unlike laminar flow reactors, jet stirred reactors are fixed volume and achieve uniform mixing by generating turbulence. To do so, a high-velocity inlet jet of fuel mixture enters and exits a chamber at constant pressure and steady state [82]. Since the mixture is highly turbulent, the assumption is made that the temperature and concentration of the exhausted gas are both homogenous. Mixing timescales are assumed to be much shorter than that of the chemical reaction time. Since this type of reactor operates under steady-state conditions, there is a lack of information about the ignition process.

2.4.3 Shock Tubes

Neither flow reactors nor jet stirred reactors can study autoignition characteristics of reactant mixtures at pressures and temperatures that are commonly found in IC engines. Such studies often use shock tubes that deduce autoignition pressures and temperatures from pressure traces. At one end of a shock tube, high-pressure inert gas that is divided by a diaphragm from the other side containing a reactant mixture. When the diaphragm is punctured, a shock wave travels down the tube and compresses the mixture [83]. Ignition delay is interpreted by the difference in shock arrival time to the start of combustion [84]. Shock tubes are capable of reaching pressures up to ~600 bar, and temperatures up to ~2800 K but reactions often have limited observation times of < 5 ms due to boundary layer effects and reflected waves.

2.4.4 RCM/RCEMs

Since the early 20th century, combustion researchers have devised many approaches to consistently measure the ignition temperature and delay of air-fuel mixtures at engine-

relevant temperatures and pressures. In addition, the study of ordinary fuel-mixture reaction evolution by isolating chemical reaction phenomena from engine-produced perturbations like fuel spray and evaporation.

Developers of the RCM identified the following five features a machine would need for studying key combustion properties:

1) the compression should be as rapid as possible

2) there should be no rebound of the piston at the end of the stroke

3) the combustion chamber should be unlubricated

4) there should be means for recording gas pressure and piston position as a function of time

5) the possibility to vary compression ratio and the initial pressure and temperature of the reaction mixture [85]

With these aims in mind, many attempts have been made to achieve them resulting in a variety of rapid compression machines.

RCMs are one of the few tools capable of studying fuel combustion and ignition delay behaviors that are representative of IC engine environments. They are designed to simulate a compression stroke event at temperatures, pressures, and realistic fuel loadings ($\phi \approx 0.5–2.0$) that are observed in modern-day spark ignition (SI) and compression ignition (CI) IC engines [86]. RCEMs are similar but also have the capability to include an expansion stroke in its trajectory. Both of these machines are capable of compressing a reactant mixture in milliseconds, nearly adiabatically, and observing its ignition characteristics in a constant volume and a constant mass reaction chamber with observation times between 1 - 150 ms. They must achieve a thermally homogenous, near-adiabatic core

of gas in the center of the cylinder to enable the study of autoignition characteristics and chemical kinetics evolution. Figure 1 exemplifies that RCMs/RCEMs can produce ignition delay times at temperatures where it is not attainable by shock tubes.

RCMs can be outfitted with gas sampling to analyze autoignition chemistry by quantifying species concentrations using off-line methods such as those described in Section 2.1. Similarly, laser diagnostics and imaging are commonly implemented techniques to study specie concentrations and temperature but also provide additional temporal and spatial fidelity in comparison to gas sampling. By outfitting the end of the combustion chamber with an optically accessible head, planar laser-induced fluorescence (PLIF) [87], chemiluminescence [78], particle image velocimetry (PIV) [88], Rayleigh scattering, and other optical diagnostics can provide in-situ measurements of species concentrations, radical lifespan, and temperature.

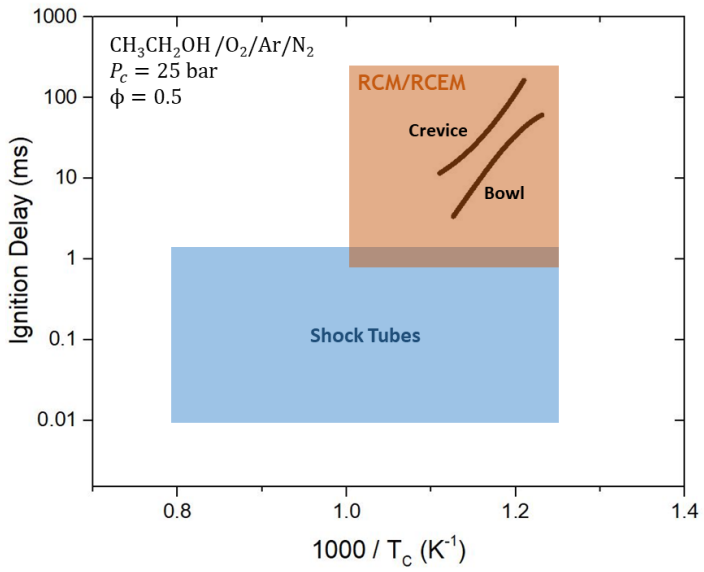

Figure 1: Comparison of ignition delay time vs. temperature for the combustion of ethanol using creviced and bowl pistons

In RCM/RCEMs, post-compression pressures and temperatures are usually greater than 10 bar and 600 K, respectively. To compensate for heat loss during compression and avoid premature ignition prior to TDC, the piston must travel at high velocities, usually greater than 6 m/s. Pressure traces from compressing non-reactive inert gases, nitrogen and argon for a typical RCM trajectory is shown in Figure 2 where a rapid rise in pressure during compression is followed by a gradual decrease post-compression due to heat loss. Another observation made in this figure is that nitrogen is closer to being isentropic during compression than argon. Also, argon can be inferred to have a higher thermal diffusivity than nitrogen that causes greater heat loss post-compression. Next, the compression of reactive *n*-butane and highly diluted dimethyl-ether (DME) fuel mixtures are shown in Figure 3. After compression, ignition delays are observed followed by the start of ignition. The *n*-butane fuel mixture is observed to have a single stage ignition delay (A) while the DME mixture exhibits a two-stage ignition delay (B).

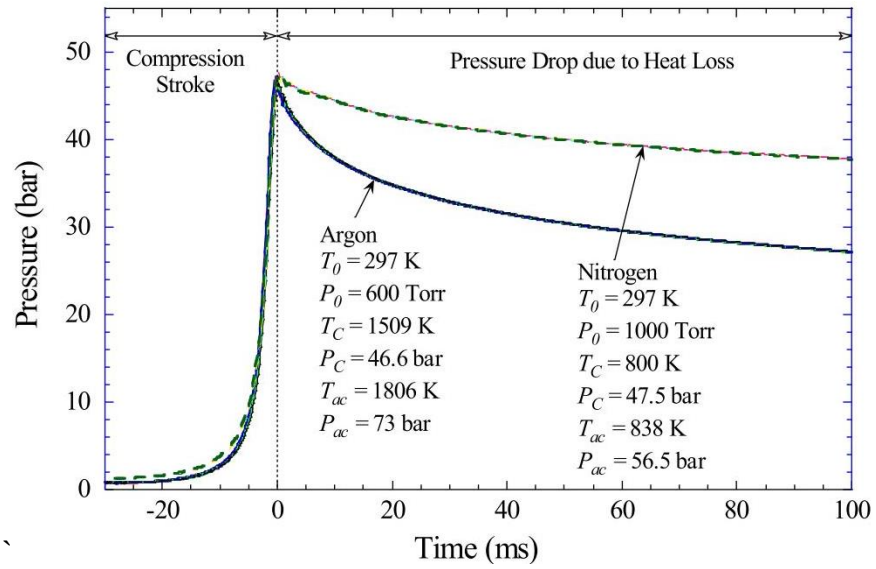

Figure 2: Compression of inert gases with a typical RCM trajectory [89]

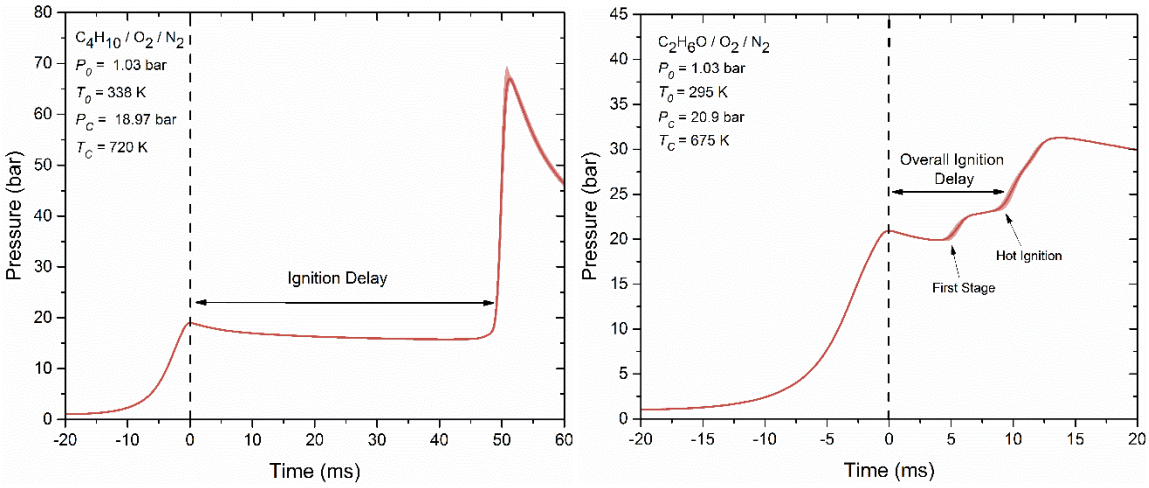

A) B)

Figure 3: Pressure traces from compression of reactive fuel mixtures: A) *n*-butane ($C_4H_{10}/O_2/N_2$ = 1/6.5/24.44) B) Dimethyl ether ($CH_3OCH_3/O_2/N_2$ = 1/4/40)

Recent efforts have been made to characterize flow field structure and heat transfer in RCMs both numerically and experimentally to validate the adiabatic core hypothesis [43], [88], [90]–[95]. In this hypothesis, the assumption is that heat losses and boundary layer effects do not directly affect the fuel mixture since its combustion is of uniform composition [96]. It is important that the adiabatic core remain intact throughout the ignition delay time to allow for accurate comparison of experiments to zero-dimensional (0-D) homogenous ignition models and to validate the volumetric ignition scenario.

Research has shown that a "roll-up" vortex forms near the piston-cylinder interface during compression in RCMs and RCEMs using flat top pistons (Figure 4) that have crevice volumes similar to pistons used in IC engines. Early CFD studies in an RCM conducted by Griffiths et al. showed spatial temperature variations in the combustion chamber and a clockwise flow pattern centered asymmetrically towards the piston face and cylinder wall [97]. Park and Keck discovered that temperature gradients could be caused

by this roll-up vortex that beset previous experimental work [98]. This vortex destroyed any thermal uniformity prior to combustion and stymied attempts to use early RCMs for detailed kinetic studies.

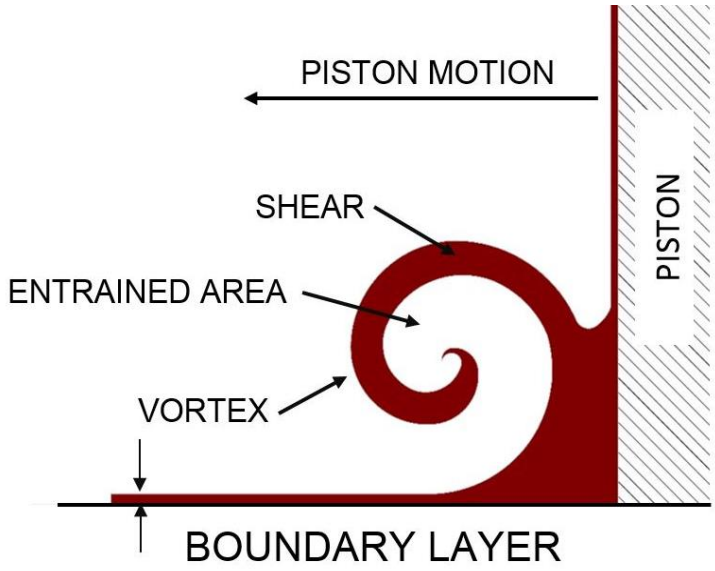

Figure 4**:** Roll-up vortex formation during compression

Researchers then introduced a novel notch crevice on the piston face edge to mitigate the influence of the roll-up vortex. Although the notch crevice design helped suppress the vortex, Lee and Hochgreb found that this type of crevice could not effectively suppress pre-ignition and questioned if reactions were occurring within the crevice volume [91]. They went on to design a channel that funneled the boundary layer into an enlarged crevice volume incorporated on the side of the piston (Figure 5). Implementing an enlarged piston crevice design helped mitigate vortex formation and provided a near quiescent adiabatic core gas. The enlarged crevice method for vortex suppression has been further investigated and has evolved over the span of almost two decades. However, the underlying geometry has stayed the same and is currently used by many RCM/RCEM facilities [84], [87]–[89], [92], [99]–[106].

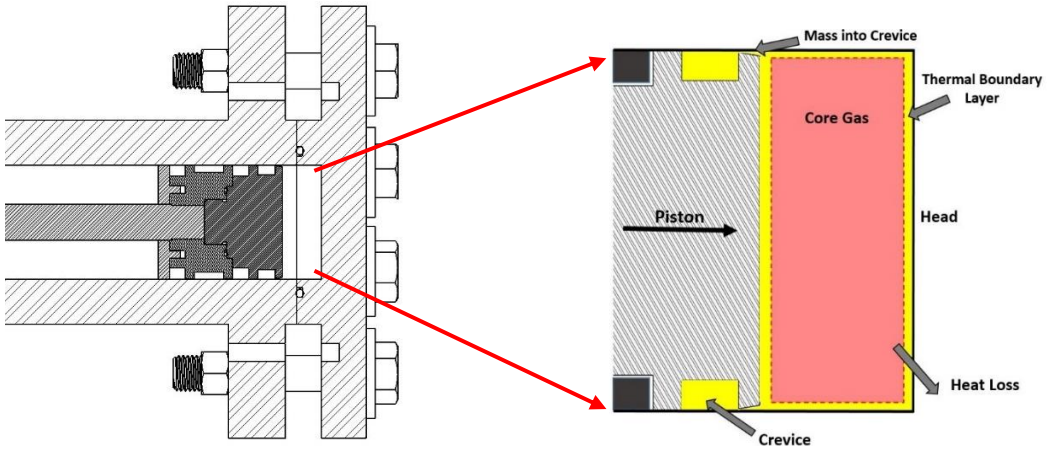

Figure 5**:** Enlarged crevice piston

Although the use of creviced pistons have been shown to sufficiently reduce the roll-up vortex in RCMs/RCEMs, their efficacy has not been extensively studied for RCEMs that implement an expansion stroke. A CFD study by Goldsborough et al. using an integrated chemical kinetics/0-D crevice model with multi-zone heat release saw a re-emerging crevice gas for a motored piston trajectory. The crevice gas was seen to emerge at the start of the expansion and create an inverted vortex near the cylinder wall [107]. The study illustrated the effect on both maximum peak and mass-averaged temperatures during expansion for both reactive and non-reactive conditions. Although it is known that gases contained in an enlarged piston crevice re-emerge during expansion in an RCEM, little work has been done to characterize the process experimentally or numerically.

The development of the controlled trajectory rapid compression and expansion machine (CT-RCEM) at the University of Minnesota – Twin Cities prompted the development of preliminary CFD models to simulate flows within the combustion chamber. During the expansion stroke, it was observed that crevice gases re-emerge creating an “inverted” vortex, opposite in direction to the roll-up vortex formed during compression. Additionally, the gas in the crevice was much cooler than the gas in the

combustion chamber; during expansion, the cool gas would exit the crevice and mix with the uniform core gas in the combustion chamber. This heterogeneous mixing and consecutive cooling of combustion gases produces a non-uniform progression of chemical kinetics. These results indicate a need for a piston that works for both compression and expansion strokes to fill this void for RCM and RCEM research.

2.4.4.1 Piston Designs

2.4.4.2 Flat Piston

Several groups have verified temperature heterogeneities in RCMs using a flat piston geometry [93], [97], [108]. Clarkson et al. observed using laser induced fluorescence (LIF) that the vortex collects cool boundary layer gas from the walls and moves it into the center of the chamber during compression [108]. The spatially non-uniform temperature field at the end of compression is relevant to the ignition process of the reactive mixture. A flat top piston with a crevice volume similar to those in IC engines (Figure 7) is used in this study to demonstrate the influence of the roll-up vortex on combustion and provide a baseline comparison for the creviced and bowl pistons.

2.4.4.3 Creviced Piston

The geometric parameters of the creviced piston used in this study were influenced by previous CFD studies that modeled the impact of varying dimensions B, C, D, F, and G in (Figure 6) for an optimal design [92], [93], [109]. It was discovered that crevice volume was the largest influencer in suppressing the roll-up vortex and that entrance channel dimensions had less impact [92]. The total crevice volume was sized to contain the boundary layer for the length of piston travel. The tapered piston face entrance angle was determined to be large enough for the boundary layer to flow into the crevice where $\delta_{99\%}$

at the end of compression (EOC). Length C in Table 1 was chosen to assist with minimizing backflow into the core gas region. The final crevice volume was determined by these parameters and was found to be approximately 25% of the final combustion chamber volume, and is well within the range of similar RCEMs [4, 8].

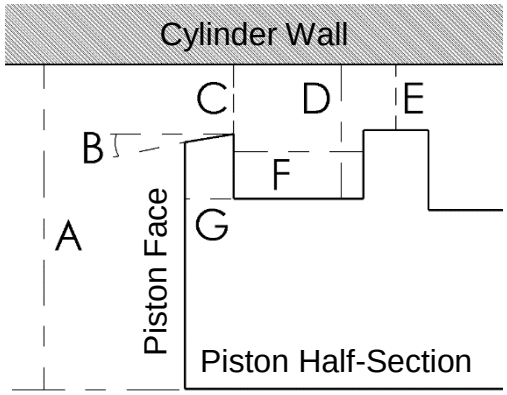

Figure 6: Half-section of creviced piston

A	25.40 mm
B	9.50º
C	0.30 mm
D	4.30 mm
E	0.05 mm
F	8.00 mm
G	3.00 mm
Total Vol.	5318 mm^3

Table 1: Corresponding values for Figure 6

Figure 7: Pistons from left to right: creviced, bowl, and flat

2.4.4.4 Bowl Piston

Bowl pistons used in compression ignition (CI) engines are designed to promote mixing of fuel and air. This type of piston is typically used in diesel engines to rid localized overly lean and rich regions during combustion in an effort to reduce UHCs and soot [110]. Air motion in diesel engines utilizing bowl style pistons can be characterized into three main categories: squish, tumble, and swirl [111]. Swirl motion is usually generated during the induction period by the design of the intake port and tumble is a large-scale rotating flow with its rotation axis perpendicular to the cylinder axis [112], [113]. Since induction time scales are orders of magnitude smaller for RCM/RCEMs, turbulence generated during fueling was neglected and only squish flows are considered in this study. Squish generates abrupt turbulence as the piston approaches TDC. This turbulent generating mechanism have been studied thoroughly using modeling and experimental techniques [111]–[121]. It was hypothesized that implementing a bowl piston design in RCEMs and RCMs would induce mixing of the cylinder's boundary layer and fuel mixture during compression and expansion, resulting in a uniform mixture composition across the reaction chamber. Generating a homogenous core gas composition provides the advantage of higher combustion efficiencies, greater volumetric ignition modes, and less deflagrative ignition characteristics.

The bowl piston was developed to mitigate the shortcomings of the creviced piston during piston expansion and dump sampling experiments in RCMs and RCEMs. The requirements for the piston included the following:

1) the core must have a higher mass fraction of fuel mixture within 50 K of the peak temperature than the creviced piston

2) there must be minimal backflow from the crevice during piston dwell at TDC and piston expansion

3) no roll-up vortex formation

CFD simulations of velocity vector profiles were performed to verify the roll-up vortex phenomena of the flat piston, boundary layer containment using the creviced piston, and bowl mixing using the bowl piston [122]. Velocity profiles for the flat piston in Figure 8A clearly demonstrates a vortex at the end of compression (EOC) while in Figure 8B, the vortex is captured in the enlarged crevice of the creviced piston. Figure 8C demonstrates large-scale rotational flow induced by the squish region.

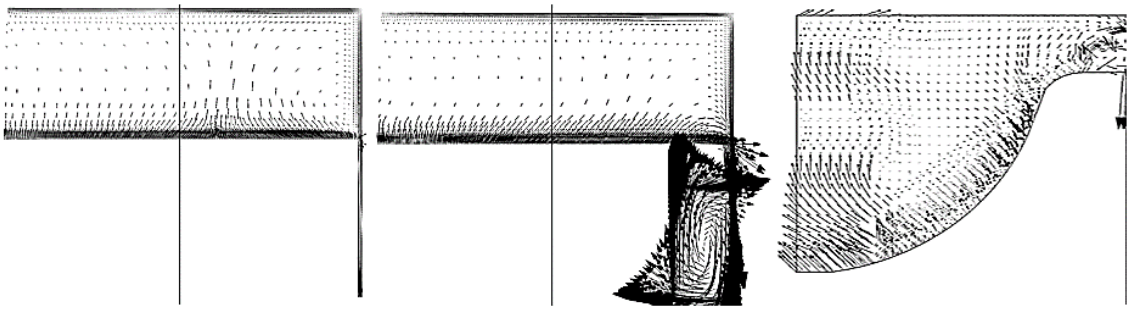

A) B) C)

Figure 8: CFD simulated velocity vectors at the end of compression A) flat piston B) creviced piston C) bowl piston

The bowl piston developed for this study is shown in Figure 9 with comparisons to the flat and creviced pistons in Figure 7. Like the flat and creviced pistons, this piston was designed to have the equivalent volume in the combustion chamber while using the same stroke. This was done by lengthening the piston to accommodate for the volume of the bowl which resulted in a 4mm squish region. A sectioned view of the piston bowl can be found in Figure 10.

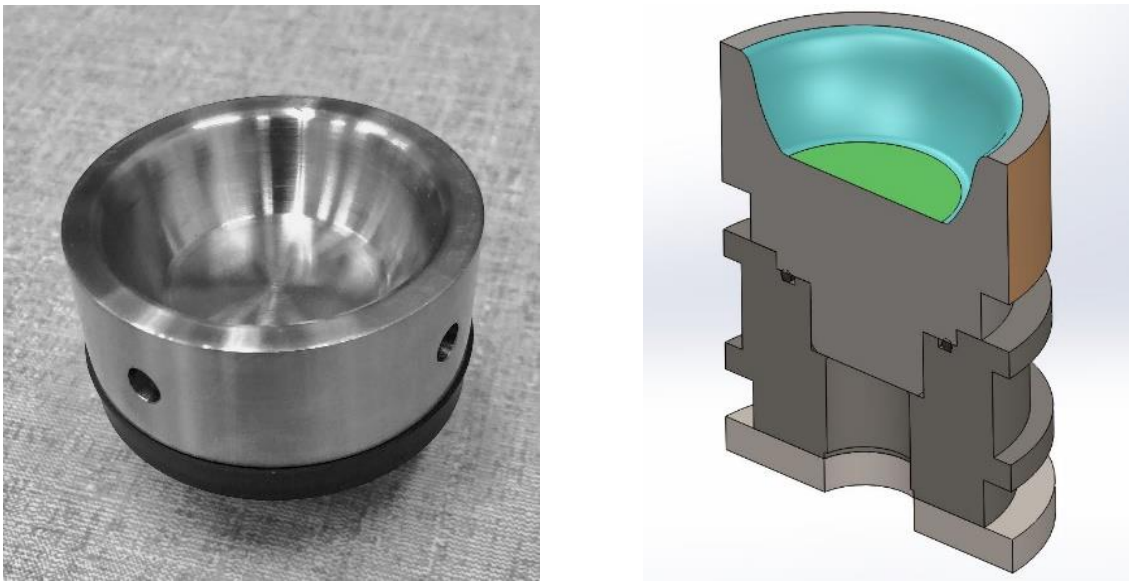

A B

Figure 9: A) bowl piston B) bowl piston assembly

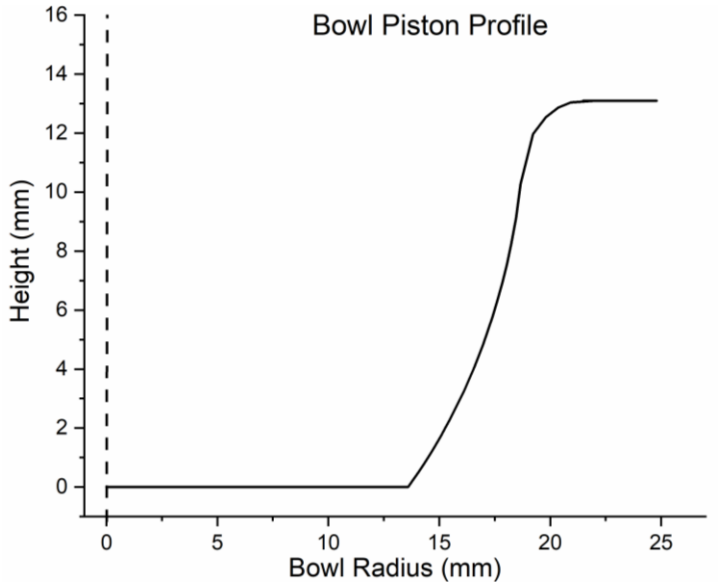

Figure 10: Bowl piston dimensions

CHAPTER 3 Experimental Methodology

3.1 Engine Setup

The first portion of this research was performed using a 4-cylinder GM A20DTH 2.0 liter turbocharged direct-injection compression ignition (CI) engine [123]. The engine was equipped with a variable geometry turbocharger (VGT), variable swirl actuation (VSA), and high-pressure common rail fuel injection. It was controlled with National Instruments hardware coupled with a fully configurable Drivven© engine control unit. A modified EGR system was used for greater control of EGR temperature, while an aftermarket PID controlled a water/air after-cooler that provided improved control over intake air temperatures. Non-oxygenated, ultra-low sulfur #2 diesel (ULSD) fuel was used in this study.

In order to achieve LTC, the engine was first motored, and then operated at the designated engine operation settings (VGT, VSA, fuel pressure) with dual injection conventional diesel combustion (CDC) until steady state operating conditions were reached. The EGR valve was then opened, pilot injection turned off, and main injection timing advanced slowly until an ELTC mode was achieved. The engine was then allowed to reach steady state.

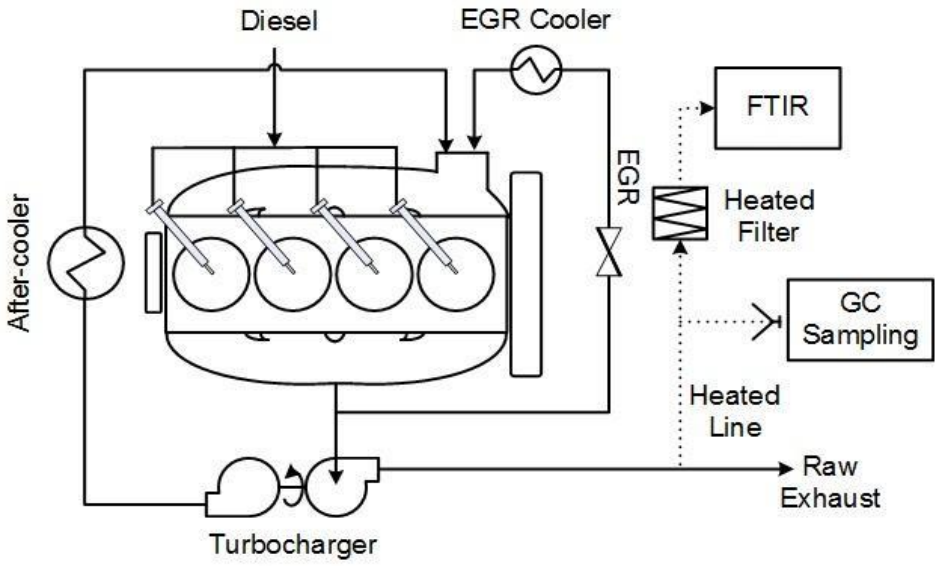

Figure 11: GM A20DTH 2.0 liter turbocharged compression ignition engine setup

Engine exhaust was sampled from the outlet of the turbocharger prior to entering a diesel oxidation catalyst (DOC) and diesel particulate filter (DPF). Heated lines at 191 °C were used to route exhaust gas to both the FTIR and GC-MS sampling system. The engine schematic is shown in Figure 11.

Table 2 shows the engine's operating conditions investigated during this study. In addition to CDC, three LTC combustion modes, produced by varying EGR rates to increase UHC concentrations ranging from low (LTC 1) to high (LTC 3), were studied. FT-IR spectra were collected at a frequency of 1 Hz for off-line analysis of each testing condition.

Table 2: Engine operating conditions

	CDC	LTC 1	LTC 2	LTC 3
Engine Speed [RPM]	1500	1500	1500	1500
BMEP [bar]	1.79	1.72	2.09	2.28
Injection Pressure [bar]	600	1000	1000	1000
Pilot Injection Timing [DBTDC]	19.0	--	--	--
Pilot Injection Duration [ms]	0.270	--	--	--
Main Injection Timing [DBTDC]	7.00	28.0	28.0	28.0
Main Injection Duration [ms]	0.560	0.475	0.480	0.485

VGT [%]	55.0	67.0	70.0	70.0
VSA [%]	70.0	5.00	5.00	5.00
EGR Valve [%]	25.0	45.0	45.0	55.0
EGR Rate [%]	17.0	30.0	57.5	59.0

3.1.1 Fourier Transform Infrared Spectroscopy (FT-IR)

FT-IR spectroscopy differs from dispersive spectroscopy in that a beam containing many frequencies of light is used instead of a monochromatic light beam. The beam is then modified to contain a different combination of frequencies to provide a second data point to allow the built in computer to analyze and infer the absorption at each wavelength. The varying frequency beam is generated through the use of a Michelson interferometer, a configuration of mirrors, one of which is moved by a motor. A broadband beam containing the full spectrum of wavelengths to be measured is directed onto the moving mirror, and as the mirror moves, each wavelength of light is periodically blocked or transmitted, causing the beam coming out of the interferometer to have a different spectrum. The raw data for light absorption at each mirror position is then processed using a Fourier Transform algorithm to determine the light absorption at each wavelength.

An AVL SESAM i60 FT bench was to measure light hydrocarbons (LHC) (C_4 and below) and limited heavy hydrocarbons (HHC) including octane and aromatic hydrocarbons (AHC) through a method designed for CDC. All measurements were made with a scanning frequency of 1 Hz. As seen in Figure 11, heated sample lines maintained at 191 °C were used to route exhaust from the test engine to a heated box equipped with a glass/PTFE filter supplied by Unique Heated Products to remove soot prior to entering the spectrometer. Prior to engine startup, the FT-IR spectrometer detector was cooled with liquid nitrogen to 65-77 K. A system leak check followed by an auto-calibration (background) were successfully performed. During testing, background values for H_2O and

CO_2 were maintained at less than 1% difference from the gas cell reference. The manufacturer supplied diesel recipe/method (Diesel-SCR) was used for quantification of UHC species. The recipe/method is designed to account for and quantify compounds commonly observed in diesel combustion exhaust. The FT-IR measures the amount of infrared light absorbed via numerous compounds in the mid-IR range (400-4000 cm^{-1}). Individual gaseous exhaust species absorb different wavelengths of infrared light, and the amount of light absorbed at specific wavelengths produces a spectrum that is iteratively fit relative to known concentrations of these same species.

3.1.2 Gas Sampling System

A gas sampling system was developed for extracting, storing and transferring engine exhaust to a GC-MS for off-line analysis. A series of four dry impingers were arranged in series and submerged in an ice bath between the sampling unit and the heated exhaust line in order to condense otherwise column damaging HCs (> C_{10}) (Figure 12). The sample reservoir section of the system was initially evacuated to a pressure of ~30 kPa. Once the engine reached a steady state, the vacuum pump pulled exhaust through the heated sample line into the impingers at ~2 liters per minute (LPM) while bypassing the sample reservoir. This allowed all lines leading to the sample reservoir to be filled with exhaust and for condensate to be collected for later GC analysis. In this study, only select light UHC species were quantified with the GC due to column restrictions.

Once approximately 6 mL of condensate was collected in the impingers (enough for 6 GC injections), the exhaust flow was directed into the sample reservoir through a throttling valve set at ~1 LPM. After exhaust filled the sample reservoir to atmospheric pressure, flow to the reservoir was stopped and the sampling system was moved to another

laboratory room for analysis. The sampling reservoir and lines were then pressurized with helium creating a 2:1 dilution for LTC modes and 1.5:1 for CDC modes.

Applying Dalton's Law, relative mole fractions for air, exhaust, and helium remaining in the system can be estimated by measuring the pressures under each condition using a pressure transducer and assuming that N_2 is the predominant gas in the exhaust after the condensation trap. The total number of moles of exhaust gas, n_{exh} was determined using the Ideal Gas Law. This value was used in the partial pressure equation where:

$$P_T = P_{exh} + P_{He} + P_{air} = (\frac{n_{exh}RT}{V}) + (\frac{n_{He}RT}{V}) + (\frac{n_{air}RT}{V}) \qquad \text{(Eq. 1)}$$

Because P_T V, n_{air} and n_{exh} are known, n_{He} is easily determined. Applying the Van Der Waals non-ideal gas correction for volume and pressure found to have negligible effects on species concentrations (< 1%).

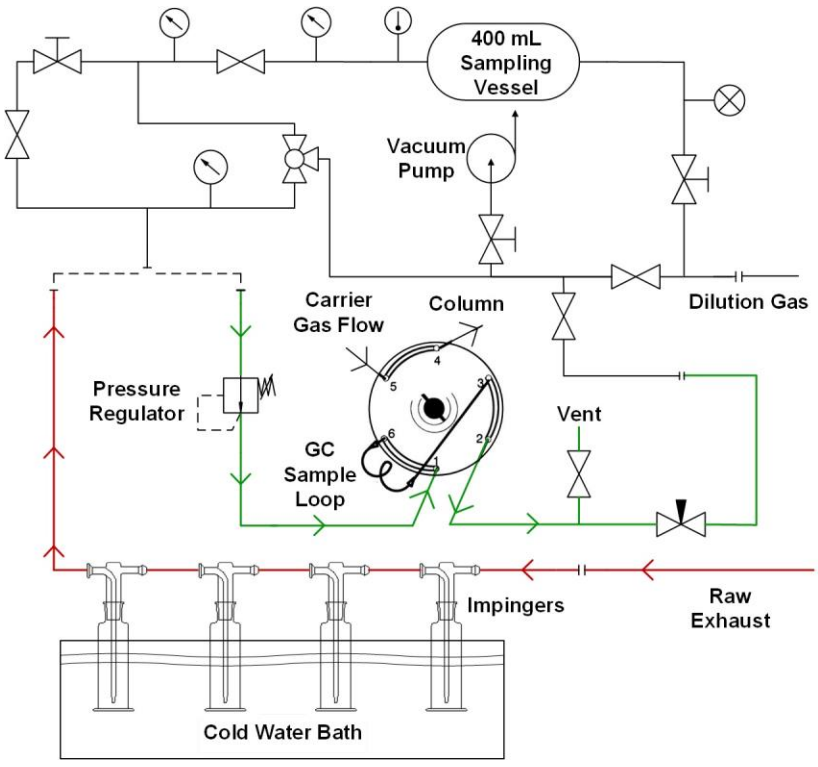

Figure 12: GC-MS gas sampling system schematic

When the vent valve was open to atmosphere, sample gases under pressure flowed out and through the GC sample loop. The use of pumps or any other mechanical devices, which can promote HC losses, were eliminated in this sampling method. With the sampling system heated to 100 °C, leftover analyte was removed by pressurizing and flowing nitrogen through for quick system turnaround.

When the sampling system was connected to the GC gas sampling line and loop (Figure 12), it was purged then evacuated before injection to minimize wasted analyte. This minimized the risk of diluting analyte with ambient room air or any other gases. Once the sample line was filled with the analyte, the vent was opened to allow flow through the sample loop as previously mentioned. A constant pressure of analyte was passed through a low-pressure regulator (6.89 kPa gauge) for increased repeatability of GC injection conditions.

3.1.3 Gas Chromatography with Mass Spectroscopy (GC-MS)

GC-MS is another instrument used in this study to quantify exhaust species. The gas chromatograph uses a capillary column with certain dimensions and stationary phase properties that interact with the gaseous compounds. The separation of these compounds depends on their interaction strength with the stationary phase of the column. The time it takes for a compound to elute from the column wall and migrate out of the column is known as the compounds retention time. Interaction strengths and retention times are influenced by many factors such as temperature, column length, carrier gas flow rate, and the amount of analyte injected. The released compounds from the column are then introduced into the mass spectrometer.

The mass spectrometer (MS) or also known as a mass selective detector (MSD) sorts ions based on their mass to charge ratio (m/z). When a compound enters a quadrupole MS through the ion source chamber, it is bombarded with electrons generated by a filament that breaks the compound into ionized fragments. A positively charged plate in the ionization chamber pushes the positively charged fragmented ions through multiple lenses where they are focused into an ion beam. The ion beam travels into the quadrupole where they are then filtered based on m/z. This filtering is done by applying a radio frequency (RF) voltage to the four rods that make up the quadrupole. An offset DC voltage is applied to a pair of rods which allow ions of a specific m/z to flow out of the quadrupole to the detector. Ions with unstable paths collide with the rods until their potential voltage is the same as the ratio of voltages on the quadrupole. Varying the potential on the rods allow for sweeping through wide ranges of m/z. The filtered ions then travel to the detector which is made up of a detector ion focus, a high energy conversion dynode (HED), and an electron multiplier (EM) horn. The detector ion focus directs the beam of ions to the HED where they strike its surface. This collision emits electrons that get attracted to a more positive EM horn that has a negative voltage at its entrance and 0 voltage at the other end. While the electrons flow through the horn to the end, they collide with the EM horn wall, freeing electrons. This addition of electrons amplifies the current generated at the end which is proportional to the number of ions that strike the HED.

The GC used in this study was an Agilent 7890B coupled to an Agilent 5977A Mass Spectrometry Detector (MSD). The GC was fitted with a 6-port 2-way pneumatic gas switching valve. A test run was performed using dry shop air before each engine mode case to ensure there were no residuals trapped within the GC column from previous runs. When

in the load position and while the carrier gas was being introduced to the column, test gases entered the sample valve, through a 0.25 mL sample loop, and vented to atmosphere. Sample gas was injected into the GC via a switching valve that simultaneously shifts the inlet and outlet to flow carrier gas into the sample loop and then on to the column. The details of the GC-MS and its parameterization are listed in Table 3.

Table 3: GC-MS parameters

Carrier Gas	Helium (99.999 %)
Gas Switching Valve	Inject: 0.01 min to 0.25 min 100 °C
Injection Port	250 °C, Constant Flow (5:1 Split) 2 mL/min column flow 14 mL/min split flow 3 mL/min purge flow
Oven	Initial: 40 °C, 0.5 min hold Ramp 1: 25 °C/min to 175 °C, 2 min hold Ramp 2: 25 °C/min to 250 °C, 8 min hold
Mass Spectrometer	Transfer Line: 280 °C Mass Scan Range: 15 - 300
Column	Agilent GS-GasPro (60 m x 0.32 mm) Type: Silica-based PLOT Stationary Phase: Bonded

Data acquisition and analysis were performed with Agilent Chemstation software. The quantification database was developed using a calibration standard that consisted of 21 different gaseous compounds balanced in nitrogen. A linear regression calibration curve was fitted for each compound having at least two concentrations consisting of three measurements each. A single background subtraction (BSB) was performed on the back end of each total ion chromatogram (TIC), and then integrated. Compounds that eluted at the same time as compounds found in the calibration standard were checked with the NIST

Standard Reference Database as well as with their target and qualifier ions to validate their identity. Quantitative analysis was then performed and a report was generated for each compound that had a calibration curve.

3.2 CT-RCEM

3.2.1 Experimental Setup

The architecture of the CT-RCEM is shown in Figure 13 and photographs of the test facility appear in Figure 14 [124]. The machine is divided into five sub-systems: combustion chamber unit, actuator unit, control module, fueling/exhaust/purge system, and diagnostics system.

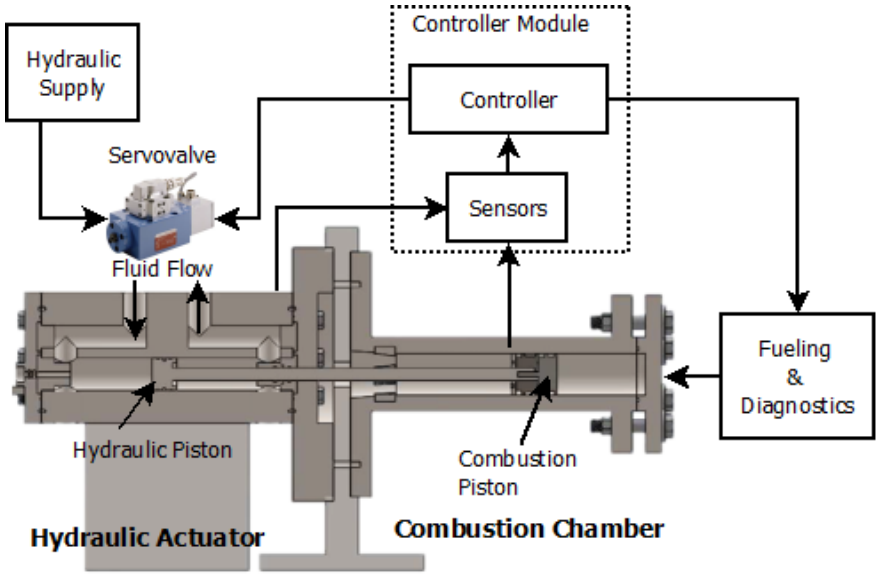

Figure 13: CT-RCEM architecture [125]


1-1/4 SAE 100 R4 200PSI HYDRAULAX 2016

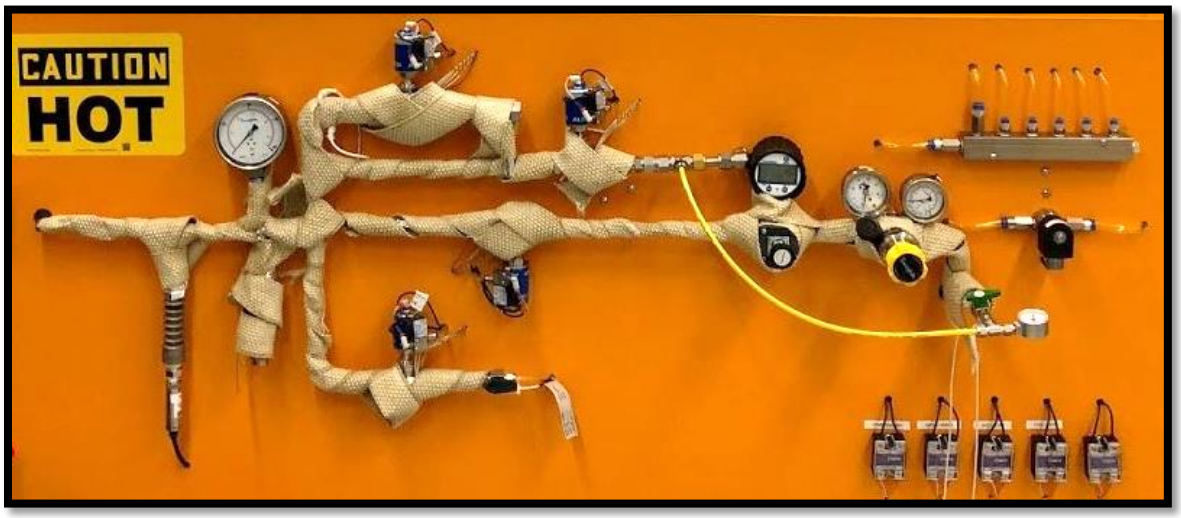
CAUTION
HOT

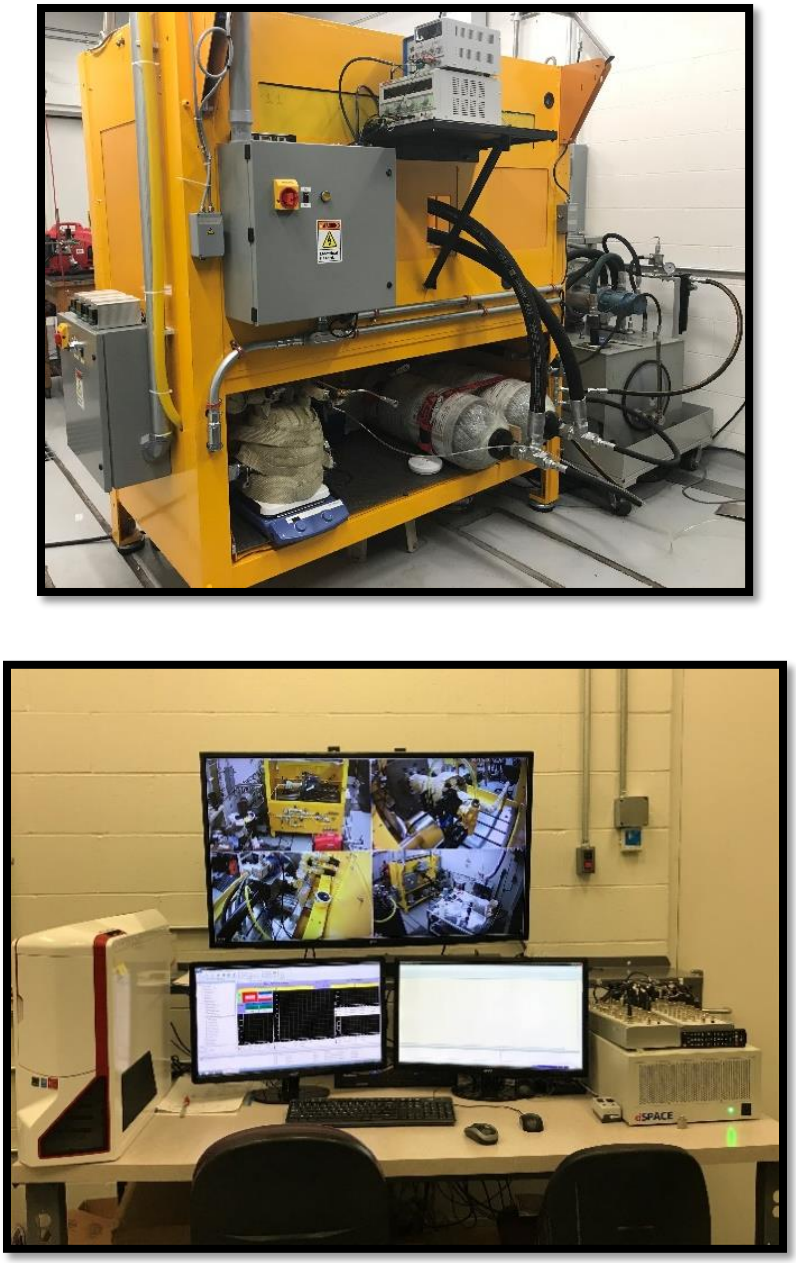

Figure 14: Controlled Trajectory Rapid Compression and Expansion Machine (CT-RCEM) at the University of Minnesota – Twin Cities

3.2.2 Actuation

Currently, RCM and RCEM actuation systems operate with open loop control and do not allow for any feedback of piston trajectory during the compression and expansion

strokes. This lack of control complicates the ability of the machine to change operating conditions such as modifying stroke, compression ratio, compression time, etc. These types of changes require replacement of parts and/or physically tuning the machine to specific parameters. This has the potential to cause repeatability error and lowered measurement accuracy. It is important that steps are taken to minimize vibrations while compressing, expanding, and during piston deceleration. At the EOC, an RCM/RCEM must have the capability to stop almost instantaneously. A constant volume reaction chamber is not attained if the piston overshoots, rebounds, or rings after its intended position. The changing volume from piston ringing can have a significant impact on the progression of chemical kinetics and the accuracy of autoignition features.

The driving mechanism of the CT-RCEM is a custom electro-hydraulic actuator with real-time trajectory control. The hydraulic actuator consists of a high bandwidth servo valve and a double acting piston. The hydraulic fluid supply system to the actuator comprises of a pump that charges two 10-gallon accumulators connected in parallel providing a peak flow rate of 1600 LPM. The hydraulic piston and combustion piston are connected by a steel rod.

By having feedback motion control, we are able to overcome the aforementioned problems with previous hydro-pneumatic RCMs/RCEMs [125]. The trajectory profile of the piston is fed to the hydraulic controller electronically and allows for complete flexibility of piston motion and operational parameters. The centralized data logging and motion controller is implemented on a dSPACE DS1007 unit with a dual core 2.0 GHz processor. A Linear Variable Differential Transformer (LVDT) position sensor which is connected to

the hydraulic piston is used for piston position feedback to the controller, with a sampling frequency of 5 kHz.

3.3.3 Combustion Chamber

The combustion chamber assembly which is also referred to as the reaction chamber assembly, consists of the combustion cylinder and head that are bolted together. The head of the reaction chamber has multiple diagnostic accessories including a high-speed pressure transducer and gas sampling capabilities. An optical head is also available for in-situ species measurements using optical diagnostic techniques. The assembly is made out of 316 stainless steel and inner diameter is coated with a thin layer of hard chrome to protect the chamber from scratching or gouging in the case of piston seal failure. The CT-RCEM has a maximum stroke of 194 mm with a minimum clearance height that can be varied from 4 – 10 mm. Total length of the combustion chamber is 200 mm. The minimum clearance height can be changed by adjusting a mechanical stop in the hydraulic actuator section of the machine. Heating elements and thermocouples are placed on the outside of the chamber to uniformly heat and keep the fuel mixture at initial temperatures. Specifications regarding the combustion chamber of the CT-RCEM can be found in Table 4.

Table 4: UMN CT-RCEM specifications

Combustion Cylinder Bore	50.8 mm
Maximum Stroke	194 mm
Maximum Geometric CR	25
Max Combustion Chamber Pressure	30 MPa
Max Peak Temperature	2100 K

The combustion piston is comprised of three pieces (Figure 15). The top is interchangeable to support multiple piston geometries such as the conventional flat and enlarged crevice pistons, and non-conventional styles like the bowl piston. The middle section houses a ring-land for a guide ring and rear piston seal. The bottom piece effectively holds the rear seal in place. The piston seals are uni-directional and are made from a unique Ryton®/carbon blend with a built in cantilever spring to help with high pressures in the combustion chamber. The guide ring is made from carbon graphite. Excellent sealing performance at low and high pressures were observed along with minimal blow-by during compression and expansion with this piston ring configuration.

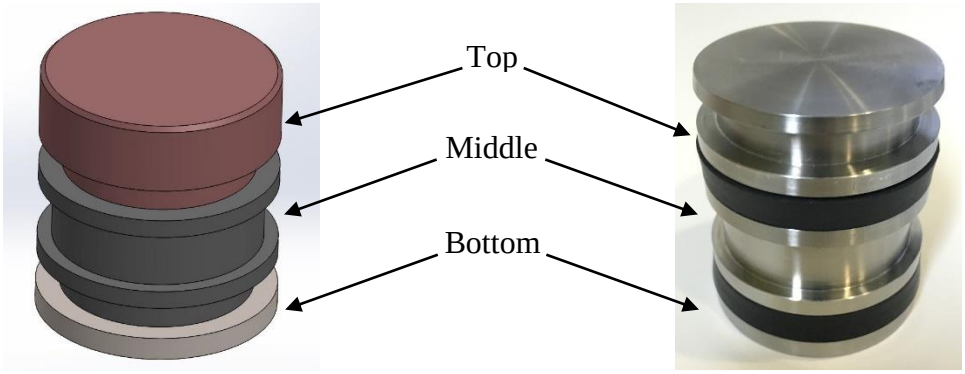

A B

Figure 15: A) model of piston assembly with flat geometry B) creviced piston assembly uni-directional piston rings

3.2.3 Fueling/Purge/Exhaust System

A system was developed to move a fuel mixture into the CT-RCEM from a mixing vessel, exhaust the combustion gases, and purge the machine after each use (Figure 16). It is electronically controlled allowing for fast turnaround times and increased safety. Swagelok ALD diaphragm solenoid valves are used to direct gas flow to and from the

combustion chamber. A HiP Hippo electro-pneumatic solenoid separates the combustion chamber and fueling system and can handle up to a maximum operating pressure of 4000 bar. Fuel and oxidizer are mixed and heated by an IKA C-MAG HS 10 magnetic stirrer heating plate. To avoid condensation of fuel mixture or exhaust when stationary or flowing, all lines and valves are heated.

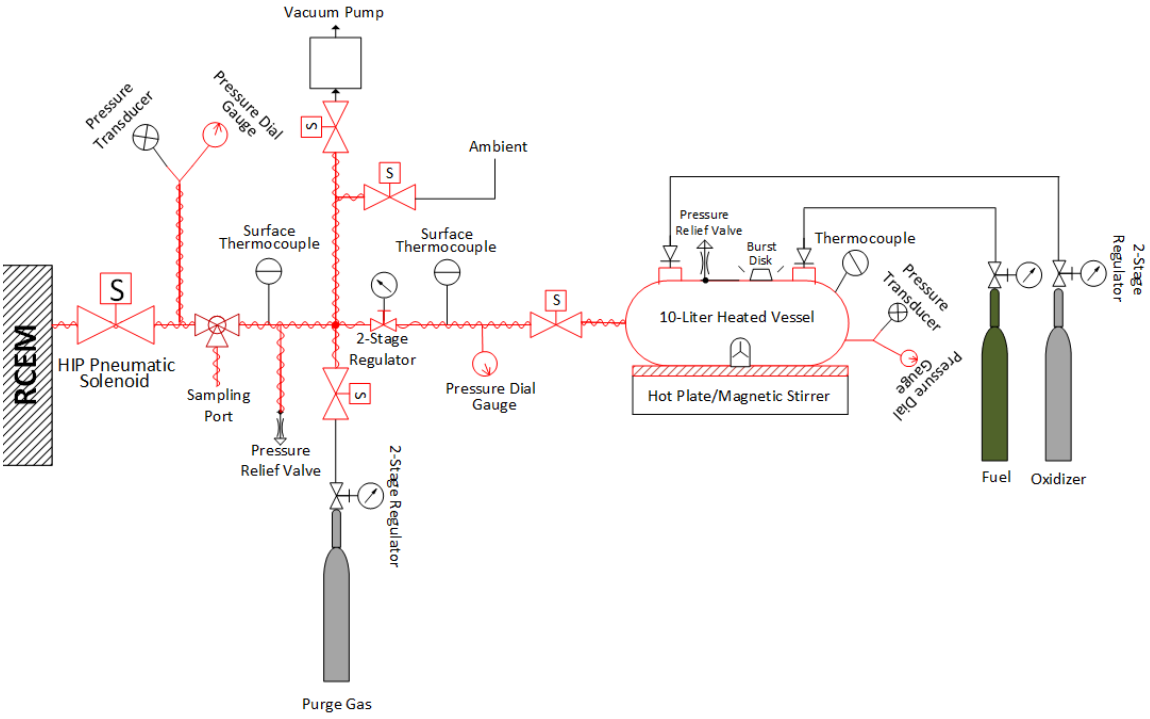

Figure 16: CT-RCEM fueling, purge, and exhaust system

3.2.4 Diagnostics

Combustion in the CT-RCEM can be characterized by three different methods. A Kistler 6045A piezoelectric pressure transducer coupled to a Kistler 5010B charge amplifier mounted in the combustion chamber provides high-speed pressure data. The pressure measurements are used to calculate ignition delay and identify anomalies like pre-ignition and knock during compression. The mobile gas sampling system described in Section 3.1.2 has the ability to connect in-line with the CT-RCEM exhaust system to

provide dump sampling capabilities. A Quantel TDL system with a tunable dye laser, 380 mJ YAG laser and iSTAR ICCD camera provide PLIF and chemiluminescence imaging capabilities. PLIF and chemiluminescence imaging provide in-situ scalar properties such temperature and specie concentrations with high spatial and temporal resolution in the combustion chamber. Figure 17 outlines the setup of the ICCD camera using the optical head.

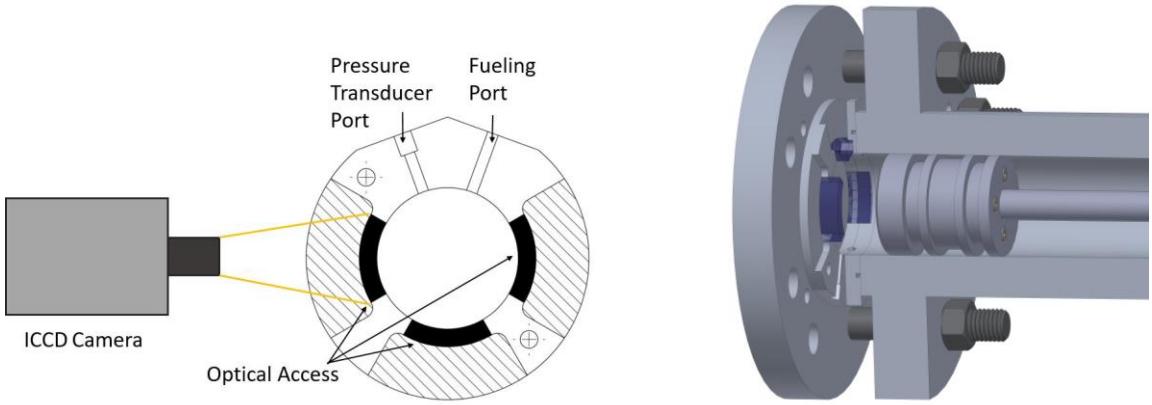

Figure 17: CT-RCEM optical head design

CHAPTER 4 Comparison and Optimization of FT-IR and GC-MS for Speciating Unburned Hydrocarbons from Diesel Low-Temperature Combustion

4.1 Overview

The work presented here combines off-line GC-MS and on-line FT-IR methods to quantify light UHCs from diesel ELTC modes. A novel sampling system was designed to collect a known quantity of exhaust gas and transfer it to a GC-MS while reducing the risk of transfer losses and unexpected dilution. GC-MS was used to identify potential compounds whose IR spectra were used together with FT-IR spectral reprocessing. GC-MS analysis is used to provide the necessary foundation for developing a more representative FT-IR method for the online quantification of light ($< C_8$) UHC species from diesel LTC operation.

4.2 Experimental Method

The FT-IR measured UHC species concentrations are summarized in Table 11 of the Appendix. Concentrations of individual hydrocarbon species in CDC exhaust were normal. As expected for LTC, these same species were present in much higher concentrations as measured by both methods. Spectra data collected during testing were reprocessed and analyzed using MKS Instruments MG2000 (v7.2) software. In order to evaluate fitting residuals, “calculate residuals/errors” was enabled in the “Setup” window with the Diesel-SCR method loaded. During the “Reprocess” function, the “Spectral Resids” display mode was chosen. After loading the Diesel-SCR method into the Spectrum Utility, “Method Analyzer”, a spectrum representative of the interfering species was loaded. A spectrum of the residual feature is revealed by successive subtraction of each

expected (Diesel-SCR method) component. Care was taken only to remove intensities associated with a given component. In an effort to reduce the residual feature intensity to zero, additional spectral methods were added to the Diesel-SCR method and the entire process was repeated.

Each LTC exhaust sample from the same test was sampled, injected and analyzed six times using GC-MS. In the first three minutes, nitrogen and oxygen co-elute, followed by the CO_2 peak; each of these exceeded the ion detector limit and therefore are not quantified in this analysis. GC-MS species concentrations and retention times can be found in Table 12 of the Appendix. A GC-MS TIC, which depicts well defined peaks of eluted compounds, from one of the CDC runs is shown in Figure 18. The Porous Layer Open Tubular (PLOT) GC column used in this study is designed for the retention of low molecular weight hydrocarbons while being highly inert and unaffected by wet samples that can influence retention stability. It was observed that acetaldehyde was retained while similar oxygenates such as formaldehyde and benzaldehyde were not. For this specific column, retention became difficult for some oxygenates and aromatics due to the chemical nature of the bonded stationary silica-based phase. Hence, identification and quantification are limited to a few aromatic and oxygenated compounds in this study.

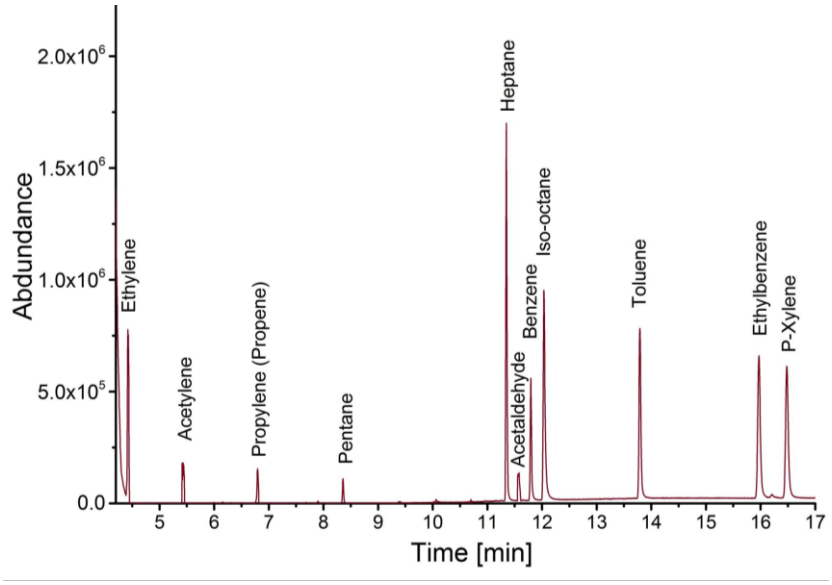

Figure 18: TIC of CDC exhaust sample with BSB

4.3 Discussion

The emissions index (EI) of species measured by the FT-IR and GC-MS are compared in Figure 19. The FT-IR is capable of measuring hydrocarbons C_1-C_8, while the GC-MS, as configured for this study, measured C_2-C_8. While the FT-IR measured aromatic hydrocarbons (toluene, benzene, and xylenes) by fitting the fine structure of toluene alone, the GC-MS was able to speciate and quantify heavier HCs (cyclo-hexane, heptane, and *iso*-octane) and specific aromatic HCs (benzene, toluene, ethylbenzene, and p-xylene). Although the FT-IR is capable of quantifying the heavier HCs, heptane and *n*-octane, the Diesel-SCR method used in this study did not include these compounds. A very good correlation between the two measurement techniques was observed for acetylene, ethylene, ethane, propene, and acetaldehyde. The GC-MS had a higher standard deviation between GC injections for the CDC case and HHCs in general.

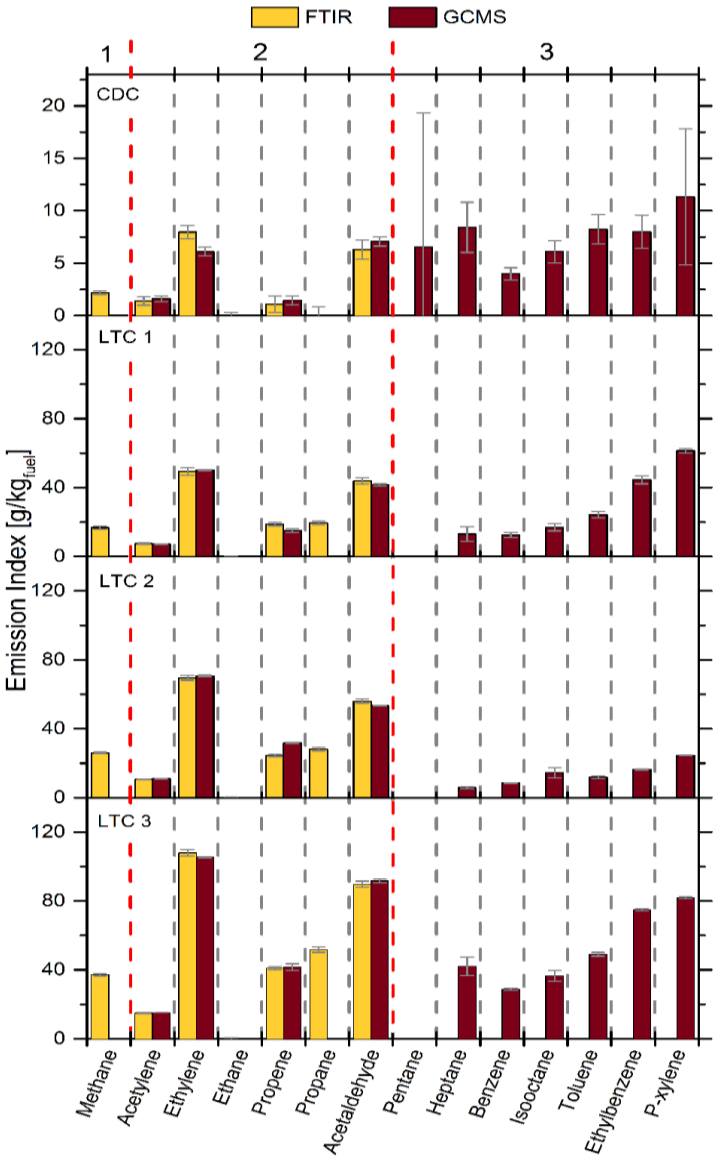

Figure 19: GC-MS vs. FT-IR emissions index. Region 1: FT-IR only; Region 2: FT-IR and GC-MS; Region 3: GC-MS only

It is important to note that the FT-IR reported propane for the LTC cases, whereas the GC-MS reported a value under its detection limit. Propane is not known to be a product of CDC or LTC [15]. As the FT-IR recipe was designed for CDC, it could suffer from unknown species interference elicited from LTC modes [14].

To verify the existence of absorption band interference, sample spectra were collected during CDC and the transition to LTC. The spectra from each LTC mode were reprocessed revealing a significant fitting residual between 2700 and 3100 cm^{-1} (Figure 20 and Figure 21 black solid line). The identical residual feature was found in both LTC 1 and 2. However, LTC 3 produced a somewhat different residual. Due to the lower temperature of these combustion modes, it was hypothesized that these features were the result of unburned diesel fuel vapor, for which the FT-IR CDC method does not account. It is clear from Figure 20 and Figure 21 that removal of diesel vapor intensity alone only partially accounts for the residual features. This is particularly evident for the LTC 3 residual (Figure 22).

In an effort to reduce the overall residual intensity, the compounds identified from GC-MS analysis were investigated. Digital spectra of these compounds and others were taken from MGRefsMaster R3 Spectral Library (251 individual compound spectra), which is available for purchase from MKS Instruments, Methuen MA. The Library contains both methods and calibration spectra for each compound. These can be incorporated into any existing method or recipe in order to identify the source of residual intensity in a complex gaseous spectrum. Information regarding the accuracy, traceability, and general quality of the methods can be found in the accompanying portable document file delivered with the library. Of the eleven compounds identified in LTC 2 and 3, only two, acetaldehyde and iso-octane, were found to have significant intensity in the residual region. Removal of the intensities of these compounds together with dodecane (or *n*-decane) and benzaldehyde reduced the intensity across the entire LTC 2 residual region to a much greater extent. Interestingly, the same kind of intensity reduction for the LTC 3 residual did not involve

acetaldehyde or *iso*-octane. Figure 21 shows that dodecane (or *n*-decane), benzaldehyde, and hexadecane were required to remove much of the residual feature intensity. Figure 22 shows that the final residuals for LTC 2 and 3 are significantly different. These results suggest that raw diesel fuel is likely not the source of the residual feature. More importantly, they suggest that the source of the residual feature is different for the LTC modes and that combustion chemistry between LTC 1 and 2 may be different from that of LTC 3.

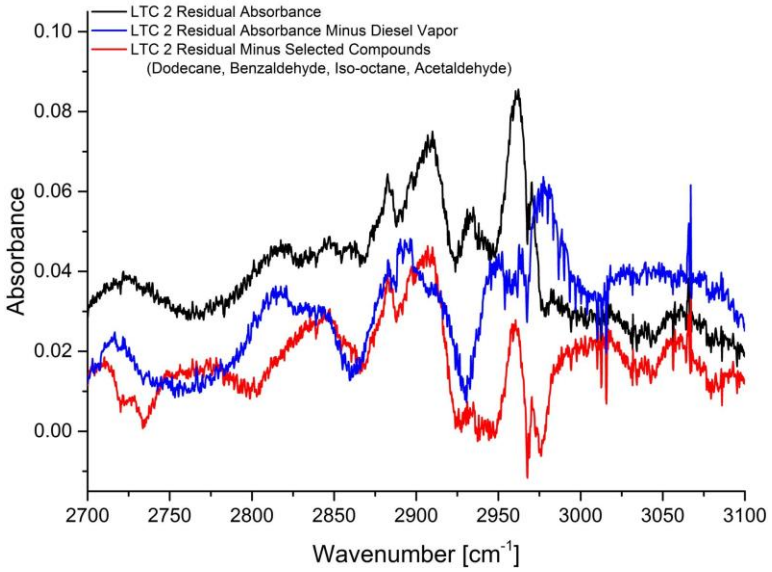

Figure 20: LTC 2 FT-IR absorbance: original LTC residual (black), original residual with diesel vapor subtracted (blue), original residual with selected compounds subtracted (red)

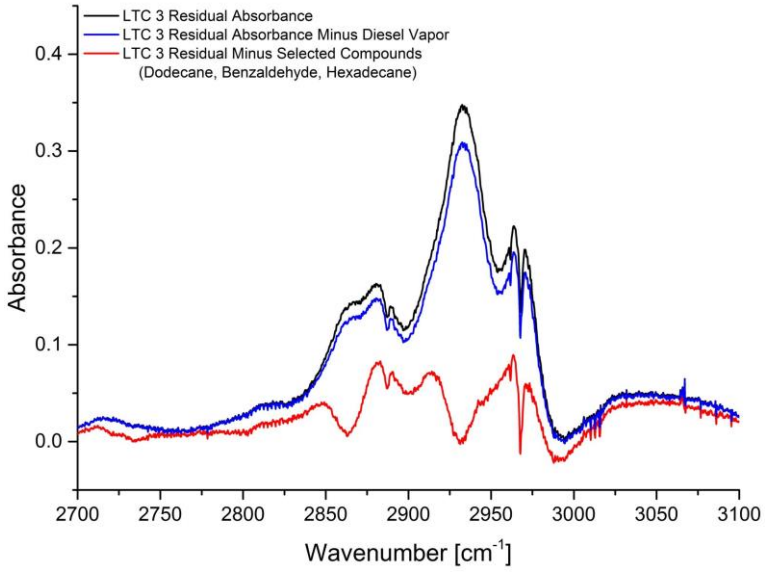

Figure 21: LTC 3 FT-IR absorbance: original LTC residual (black), original residual with diesel vapor subtracted (blue), original residual with selected compounds subtracted (red)

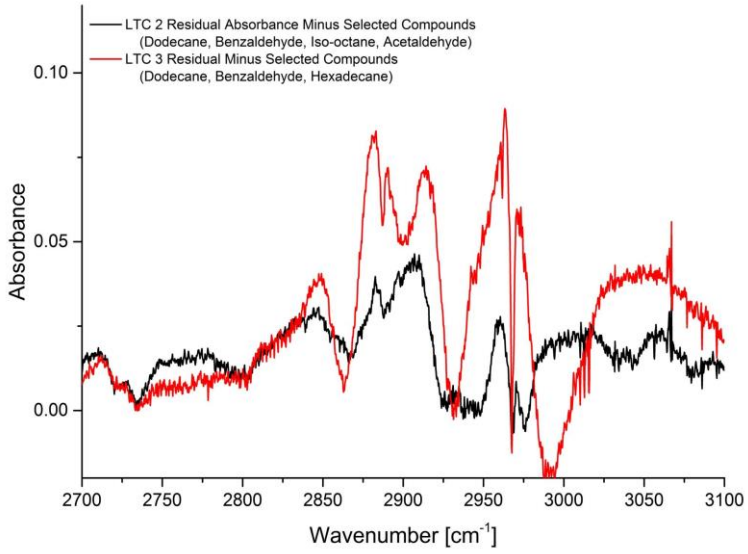

Figure 22: LTC 2 & LTC 3 residual absorbance after subtraction of selected compounds

Figure 22 shows that the intensity of each residual is not fully accounted for in the current analysis. The next steps in method development are to carefully record calibration spectra for each identified component and incorporate these calibrations into the CDC method, Diesel-SCR. This requires careful analysis of interferences and selection of fitting

regions. It may also require altering fitting regions for other components in the standard method. Finally, the method must be evaluated by collecting spectra from each LTC mode and reprocessing them. Evaluation of the spectral residual fittings will reveal how well the new method measures the new components and accounts for the majority of the intensity in the 2700-3100 cm^{-1} region. Significant improvements in the utility of the GC-MS in this process might include incorporation of two or more stationary phase columns in parallel as well as the ability to sample the condensate where additional exhaust gas components may be found. Alternatively, utilizing a stationary phase column designed for speciation of HHCs (> C_8) could replace the need for condensate trapping altogether.

The results indicate that care must be taken when applying FT-IR methods optimized for CDC modes to unconventional modes such as LTC. Specifically, one should routinely evaluate FT-IR spectral fitting residuals to ensure that compounds and concentrations are accurately identified and quantified. In this way, the FT-IR can be used as a discovery tool itself or in conjunction with other speciation methods like GC-MS in the evaluation of exhaust from alternative combustion modes and/or fuels. The results of this study [126], [127] suggest that not only can FT-IR and GC-MS be used in conjunction to measure a variety of compounds from unconventional combustion modes, alternative fuels, or new catalyst materials, but they can also be used together as investigative tools in the discovery of unsuspected or new intermediates arising from future combustion strategies or catalyst materials.

CHAPTER 5 Investigation of Piston Geometry in Rapid Compression Machines

5.1 Overview

The purpose of the work described in this section was to investigate how a non-conventional bowl-style piston design can impact chemical and thermal uniformity in RCMs. Increased uniformity is directly linked with the conversion of unburned fuel to products of combustion and is critical for accurate measurement of species concentrations and development of chemical kinetic mechanisms [43], [128]. Conversion efficiencies are significantly lowered when using a flat piston design due to boundary layer development and thermal and chemical non-uniformities caused by roll-up vortex phenomena [89]. Similarly, the creviced style piston inhibits conversion since unburned fuel mixture stored in the enlarged crevice on the piston periphery is too cool to ignite. It is hypothesized that implementation of a bowl-style piston can lead to improved uniformity and greater conversion of unburned fuel to products. This is due to the absence of an enlarged crevice and enhanced mixing of boundary layer and fuel mixture caused by squish flows during compression and combustion. It is also hypothesized that a bowl-style piston will exhibit less mixed mode ignition by increasing turbulent Damköhler and turbulent Reynolds numbers.

5.2 Experimental Results

Experimental results for four different fuel mixtures using the flat, creviced, and bowl pistons are presented in this section. Sections 5.2.1 and 5.2.2 describe experiments used to depict trends of the CT-RCEM performance and the varying piston designs. Section

5.2.3 describes an in-depth experiment done over a range of temperatures with ethanol to characterize the piston performance with respect to each other.

Fuel mixture compositions, as well as compressed pressures and temperatures, are presented in Table 5. It should be noted that compressed temperature, T_C, was deduced from compressed pressure, P_C, using the isentropic relation (Equation 2) where P_0 is initial pressure, T_0 is initial temperature, and γ is the specific heat ratio of the fuel mixture.

$$\int_{T_0}^{T_c} \frac{\gamma}{\gamma-1} \frac{dT}{T} = \ln\left(\frac{P_C}{P_0}\right) \quad \text{(Eq. 2)}$$

Table 5: Test matrix for combustion studies

Fuel	**Piston Type**	ϕ	**Fuel (mole)**	**O_2 (mole)**	**Ar (mole)**	**N_2 (mole)**	**P_C (MPa)**	**T_C (K)**
Dimethyl ether	Creviced	0.33	1.00	4.00	0	40	2.12	685
	Creviced	0.33	1.00	4.00	0	50	2.11	683
	Flat	0.33	1.00	4.00	0	40	2.15	690
	Flat	0.33	1.00	4.00	0	50	2.14	689
	Bowl	0.33	1.00	4.00	0	40	2.13	687
	Bowl	0.33	1.00	4.00	0	50	2.12	685
***n*-Butane**	Creviced	1.00	1.00	6.50	0	24.44	1.90	719
	Flat	1.00	1.00	6.50	0	24.44	1.94	726
	Bowl	1.00	1.00	6.50	0	24.44	1.91	721
Ethanol	Creviced	0.50	1.00	6.00	13.56	9.00	2.50	817-880
	Bowl	0.50	1.00	6.00	13.56	9.00	2.50	812-888

Generally, the ignition delay of a fuel is defined as the time it takes to autoignite when exposed to autoignition conditions. For this study, the duration of the first stage of ignition delay is defined as the time between the end of compression (EOC) and the local maximum of the time derivative of the pressure trace between the EOC and hot ignition.

Similarly, the duration of the second stage of ignition delay is between the end of the first stage of ignition delay to the global maximum of the time derivative of the pressure trace.

5.2.1 Dimethyl ether

In this study, the ignition delay is collected for two highly dilute DME fuel mixtures. First, results are shown for the combustion mixture of DME, oxygen, and nitrogen consisting of 1 mole, 4 moles, and 40 moles, respectively. A non-reactive experiment was performed to observe the heat loss to the chamber walls and piston by replacing the moles of oxygen with extra nitrogen. Observed in Figure 23 is the relationship between non-reactive and reactive pressure traces which are seen to match exactly during compression when using the creviced piston. Heat loss is apparent via the pressure decay following the EOC for both reactive and non-reactive mixtures.

DME autoignition at low-to-intermediate temperatures and elevated temperatures is known to show characteristics of two-stages of ignition delay and a negative temperature coefficient region. After the reactive mixture undergoes the first stage of ignition delay (τ_1), it is followed by the second stage of ignition delay (τ_2), then subsequently hot ignition. The flat piston presented a longer LTHR than the ITHR and a total ignition delay of 5.3 ms (Figure 23). In contrast, the creviced piston exhibited slower rates of pressure rise during the transition to ITHR and hot ignition lengthening the ignition delay to 9.3 ms (Figure 24). The bowl piston displayed similar rates of pressure rise to the flat piston but had a significantly longer LTHR period and short ITHR when compared to the other pistons (Figure 25). Ignition delay time for the bowl piston fell between the flat and creviced pistons at 7.7 ms. Figure 26 shows the overlaid pressure traces for the three pistons.

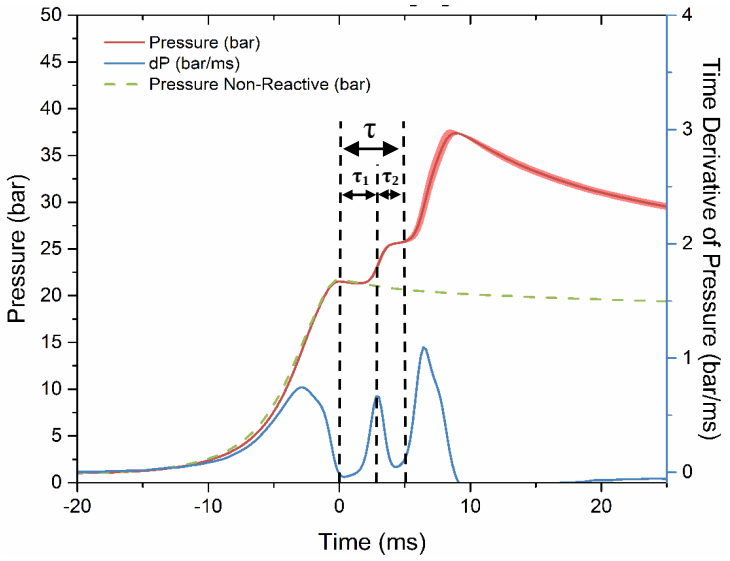

Figure 23: Pressure profile for autoignition of dimethyl ether mixtures using a flat piston. Molar composition: $CH_3OCH_3/O_2/N_2$ = 1/4/40. Initial conditions are T_o = 300 K and P_o = 1.034 bar.

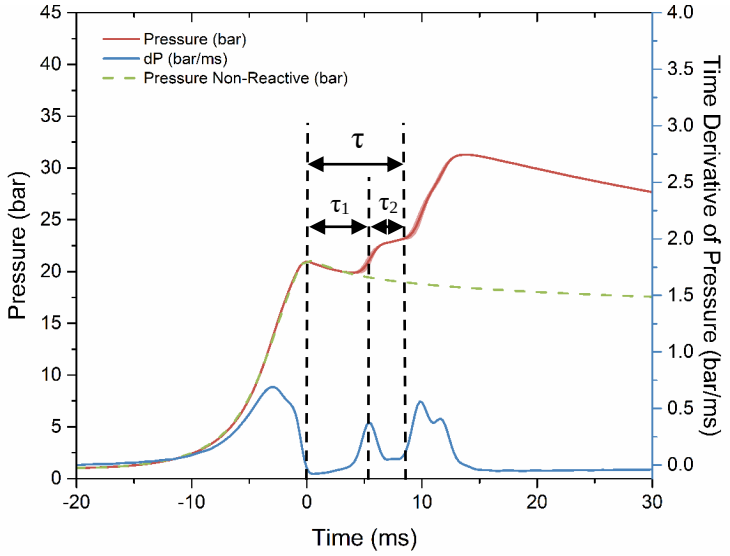

Figure 24: Pressure profile for autoignition of dimethyl ether mixtures using creviced piston. Molar composition: $CH_3OCH_3/O_2/N_2$ = 1/4/40. Initial conditions are T_o = 300 K and P_o = 1.034 bar.

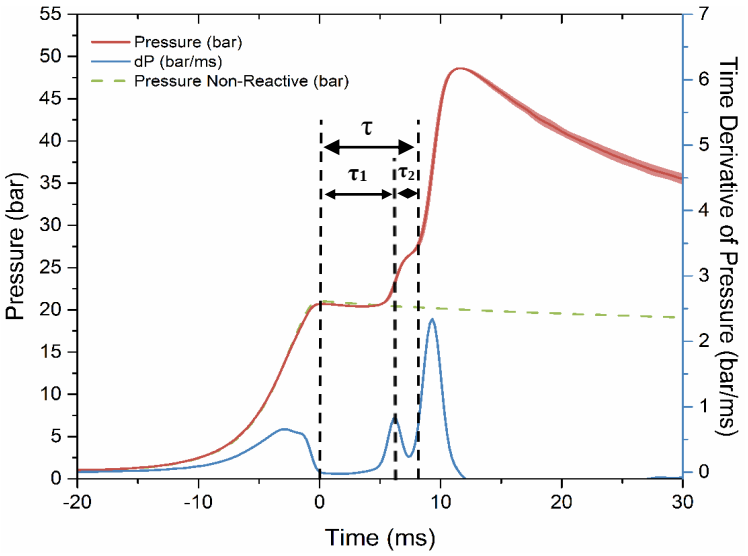

Figure 25: Pressure profile for autoignition of dimethyl ether mixtures using a bowl piston. Molar composition: $CH_3OCH_3/O_2/N_2$ = 1/4/40. Initial conditions are T_o = 300 K and P_o = 1.034 bar.

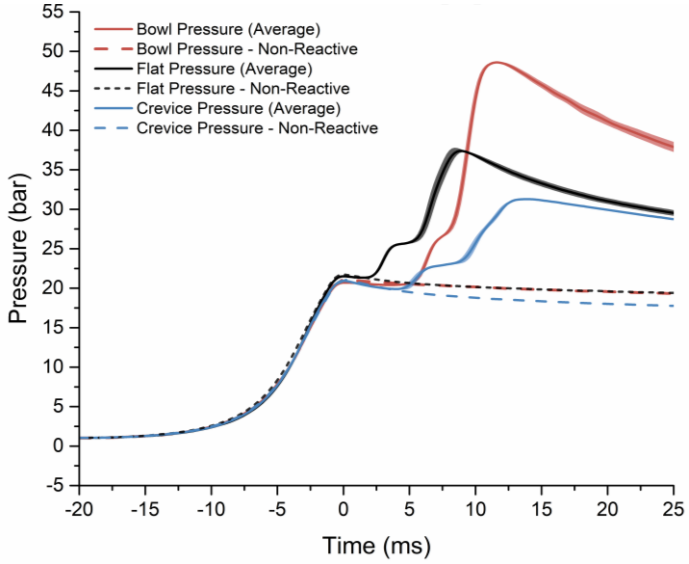

Figure 26: Pressure profiles for autoignition of dimethyl ether mixtures using a creviced piston, flat piston, and bowl piston. Molar composition: $CH_3OCH_3/O_2/N_2$ = 1/4/40. Initial conditions are T_o = 300 K and P_o = 1.034 bar.

Next, DME experiments were conducted with 50 moles of nitrogen to study the influence of increasing dilution. The three pistons exhibited longer ignition delays and slow rates of pressure rise depictive of weak ignition (Figure 27-Figure 30). Interestingly, the increase in dilution resulted in shorter LTHRs for the creviced and bowl pistons and extended ITHR for all three pistons.

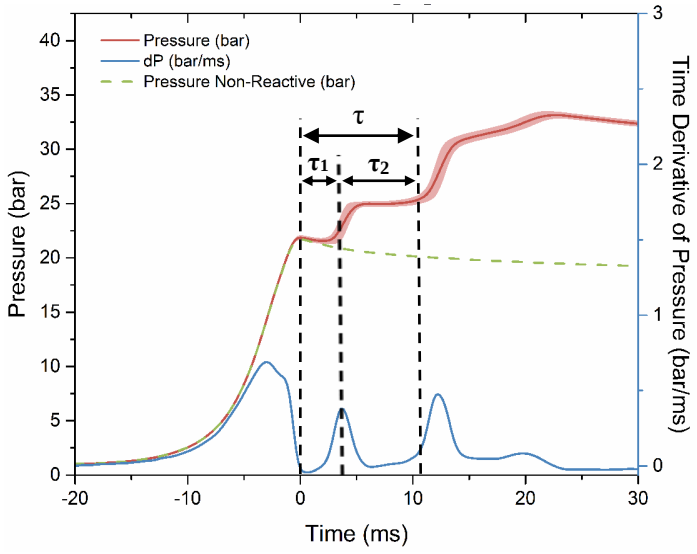

Figure 27: Pressure profile for autoignition of dimethyl ether mixtures using flat piston. Molar composition: $CH_3OCH_3/O_2/N_2$ = 1/4/50. Initial conditions are T_o = 300 K and P_o = 1.034 bar.

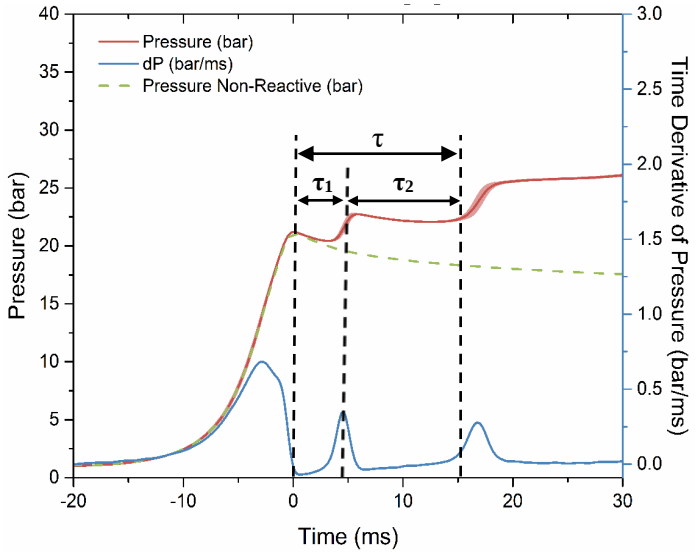

Figure 28: Pressure profile for autoignition of dimethyl ether mixtures using creviced piston. Molar composition: $CH_3OCH_3/O_2/N_2$ = 1/4/50. Initial conditions are T_o = 300 K and P_o = 1.034 bar.

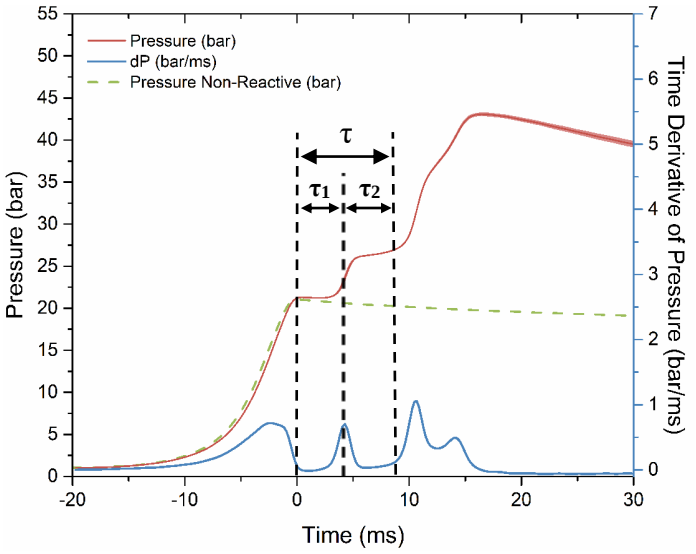

Figure 29: Pressure profile for autoignition of dimethyl ether mixtures using bowl piston. Molar composition: $CH_3OCH_3/O_2/N_2$ = 1/4/50. Initial conditions are T_o = 300 K and P_o = 1.034 bar

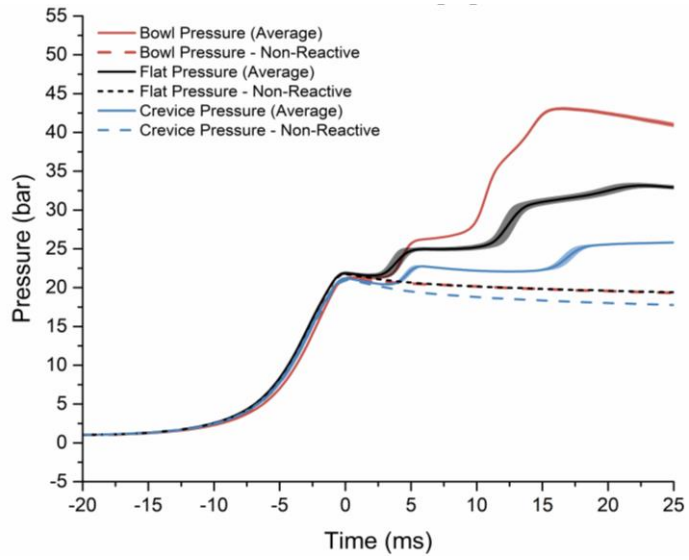

Figure 30: Pressure profiles for autoignition of dimethyl ether mixtures using a creviced piston, flat piston, and bowl piston. Molar composition: $CH_3OCH_3/O_2/N_2$ = 1/4/50. Initial conditions are T_o = 300 K and P_o = 1.034 bar.

5.2.2 n-Butane

A stoichiometric *n*-butane fuel mixture with no dilution was tested across the three different pistons at one condition. Unlike the highly dilute DME experiments, *n*-butane presented only one stage of ignition delay and rapid pressure rise during hot ignition (Figure 31-Figure 34). The flat piston had the shortest ignition delay of 26.8 ms, followed by the bowl and creviced pistons at 30.3 ms and 48.1 ms, respectively.

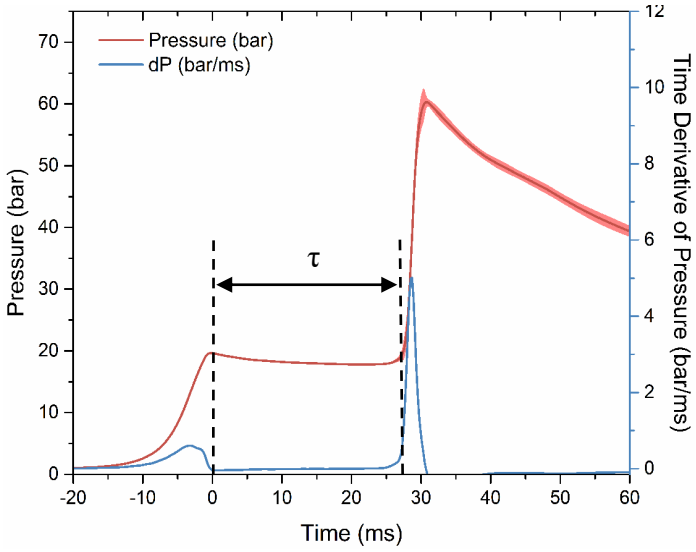

Figure 31: Pressure profile for autoignition of *n*-butane mixtures using flat piston. Molar composition: $C_4H_{10}/O_2/N_2$ = 1/6.5/24.44. Initial conditions are T_o = 300 K and P_o = 1.034 bar

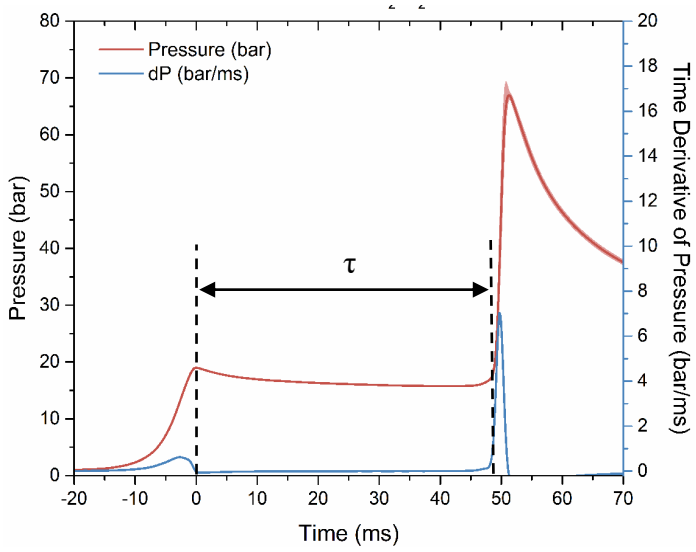

Figure 32: Pressure profile for autoignition of *n*-butane mixtures using creviced piston. Molar composition: $C_4H_{10}/O_2/N_2$ = 1/6.5/24.44. Initial conditions are T_o = 300 K and P_o = 1.034 bar

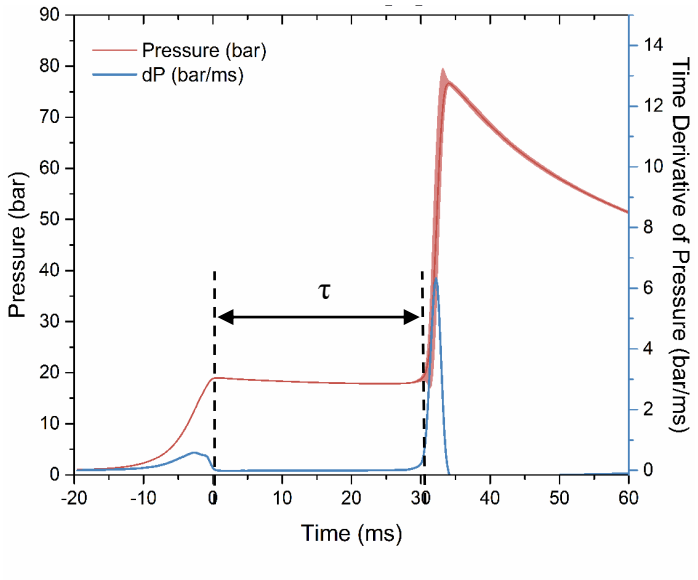

Figure 33: Pressure profile for autoignition of *n*-butane mixtures using bowl piston. Molar composition: $C_4H_{10}/O_2/N_2$ = 1/6.5/24.44. Initial conditions are T_o = 300 K and P_o = 1.034 bar

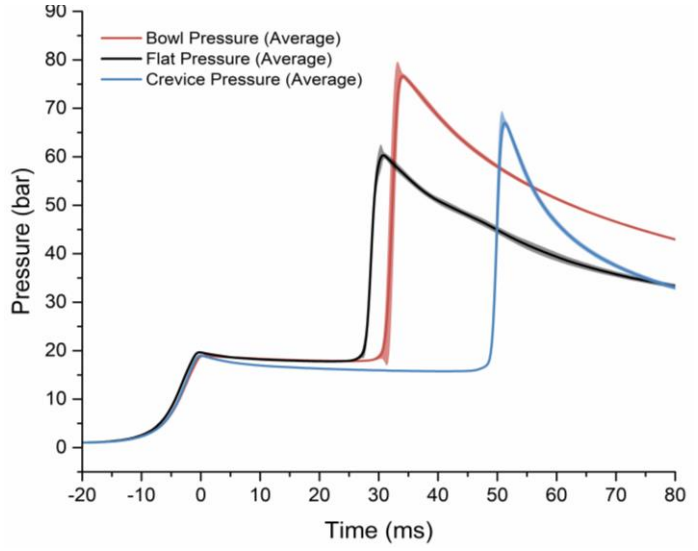

Figure 34: Pressure profile for autoignition of *n*-butane mixtures using flat, creviced, and bowl pistons. Molar composition: $C_4H_{10}/O_2/N_2$ = 1/6.5/24.44. Initial conditions are T_o = 300 K and P_o = 1.034 bar

5.2.3 Ethanol

In this study, ethanol was the primary fuel used to characterize combustion performance between the creviced and bowl piston. Ethanol was chosen because its combustion performance is well documented and does not typically exhibit NTC behavior. Since ethanol is a liquid at standard temperature and pressure (STP), precautionary steps were taken to ensure ethanol was in the gas phase during fuel preparation. An Engineering Equation Solver (EES) model was used to determine the amount of ethanol and corresponding temperatures needed to stay within the super-heated vapor region (Figure 35) when using the CT-RCEM fuel preparation system. Initial fuel mixture temperatures in the range of 353 K – 383 K were used in this study.

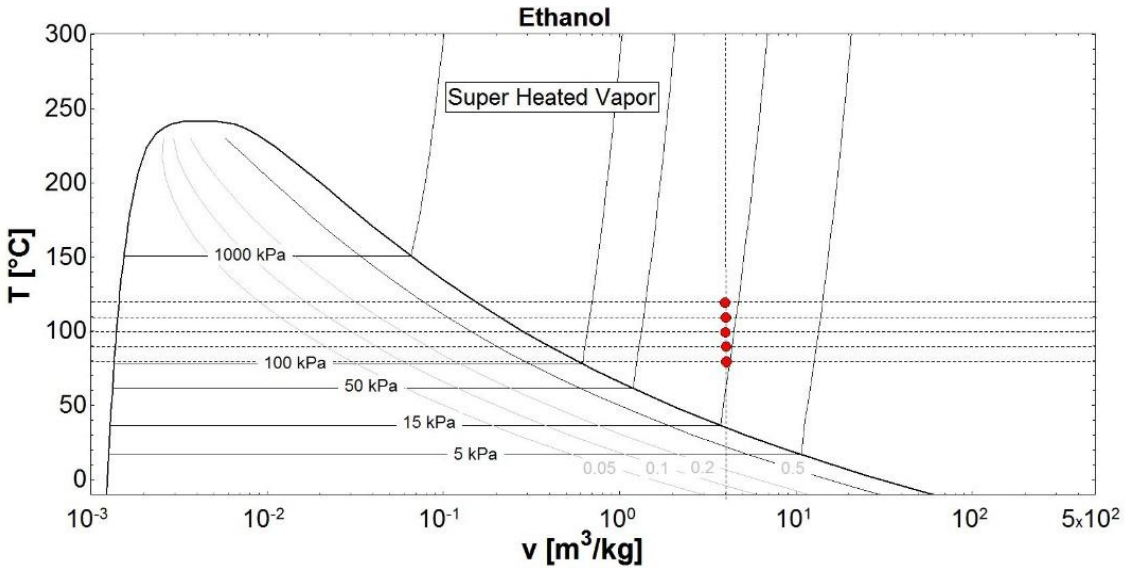

Figure 35: Temperature-specific volume diagram for ethanol in the super-heated vapor region

Experiments were conducted with a lean mixture ($\phi = 0.5$) at a compressed pressure of 25 bar to compare baseline creviced piston results with work done by Mittal et

al. [77]. It was important to match the oxidizer/dilution ratio while adjusting the argon/nitrogen ratio to attain the ideal γ for autoignition over the range of temperatures.

Figure 36 shows the pressure profiles obtained for the creviced piston at compressed temperatures in the range of 810-870 K at a compressed pressure of 2.5 MPa. The pressure decay after the piston has reached TDC is 21% over a 50 ms interval. This is largely due to the continued mass flow into the crevice after the piston has stopped at TDC. The lack of an enlarged crevice on the bowl piston's periphery significantly reduces the pressure decay to 8% over a 50 ms interval (Figure 37). It is noted that the rate of pressure drop does not increase with increasing temperatures since the surface area to volume ratio stays constant for all tests. This constant decay is not observed when clearance height is modified to achieve compressed temperatures [106]. It is also noted that the adiabatic core assumption is used to roughly estimate compressed temperatures for the bowl piston since turbulent mixing may reduce overall in-cylinder temperatures during compression.

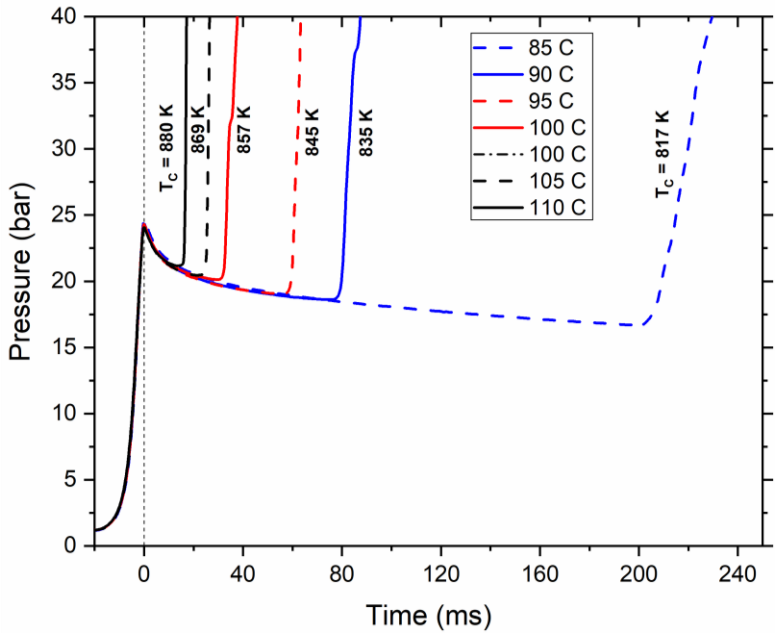

Figure 36: Pressure profiles for autoignition of ethanol mixture using creviced piston. Molar composition: CH_3CH_2OH /O_2/Ar/N_2 = 1.0/6.0/13.6/9.0.

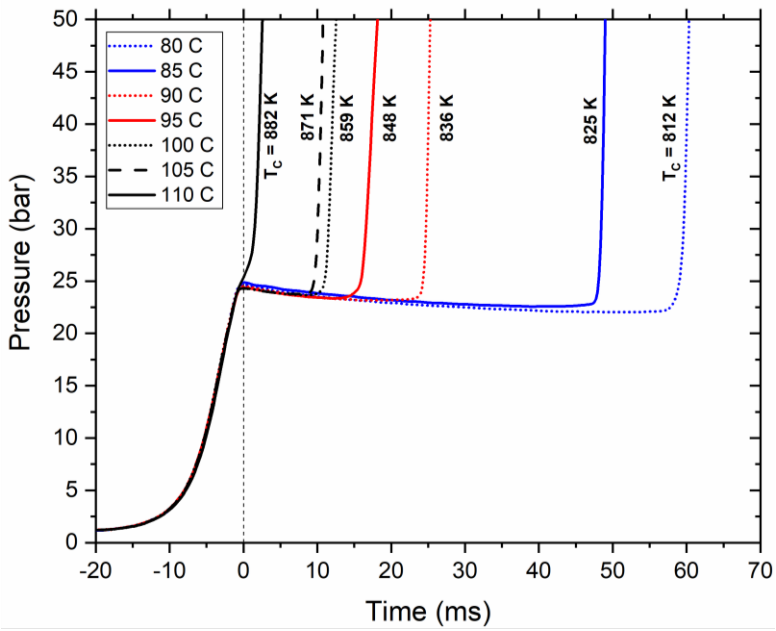

Figure 37: Pressure profiles for autoignition of ethanol mixture using bowl piston. Molar composition: CH_3CH_2OH /O_2/Ar/N_2 = 1.0/6.0/13.6/9.0.

A regression analysis of the ignition delay data for both creviced and bowl pistons yields the correlation,

$$\tau = A\, {P_C}^{a}\, \emptyset^{b}\ \exp(T_a/T_C)$$

$$\tau = 3.4 \times 10^{-10}\ {P_C}^{-1.6}\, \emptyset^{-0.75}\ \exp(25{,}739/T_C)$$

where activation temperature, $T_{a,}$ is 25,739 Kelvin [129], A is a constant, 'a' is the pressure exponent, 'b' is the equivalence ratio exponent and the regression correlation coefficient is $R^2 \geq 0.978$. The correlation and experimental data is plotted in Figure 38.

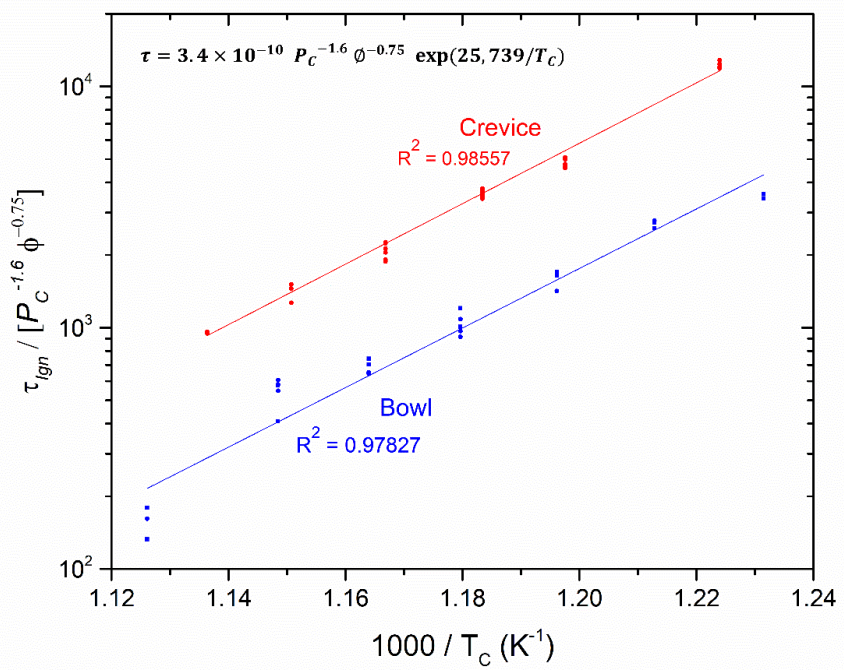

Figure 38: Experimental ignition delay correlations for creviced and bowl pistons

As a comparison, ignition delay is plotted against inverse compressed gas temperature and data from Mittal and co-workers (Figure 39) [77]. Excellent agreement with Mittal et al. is seen with the creviced piston throughout the tested temperature range. The bowl piston exhibited shortened ignition delays overall when compared to the creviced piston. Interestingly, the bowl piston achieved higher compressed temperatures than the creviced piston at the same initial temperatures (Table 6).

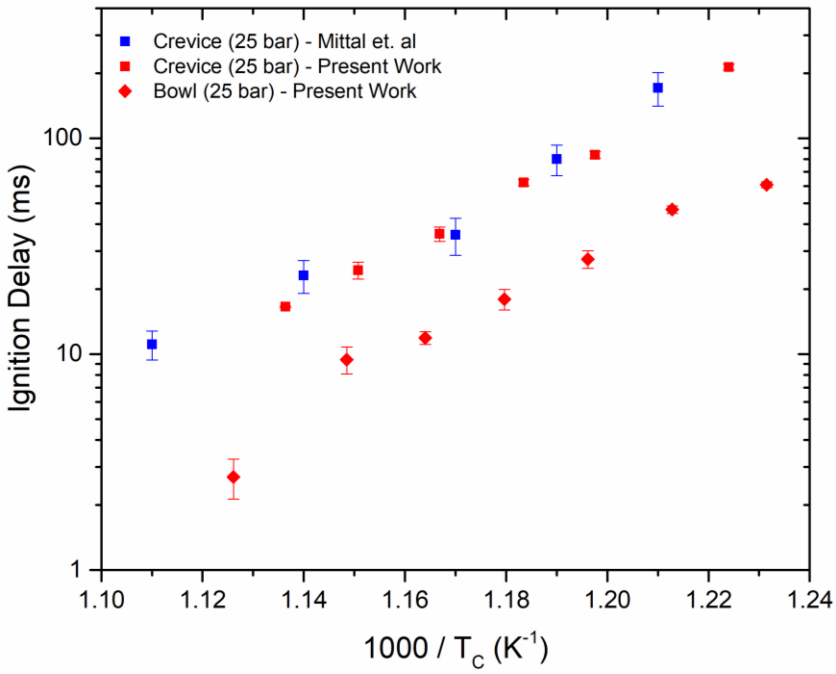

Figure 39: Ignition delay correlation with Mittal et al.

Table 6: Initial temperatures vs compressed temperatures

Initial Temperature (K)	Creviced Piston Compressed Temperature (K)	Bowl Piston Compressed Temperature (K)
353	No Ignition	812
358	817	825
363	835	836
368	845	848
373	857	859
378	869	871
383	880	882

5.3 Discussion

Data presented in Section 5.2 is analyzed and discussed in this section to explore the effects each piston design has on combustion. Examining data in terms of turbulent Damköhler number and turbulent Reynolds number characterizes the ignition event each piston achieves. Heat release analysis (HRA) is conducted to quantify combustion efficiency and supplement the ignition analysis to exemplify piston performance for the

fidelity of dump sampling and RCEM use. HRA also provides insight into phenomena not yet documented in RCM literature.

5.3.1 Ignition Analysis

Ignition analysis has long been performed to understand how turbulence, thermal and mixture stratification, and other phenomena can influence a fuel mixture's exothermicity. Characteristic time scales like compression, diffusion, heat release, and shockwave/flame propagation help differentiate the autoignition regimes: strong, mild, and mixed [43].

Strong ignition behavior is most correlated with the homogenous ignition of an unburned gas volume and depicted by steep pressure rises. In contrast, mild ignition or also referred to as "deflagration ignition" occurs when flames develop in the reaction chamber triggered by the formation of localized ignition kernels or hot spots on the walls of the chamber. To better understand mild ignition, Schlieren techniques have been used by many groups to identify regions of thermal and reactivity gradients in shock tubes [130]–[134] and RCMs [135]–[138]. The combination of strong and mild ignition behavior is the transition from a deflagration flame kernel to an explosion first termed by Urtiew and Oppenheim [139] as "explosion in explosion". Following work performed by Pfahl et al. [36] and Fieweger et al. [133] termed it "deflagration to detonation (DDT)". In this work, DDT will be referred to as "mixed ignition".

Grogan et al. created an ignition regime diagram in terms of non-dimensional turbulent Reynolds (Re_t) and turbulent Damköhler (Da) numbers to parameterize ignition behavior for RCM/RCEMs tests [86]. Damköhler number is used to relate the characteristic diffusion time to the characteristic reaction time in the system:

$$Da_t = \frac{\tau_t}{\tau_{ign}} \quad \text{(Eq. 3)}$$

where τ_t is the ratio of integral length scale l to the turbulent velocity fluctuation u'. Ignition delay τ_{ign} is used as the characteristic reaction time. Since turbulence is a difficult parameter to measure in RCM/RCEMs, it is estimated using the following:

$$\tau_t = \frac{C_l}{\tau_u} * \frac{d}{U_{piston}} \quad \text{(Eq. 4)}$$

where C_l is a proportionality constant dependent on machine design, $\tau_u$is turbulent intensity, d is bore diameter of the reaction chamber, and U_{piston} is characteristic velocity of the piston. The turbulent Reynolds number is the ratio of inertial forces to the viscous forces:

$$Re_t = \frac{u\prime l}{\nu} \quad \text{(Eq. 5)}$$

where ν is the kinematic viscosity of the fuel mixture. The derivations for demarcations that characterize the ignition regimes in RCM/RCEMs is laid out by Grogan and co-workers [86].

Ignition type was determined for the combustion events in Section 5.2 by calculating the turbulent Reynolds and turbulent Damköhler numbers. For the creviced piston, the parameters τ_u and C_l were taken to be 2% and 10%, respectively [86]. As for the flat and bowl pistons, the parameters τ_u and C_l were taken to be 6% and 18%, respectively [117], [119], [140].

Delineations that separate strong, mixed, and mild regimes are derived from the Shock Wave Amplification by Coherent Energy Release (SWACER) and Sankaran criteria. The SWACER mechanism proposed by Lee et al. explains the transition from a shock wave created by a hot spot or flame kernel to an overdriven detonation. SWACER

theory is strongly based on the synchronization of gas dynamic perturbations with the energy release from a chemical reaction which is essentially Rayleigh's stability criterion applied to a traveling compression pulse [141]. The SWACER criterion can be expressed as:

$$Da_t = \left(\frac{T_T}{T_u}\right) \frac{A}{\mathrm{M}\sqrt{10}} Re_t^{1/2} \quad \text{(Eq. 6)}$$

where T_T is temperature fluctuation level, A is the Arrhenius factor, and M is the relevant Mach number. By taking into account chemistry and compressibility, the SWACER criterion determines the susceptibility of a mixture to either ignite as a detonation or a volumetric ignition event (strong ignition).

The Sankaran criterion was postulated to identify the likelihood of mild ignition by comparing laminar flame speed to the velocity front of an ignition kernel [142]. It is expressed as:

$$Da_t = \frac{T_T^2 A}{5Pr\gamma\beta Y_F} e^{A\frac{\beta}{\beta+1}} \quad \text{(Eq. 7)}$$

where γ is the heat capacity ratio, Pr is the Prandtl number, β is the heat release parameter, and Y_F is the mass fraction of fuel. Unlike the SWACER criterion, the Sankaran criterion is independent of the turbulent Reynolds number. The region bound between the SWACER and Sankaran criteria is where flame kernels have the propensity to transition into a detonation (mixed ignition).

Table 7 specifies the ignition type for the experiments performed in Section 5.2. It is perceived for both DME mixtures that mixed ignition is predominately realized excluding the highly dilute creviced piston case. In that case, the creviced piston achieved a lengthened ignition delay that caused it to be less than the Sankaran criterion resulting in mild ignition. Interestingly, extremely slow rates of pressure rise during hot ignition were

observed for the highly dilute DME mixture indicative of mixed ignition. *n*-butane observed ignition bordering the strong ignition limit. The lengthened ignition delay produced by the creviced piston placed the turbulent Damköhler number in the mixed ignition region. Since ethanol tests were swept over a large temperature range, multiple ignition types were observed. As ignition delay increased with lowered compression temperatures for ethanol, Damköhler number decreased placing a number of creviced piston tests in the mixed ignition regime.

Ignition regime results indicate stronger, more adiabatic ignition when using the bowl-style piston compared to flat and creviced pistons across four fuel mixtures (Figure 40). Increased uniform burning due to stronger ignition increases the amount of fuel converted to products of combustion. Combustion efficiency analysis in Section 5.3.2 will supplement ignition findings described in this section. Although ignition classification calculations favor bowl piston performance, results are not confirmed without experimental verification using LIF, PLIF, Schlieren, or chemiluminescence imaging techniques. Future work recommendations to study ignition behavior are found in Chapter 6.

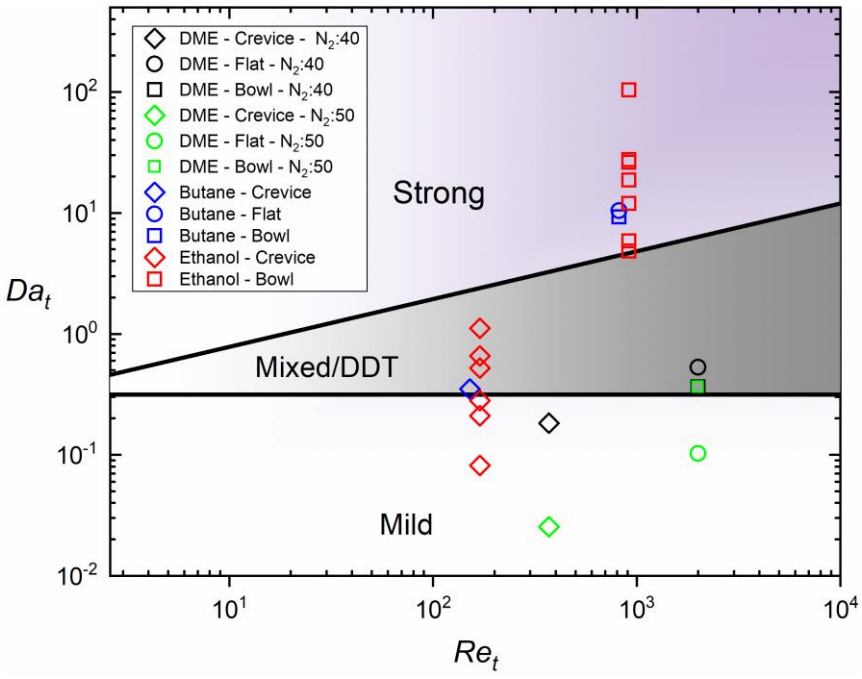

Figure 40: Ignition regime classification for dimethyl ether, *n*-butane, and ethanol experiments

Table 7: Classification of ignition behavior

Fuel Mixture	Piston Type	Ignition Classification
Dimethyl ether/O_2/N_2 N_2 = 40 moles	Creviced	Mild Ignition
	Flat	Mixed Ignition
	Bowl	Mixed Ignition
Dimethyl ether/O_2/N_2 N_2 = 50 moles	Creviced	Mild Ignition
	Flat	Mild Ignition
	Bowl	Mixed Ignition
n-butane/O_2/N_2	Creviced	Mixed Ignition
	Flat	Strong Ignition
	Bowl	Strong Ignition
Ethanol/O_2/Ar/N_2	Creviced	Mild/Mixed Ignition
	Bowl	Strong Ignition

5.3.2 Heat Release Analysis

Heat release analysis (HRA) is applied largely to internal combustion engine research [143]–[148] and fundamental combustion instruments [149]–[151] to better understand chemical and physical processes which are difficult or otherwise impossible to measure directly. In IC engines, the amount of heat released during a combustion cycle is deduced based on crank-angle resolved pressure diagnostics and energy conservation principles. This deduction is key when quantifying exothermicity, evaluating chemical kinetic models, and detecting non-uniform ignition phenomena. Although extensive HRA has been conducted on internal combustion engines, this analysis technique has not been immensely applied to RCM/RCEM studies. Previous work has mentioned the difficulties with applying HRA to RCM/RCEMs, i.e. appropriately accounting for physical phenomena like heat loss to the walls of the combustion chamber, thermal boundary layer growth, condensation of fuel mixtures due to wall temperature gradients, and perturbations in sensor signal and data acquisition system [152].

Numerous groups have mentioned the challenges with applying the conservation equation to RCM/RCEMs and internal combustion engines [148], [152]. Physical processes such as quantifying the volume of the chamber during compression in RCMs/RCEMs is, for the most part, extrapolated from models and pressure data due to the lack of in-situ measurement of piston position. The CT-RCEM allows for a direct measurement of piston position via an LVDT which greatly reduces the uncertainty associated with volume calculations.

The first step of HRA is to apply the first law of thermodynamics to the gas in the reaction chamber. It is expressed as:

$$\frac{dU}{dt} = \dot{Q}_{comb} - \dot{Q}_{loss} - \dot{W}_{piston} + \dot{H}_{in} - \dot{H}_{ex} \quad \text{(Eq. 8)}$$

where U is internal energy, $\dot{Q}_{comb}$ is the rate of heat released from combustion, $\dot{Q}_{loss}$ is the rate of heat lost to the surrounding walls of the reaction chamber, $\dot{W}_{piston}$ is the work done by the piston, and $\dot{H}_{in}$, $\dot{H}_{ex}$ are the rates of enthalpy flow in and out of the reaction chamber, respectively.

For this analysis, enthalpy flows are ignored and it is assumed that the fuel mixture is homogeneous and does not change composition during the filling process. Using this approach is acceptable to differentiate key features like the rate of heat release (ROHR) and combustion efficiency between pistons.

To simplify, Equation 8 can be written as:

$$mC_v \frac{dT}{dt} = \dot{Q} - p\frac{dV}{dt} \quad \text{(Eq. 9)}$$

where $\dot{Q}$ is the combination of the heat transfer across the cylinder walls and the heat release rate from combustion. Assuming ideal gas behavior, Equation 10 can be applied:

$$PV = mRT \quad \text{(Eq. 10)}$$

Assuming constant mass in the reaction chamber, Equation 10 can be differentiated as:

$$\frac{dT}{dt} = \left(p\frac{dV}{dt} + V\frac{dp}{dt}\right)\frac{1}{mR} \quad \text{(Eq. 11)}$$

Combining Equation 9 and Equation 11, the heat release equation becomes:

$$ROHR = \frac{\gamma}{\gamma-1} P \frac{dV}{dt} + \frac{1}{\gamma-1} V \frac{dP}{dt} \quad \text{(Eq. 12)}$$

where γ is the ratio of specific heats, *V* is the cylinder volume, and *P* is the cylinder gas pressure, and $\dot{Q}$ is replaced with ROHR.

Rate of heat release rates are plotted against pressure traces in Figure 41 for the highly dilute DME case presented in Section 5.2.1. Correlation between the start of the first

and second stages of ignition delay and ROHR are apparent. This preliminary exothermicity, LTHR and/or ITHR, happens prior to the autoignition point and is common in degeneratly branched systems [152], [153]. It is observed that the bowl piston has the largest ROHR followed by the flat and then the creviced pistons. The link between ROHR, net heat release, and combustion efficiency will be discussed in the following sub-section.

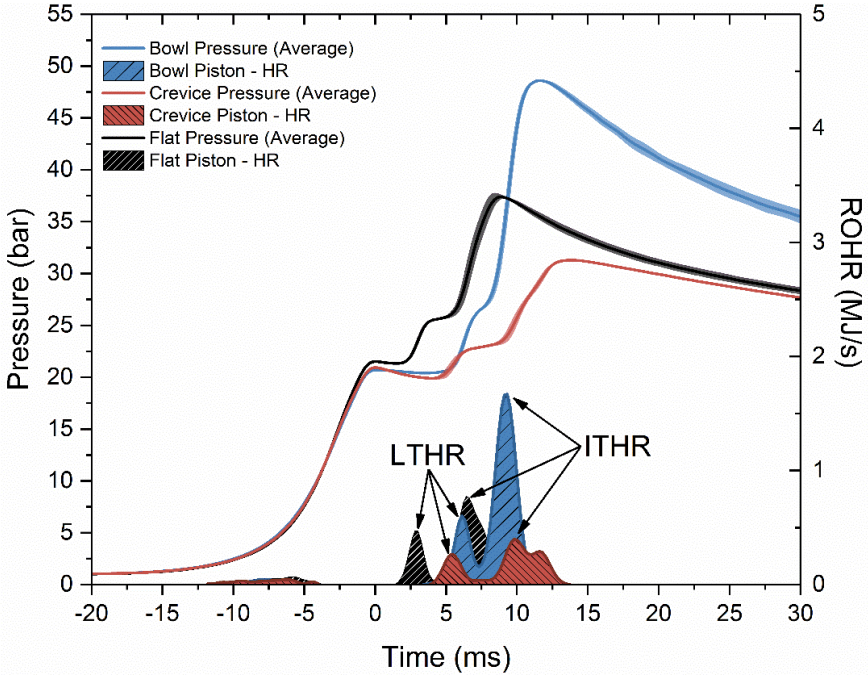

Figure 41: DME/O_2/N_2 = 1/4/40 ROHR and averaged pressure trace for creviced, flat, and bowl pistons

5.3.2.1 Combustion Efficiency

Combustion efficiency, η_c, defines how well fuel is being converted to products of combustion and is commonly used as a parameter to benchmark combustion systems. It is the ratio between the amount of energy released during the combustion process and the actual energy content of the fuel. In this work, combustion efficiency is used to show which piston is effectively converting the most fuel to products of combustion. In equation form:

$$\eta_c = \frac{Q_{heat}}{m_{fuel^*}\, q_{LHV}} \quad \text{(Eq. 13)}$$

where Q_{heat} is the net heat released, m_{fuel} is the mass of fuel in the reaction chamber, and q_{LHV} is the lower heating value (LHV) of the fuel.

Figure 42 shows ROHR against combustion efficiency for lean, highly dilute DME fuel mixtures. First, the less dilute mixture was shown to achieve a 71% combustion efficiency for the bowl piston and only 40% and 29% for the flat and creviced piston, respectively. The more dilute DME mixture achieved significantly lower combustion efficiencies for the three pistons. Increased dilution has long been associated with lower combustion efficiency because the premixed flame propagation is slowed by the reduced reactivity that consequently lowers the ROHR [23], [154]–[157].

Interestingly, Figure 42B clearly identifies two expected stages of ignition delay prior to hot ignition and instances where ROHR starts to decrease then subsequently recovers during the main stage of combustion. This extra stage of heat release is not commonly seen with DME fuel mixtures or in RCMs but can be associated with highly dilute fuel blends. Shao et al. [158] performed shock tube experiments using a near stoichiometric methane mixture which was highly diluted with carbon dioxide. They observed a similar occurrence in pressure and OH* emission near 306 nm where an additional mode of heat release occurred during the main stage of ignition, however, it was not discussed in the work. For this instance, shock bifurcation is a possible explanation since it is a known mechanism for non-ideal ignition behavior in shock tubes. Shock bifurcation is a condition where the reflected shock interacts with the boundary layer and bifurcates causing velocity fluctuations and non-uniformities in the mixture composition. Ihme et al. and group [159] have done significant work numerically modeling shock

bifurcation to understand its formation and progression. To correlate mild/mixed ignition to bifurcation, it is realistic to assume that mild ignition will not occur if the ignition delay of the fuel mixture is much less than the characteristic time scale for the bifurcation [160]. This is reasonable to assume since the kinetics of the mixture will not be affected by the physical processes of the bifurcation. To determine the bifurcation timescale in the CT-RCEM, Equation 14 is used to estimate τ_{BIF}:

$$\tau_{BIF} = \frac{D}{4Uh'} \qquad \text{(Eq. 14)}$$

where D is the diameter of the combustion chamber, h equals half the radius of the combustion chamber, and U is the speed of the wave front which can be approximated by the piston velocity. Results indicate that $\frac{\tau_{BIF}}{\tau_{ign}} = 5.3$ suggesting that bifurcation is not likely the cause of the mild/mixed ignition and cool flame behavior during the main stage of heat release.

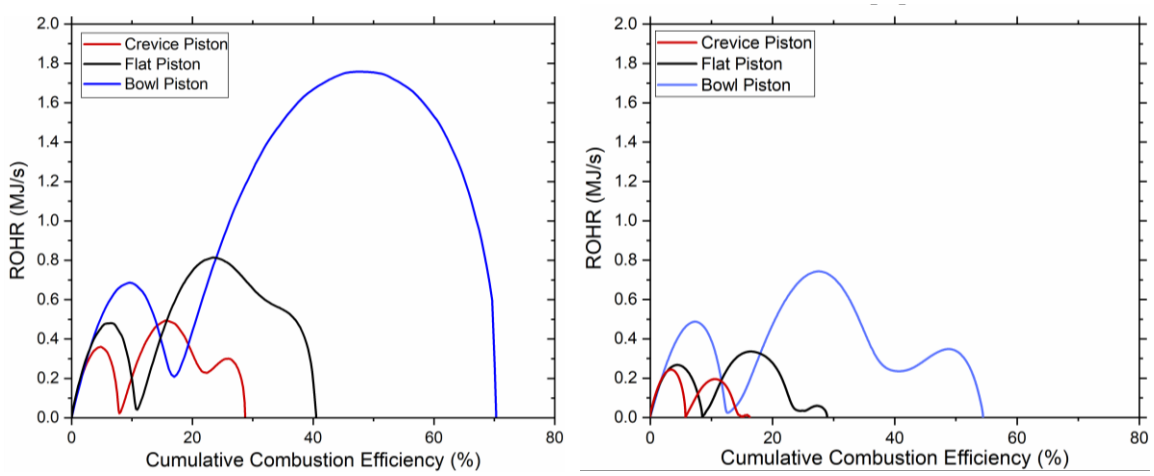

A B

Figure 42: A) DME/O_2/N_2 = 1/4/40 ROHR vs cumulative combustion efficiency for creviced, flat, and bowl pistons B) DME/O_2/N_2 = 1/4/50 ROHR vs cumulative combustion efficiency for creviced, flat, and bowl pistons

To further investigate potential explanations why there is a secondary heat release during the main stage of ignition, a distribution of cumulative combustion efficiency was derived for both DME mixtures using the bowl piston (Figure 43). The normal distributions clearly outline two and three modes of heat release for the 40 and 50 moles of nitrogen dilution mixtures, respectively. There is a high probability that the third stage of ignition is likely a secondary cool flame event due to a large amount of fuel left in the chamber at the end of main ignition. Multiple groups have both numerically and experimentally confirmed the extinction and reignition of premixed and non-premixed flames [161], [162]. The mild and mixed ignition characteristics identified for the DME fuel mixtures in Section 5.3.1 suggest that thermal inhomogeneities in the reaction chamber can act as localized ignition kernels that eventually transition to a detonation wave promoting the secondary cool flame event. It is inferable from Figure 43 that the third mode is not achieved if ROHR during the main stage of the ignition is great enough to overcome these homogeneities and decelerating chemical kinetics caused by the large heat capacity of the highly dilute mixtures. It is recommended that future work be conducted to confirm and further investigate this secondary cool flame behavior using optical methods.

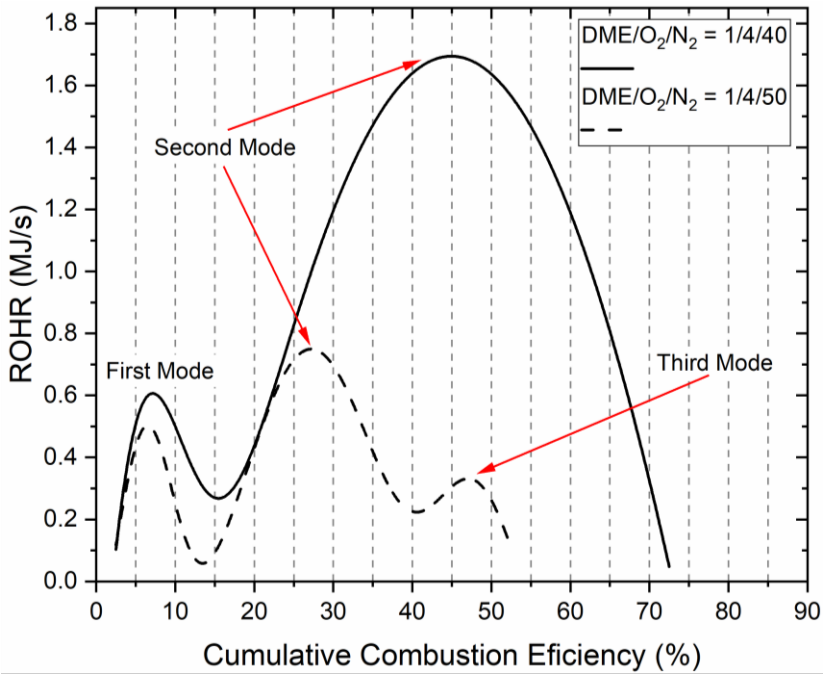

Figure 43: Distributions for DME/O_2/N_2 = 1/4/40 and DME/O_2/N_2 = 1/4/50 using bowl piston

Table 8 shows the distributions for each mode of heat release during DME combustion using a Gaussian fitting routine and a Levenverg Marquardt iteration algorithm. R-Square for both curves were > 0.97 after 200 iterations. Comparing first mode heat release between the two mixtures, there is approximately a 10% and 3% difference when using the creviced and flat pistons, respectively, but only a 1% difference when using the bowl piston. It can be inferred that the bowl piston produces more repeatable results across dilution ratios.

Table 8: DME/O_2/N_2 = 1/4/40 and DME/O_2/N_2 = 1/4/50 distributions

DME/O_2/N_2 = 1/4/40			
	First Mode	Second Mode	Third Mode
Crevice	25.8%	49.1%	25.1%
Bowl	22.3%	77.7%	0%
Flat	26.8%	73.2%	0%

DME/O_2/N_2 = 1/4/50			
	First Mode	Second Mode	Third Mode
Crevice	35.5%	57.3%	7.2%
Bowl	23.3%	51.1%	25.6%
Flat	29.4%	55.2%	15.4%

Similar trends were observed with the stoichiometric *n*-butane fuel mixture when compared to DME. In this case, the bowl piston also exhibits a higher peak ROHR followed by the creviced and flat pistons (Figure 44). The bowl piston achieves a 98% combustion efficiency which is significantly greater than the creviced and flat piston designs. The high combustion efficiency displayed by the bowl piston would provide ideal dump sampling conditions to accurately analyze combustion products with minimal unburnt fuel that would skew speciation results.

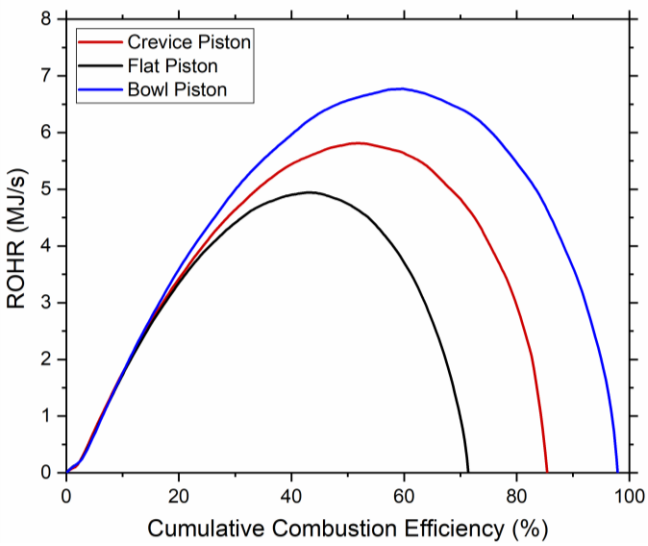

Figure 44: *n*-butane/O_2/N_2 = 1/6.5/24.44 ROHR vs Cumulative combustion efficiency for creviced, flat, and bowl pistons

HRA for ethanol is shown in Figure 45 and Figure 46 and maintains confidence that the bowl piston provides an environment for a greater fraction of fuel to be burnt during combustion when compared to the creviced piston. It is observed that the creviced piston consistently achieves a combustion efficiency in the range of 74% and 81%, with the exception of the lowest compressed temperature fuel mixture that bordered the autoignition temperature. The bowl piston produced far greater efficiencies that were greater than 98% across the tested temperature range.

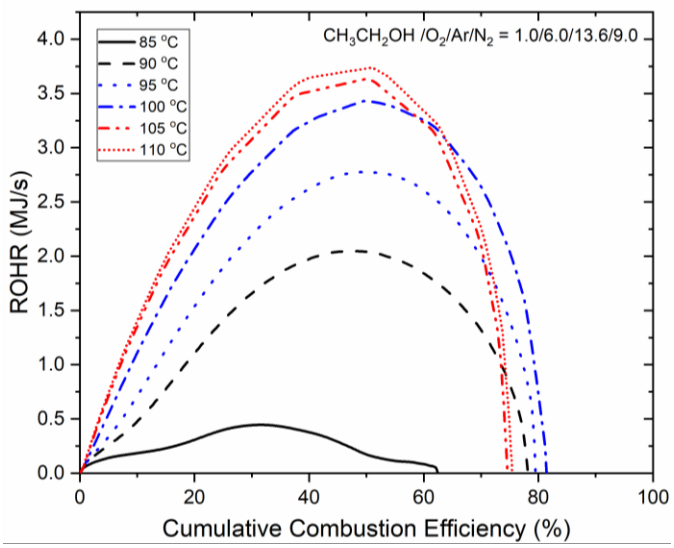

Figure 45: CH_3CH_2OH /O_2/Ar/N_2 = 1.0/6.0/13.6/9.0 ROHR vs Combustion efficiency for creviced piston

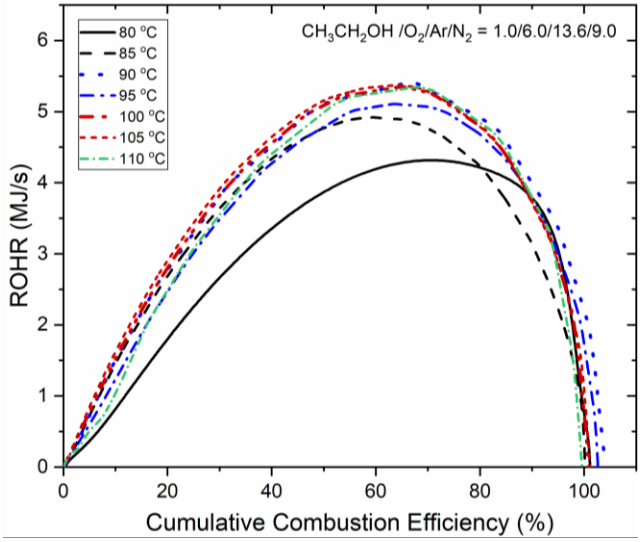

Figure 46: $CH_3CH_2OH/O_2/Ar/N_2$ = 1.0/6.0/13.6/9.0 ROHR vs Combustion efficiency for bowl piston

It is intuitive that the creviced piston will have a lower combustion efficiency due to the amount of fuel in the enlarged crevice not able to react. This is largely due to the amount of heat transfer to the walls of the piston and reaction chamber. The creviced piston is not designed to maximize the amount of fuel burnt but produce an environment suitable

for ignition delay studies as outlined in Section 2.2.4. Hence, the creviced piston is not appropriate when the objective is to evacuate the contents of an entire cylinder for speciation studies. The data presented clearly demonstrates improved ignition modes and combustion efficiencies when using the bowl piston over conventional flat and creviced pistons. With nearly all fuel being converted to products of combustion for certain fuel mixtures and environmental conditions, speciation via dump sampling using the bowl piston, in theory, will improve the detection and mass measurement of combustion products. In this research, HRA has proven to be an essential application in understanding important phenomena like unconventional ignition modes, combustion efficiency, and fuel exothermicity.

5.3.3 CFD Verification

CFD simulations were conducted in collaboration with Carnegie Mellon University (CMU) in an effort to qualitatively corroborate experimental results. Non-reactive simulations of the bowl piston were performed with initial and boundary conditions found in Table 9 and Table 10, respectively.

Table 9: Initial conditions for bowl simulations

Parameter	Value
Temperature	300 K
Pressure	1.034 bar
Compression Ratio	10.15
Mixture Composition (by mass)	DME: 3.55%, O_2: 9.9%, N_2: 86.55%

Table 10: Boundary conditions for bowl piston simulations

Boundary No.	Boundary Name	Boundary Type	Temperature B.C.	Pressure B.C.	Velocity B.C.
1	Piston	Moving	Dirichlet: 503 K	Neumann	No Slip
2	Periodic Face 1	Stationary	Periodic	Periodic	Periodic
3	Periodic Face 2	Stationary	Periodic	Periodic	Periodic
4	Liner	Stationary	Dirichlet: 503 K	Neumann	No Slip
5	Head	Stationary	Dirichlet: 503 K	Neumann	No Slip

Figure 47 compares modeled and experimental pressure traces for a compress and dwell trajectory using the bowl piston. The modeled trajectory was determined by the experimental trajectory realized by the LVDT on the CT-RCEM. Both pressure traces match well with each other, although the CFD simulation predicts a slightly higher pressure at TDC and a slightly faster rate of pressure reduction during the dwell phase.

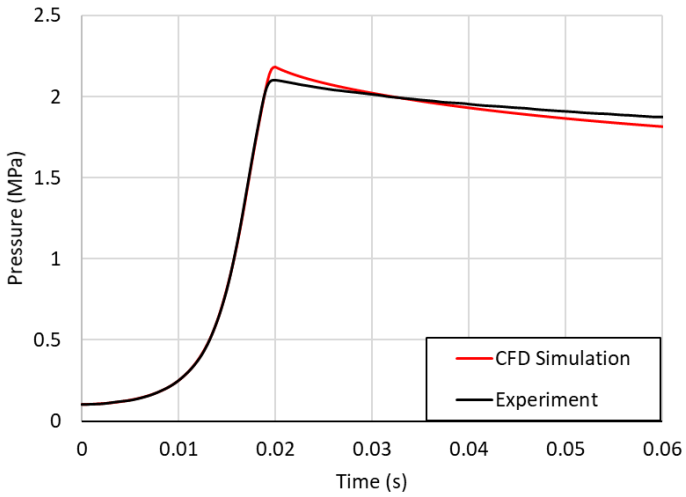

Figure 47: Comparison of non-reactive experimental and CFD simulation pressure traces for bowl piston

Figure 48 shows the velocity vectors for the bowl piston at TDC; the roll-up vortex moves to the base of the bowl, and the bowl profile enhances overall mixing using the high-velocity gases evacuating the squish region. The temperature contour in Figure 49 indicates

a uniform temperature core at TDC. Though the bowl piston does not completely suppress the roll-up vortex, the impact to core temperature homogeneity is significantly less when compared to the flat piston. When comparing the bowl and creviced piston, the absence of the enlarged crevice on the piston periphery allows for nearly all of the fuel mixture to be in the bowl at the end of compression. By lessening the amount of unburnt fuel mixture at the end of combustion by removing the enlarged crevice, combustion efficiency is improved. Results are further discussed in Dasrath et al. [122].

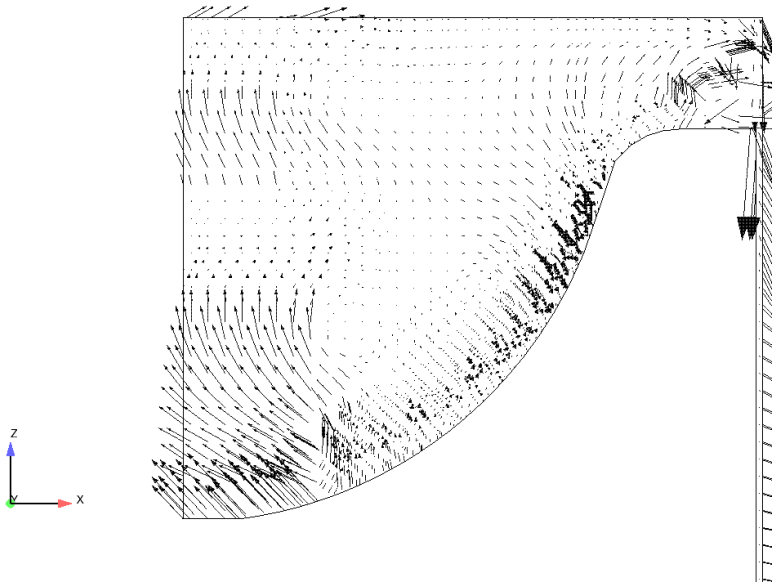

Figure 48: Velocity vectors at TDC for bowl piston using CT-RCEM combustion chamber geometry

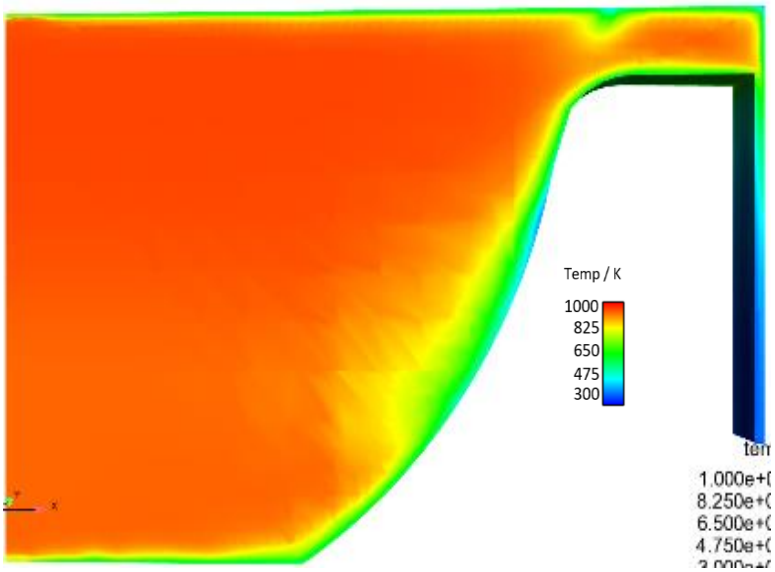

Figure 49: Temperature contour for bowl piston at TDC using CT-RCEM combustion chamber geometry

CHAPTER 6 Conclusions & Suggested Future Work

Growing concerns about IC engine emissions and associated health risks have driven fundamental combustion research to explore novel engine designs and utilization of renewable fuels. Speciation of intermediates and products of combustion is necessary for the verification and validation of detailed chemical kinetic mechanisms. Development of accurate chemical kinetic models is necessary to predict the operation of novel IC engine designs and combustion of unconventional fuels under conditions that are difficult and expensive to study with real combustors. This body of work demonstrated improved speciation methods for IC engines, RCMs and RCEMs. Based on the findings of this study, the following conclusions and recommendations for future work are made.

6.1 Comparison and Optimization of FT-IR and GC-MS for Speciating Unburned Hydrocarbons from Diesel Low-Temperature Combustion

LHCs sampled from engine exhaust post-turbo were speciated using an AVL SESAM i60 FT AVL bench equipped with an FID and an Agilent 7890B coupled to an Agilent 5977A Mass Spectrometry Detector (MSD). A heated fixed-volume gas sampling system was developed for extracting exhaust and injecting it into a GC that showed to minimize unknown dilution and light unburned hydrocarbons (LHC) losses. Comparison of GC-MS and FT-IR concentrations indicated that measurements were within 10 % of each other for C_2H_2, C_2H_4, C_2H_6, and C_2H_4O species. Along with the wide range of LHCs quantified in this study, focus was directed towards the misidentification of propane by the FT-IR during LTC modes. In the region where propane is absorbed (2700 and 3100 cm^{-1}), analysis of the FT-IR spectra indicated absorption band interference in the wavelength range where saturated hydrocarbons are measured. One of the primary findings of this work

demonstrates how speciation using GC-MS can aid in the identification of falsely identified compounds in FT-IR spectra and elucidate the breakdown of this technique during unconventional engine operation.

The results of this study suggest that not only can FT-IR and GC-MS be used in tandem to measure a variety of compounds from unconventional combustion modes, alternative fuels, or new catalyst materials, but they can also be used together as investigative tools in the discovery of unsuspected or new intermediates arising from future combustion strategies or catalyst materials.

The work in Chapter 4 presented speciation results for LHCs using FT-IR and GC-MS. A series of impingers were connected to the inlet of the gas sampling system which collected semi-volatile organic compounds (SVOCs) from the engine exhaust. It is proposed to use a Restek Rxi-624-MS column to speciate the collected condensate to widen the range of hydrocarbons speciated from engine exhaust.

6.2 Investigation of Piston Geometry in Rapid Compression Machines

A controlled trajectory RCEM was developed at the University of Minnesota – Twin Cities to investigate combustion properties of fuel mixtures and produce data to aid the development of chemical kinetic mechanisms. These machines work well for measuring a fuel mixtures ignition delay but are currently restricted for use in dump sampling speciation studies. This is mostly due to incomplete combustion from unburnt fuel mixture left in the piston crevice that causes difficult differentiation and quantification amongst products and intermediates of combustion.

Research groups have shown the drawbacks of using flat and enlarged piston crevice designs for sampling reaction chamber gases during and after combustion.

Complex and expensive fast-sampling systems have been implemented by a few research groups to extract small quantities of gas from the center of the chamber before mixing of chamber and crevice gases occur. The drawbacks with this approach include small sample volumes, local composition non-uniformities, and non-uniform progression of chemical kinetics during sampling.

A bowl piston was designed to overcome the issues that stymie dump sampling in RCMs/RCEMs. Experiments to characterize piston performance included four fuel mixtures with flat, enlarged crevice, and bowl piston profiles. Heat release analysis indicates greater combustion efficiencies when using the bowl piston as opposed to the standard flat and enlarged creviced pistons. This is indicative of smaller fractions of unburnt fuel left in the combustion chamber after combustion, ideal for dump sampling and the differentiation of unburnt fuel from combustion products. Also, compared to the creviced piston, results point toward greater fuel conversion due in part to stronger ignition characteristics. The environmental conditions created by the implementation of the bowl piston provided better performance over the flat and creviced pistons for dump sampling speciation methods in RCMs and RCEMs.

To support findings of this research, one of the portions of future work would be to confirm ignition results and multi-cycle burning modes using PLIF and/or chemiluminescence. As a preliminary stage of research to check optical capabilities, an image (Figure 50) using natural chemiluminescence of the OH* radical was captured after the EOC using the creviced piston and a highly dilute DME fuel mixture. Multiple ignition kernels are observed that help support findings of the mild and mixed ignition modes of highly dilute DME combustion.

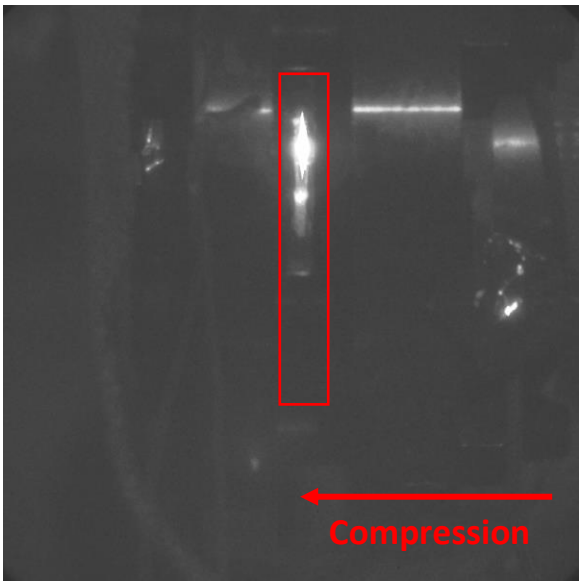

Figure 50: OH* measurement at EOC using a DME fuel mixture

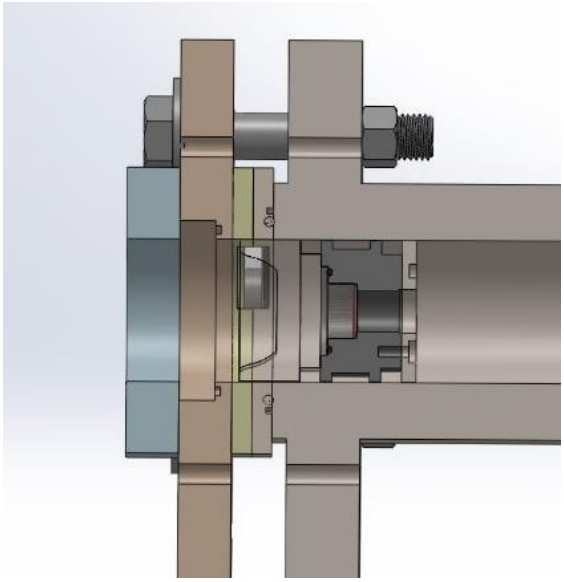

Figure 51: Implementation of an optical bowl piston for use with CT-RCEM optical head

Finally, to confirm ignition results using the bowl piston design, it is suggested that an optical bowl piston be manufactured for use with PLIF and chemiluminescence studies (Figure 51). An optical piston will allow for spatial measurement of combustion occurring in the bowl of the piston as well the squish region. Lastly, it is suggested to perform

speciation using dump sampling to confirm the bowl piston does improve the detection and mass measurement of combustion products.

Bibliography

[1] "Optima: Co-optimization of fuels and engines, accelerating the path to economic and sustainable fuels and vehicles," 2015.

[2] J. M. Melillo, T. C. Richmond, and G. Yohe, *Highlights of Climate Change Impacts in the United States: The Third National Climate Assessment*. 2014.

[3] Epa, "Conversion Factors for Hydrocarbon Emission Components," no. 002, pp. 1–4, 2010.

[4] Yuki Hanai, "Combustion engines still worth improving, say Mazda and Nissan - Nikkei Asian Review," 2018.

[5] J. Peckham, "GM's 'Clean Diesel Combustion' R&D: VVA, LTC Focus," 2007.

[6] J. Hyvönen, G. Haraldsson, and B. Johansson, "Operating Conditions Using Spark Assisted HCCI Combustion During Combustion Mode Transfer to SI in a Multi-Cylinder VCR-HCCI Engine," *SAE Tech. Pap. Ser.*, vol. 1, no. 724, 2010.

[7] G. Paczko, N. Peters, K. Seshadri, and F. A. Williams, "The role of cool-flame chemistry in quasi-steady combustion and extinction of n-heptane droplets," *Combust. Theory Model.*, vol. 18, no. 4–5, pp. 515–531, Sep. 2014.

[8] C. K. Law, *Combustion physics*, vol. 9780521870. Cambridge: Cambridge University Press, 2006.

[9] C. A. Gierczak *et al.*, "FTIR: Fundamentals and applications in the analysis of dilute vehicle exhaust," *Sociol. J. Br. Sociol. Assoc.*, 1991.

[10] A. Sedlmaiera *et al.*, "Determination of VOCs in traffic exhaust by FTIR absorption

spectrometry," vol. 3821, no. June, 1999.

[11] W. F. Northrop and A. S. Avenido, "Fractionation of engine exhaust hydrocarbons using flame ionization detection with variable temperature sample conditioner," *Int. J. Engine Res.*, vol. 17, no. 2, pp. 235–245, 2015.

[12] M. T. Sherman, M. L. Akard, and H. Nakamura, "Flame Ionization Detector Oxygen Quench Effects on Hydrocarbon Emission Results," *SAE Tech. Pap. Ser.*, vol. 1, no. 724, 2010.

[13] C. P. Koci *et al.*, "Detailed Unburned Hydrocarbon Investigations in a Highly-Dilute Diesel Low Temperature Combustion Regime," *SAE Int. J. Engines*, vol. 2, no. 1, pp. 858–879, 2009.

[14] M. Han, D. N. Assanis, and S. V. Bohac, "Sources of Hydrocarbon Emissions from Low-Temperature Premixed Compression Ignition Combustion from a Common Rail Direct Injection Diesel Engine," *Combust. Sci. Technol.*, vol. 181, no. 3, pp. 496–517, Feb. 2009.

[15] T. a Sasaki and C. L. Wilkins, "Gas chromatography with Fourier transform infrared and mass spectral detection," *Most*, vol. 842, pp. 341–349, 1999.

[16] P. Dagaut and A. Nicolle, "Experimental study and detailed kinetic modeling of the effect of exhaust gas on fuel combustion: Mutual sensitization of the oxidation of nitric oxide and methane over extended temperature and pressure ranges," *Combust. Flame*, vol. 140, no. 3, pp. 161–171, 2005.

[17] T. J. Jacobs and D. N. Assanis, "The attainment of premixed compression ignition

low-temperature combustion in a compression ignition direct injection engine," *Proc. Combust. Inst.*, vol. 31 II, pp. 2913–2920, 2007.

[18] D. Han, A. M. Ickes, S. V. Bohac, Z. Huang, and D. N. Assanis, "HC and CO emissions of premixed low-tempearture combustion fueld by blends of diesel and gasoline," 2012.

[19] W. F. Northrop, S. V. Bohac, and D. N. Assanis, "Premixed Low Temperature Combustion of Biodiesel and Blends in a High Speed Compression Ignition Engine," 2009.

[20] C. P. Koci *et al.*, "Multiple-Event Fuel Injection Investigations in a Highly-Dilute Diesel Low Temperature Combustion Regime," *SAE Int. J. Engines*, vol. 2, no. 1, pp. 837–857, 2009.

[21] X. Feng, M. Huo, C.-F. Lee, and H. Liu, "The Effects of EGR and Injection Timing on the Engine Combustion and Emission Performances Fueled by Butanol-Diesel Blends," vol. c, 2012.

[22] M. Zheng, G. T. Reader, and J. G. Hawley, "Diesel engine exhaust gas recirculation––a review on advanced and novel concepts," *Energy Convers. Manag.*, vol. 45, no. 6, pp. 883–900, Apr. 2004.

[23] A. Abu-Jrai *et al.*, "Performance, combustion and emissions of a diesel engine operated with reformed EGR. Comparison of diesel and GTL fueling," *Fuel*, vol. 88, no. 6, pp. 1031–1041, 2009.

[24] J. Kashdan, S. Mendez, and G. Bruneaux, "An Investigation of Unburned

Hydrocarbon Emissions in Wall Guided , Low Temperature Diesel Combustion Region of Interest Revolutions per Minute Start of Injection," vol. 63, no. 4, pp. 433–459, 2008.

[25] M. Han, D. N. Assanis, T. J. Jacobs, and S. V. Bohac, "Method and Detailed Analysis of Individual Hydrocarbon Species From Diesel Combustion Modes and Diesel Oxidation Catalyst," *J. Eng. Gas Turbines Power*, vol. 130, no. 4, p. 042803, 2008.

[26] W. F. Northrop, T. J. Jacobs, D. N. Assanis, and S. V Bohac, "Deactivation of a diesel oxidation catalyst due to exhaust species from rich premixed compression ignition combustion in a light-duty diesel engine," *Int. J. Engine Res.*, vol. 8, no. 6, pp. 487–498, 2007.

[27] R. P. Verbeek, A. van Doorn, and M. van Walwijk, "Global Assessment of Dimethyl-ether as an Automotive Fuel (second edition)," pp. 1–75, 1996.

[28] C. Arcoumanis, C. Bae, R. Crookes, and E. Kinoshita, "The potential of di-methyl ether (DME) as an alternative fuel for compression-ignition engines: A review," *Fuel*, vol. 87, no. 7, pp. 1014–1030, Jun. 2008.

[29] D. A. Good, J. S. Francisco, A. K. Jain, and D. J. Wuebbles, "Lifetimes and global warming potentials for dimethyl ether and for fluorinated ethers: CH 3 OCF 3 (E143a), CHF 2 OCHF 2 (E134), CHF 2 OCF 3 (E125)," *J. Geophys. Res. Atmos.*, vol. 103, no. D21, pp. 28181–28186, 1998.

[30] D. A. Good, J. Hanson, J. S. Francisco, Z. Li, and G.-R. Jeong, "Kinetics and Reaction Mechanism of Hydroxyl Radical Reaction with Methyl Formate," *J. Phys.*

Chem. A, vol. 103, no. 50, pp. 10893–10898, 1999.

[31] G. Mittal, M. Chaos, C. J. Sung, and F. L. Dryer, "Dimethyl ether autoignition in a rapid compression machine: Experiments and chemical kinetic modeling," *Fuel Process. Technol.*, vol. 89, no. 12, pp. 1244–1254, 2008.

[32] N. Lida. and T. Igarash., "Auto-Ignition and Combustion of n-Butane and DME/Air Mixtures in a Homogeneous Charge Compression Ignition Engine," *SAE Tech. Pap.*, no. 724, pp. 2000-01-1832, 2000.

[33] K. Wattanavichien, "Development of a DME fuelled HCCI Engine," *4th AUN/SEED-Net RC MeAe*, 2012.

[34] C. M. Zinner, "Methane and Dimethyl Ether Oxidation at Elevated Temperatures and Pressure," *Electron. Theses Diss.*, no. 3695, 2008.

[35] N. Leplat, P. Dagaut, C. Togbé, and J. Vandooren, "Numerical and experimental study of ethanol combustion and oxidation in laminar premixed flames and in jet-stirred reactor," *Combust. Flame*, vol. 158, no. 4, pp. 705–725, 2011.

[36] U. Pfahl, K. Fieweger, and G. Adomeit, "Self-ignition of diesel-relevant hydrocarbon-air mixtures under engine conditions," *Symp. Combust.*, vol. 26, no. 1, pp. 781–789, Jan. 1996.

[37] U. Burke *et al.*, "An ignition delay and kinetic modeling study of methane, dimethyl ether, and their mixtures at high pressures," *Combust. Flame*, vol. 162, no. 2, pp. 315–330, 2015.

[38] R. D. Cook, D. F. Davidson, and R. K. Hanson, "Shock tube measurements of

ignition delay times and OH time-histories in dimethyl ether oxidation," *Proc. Combust. Inst.*, vol. 32, no. 1, pp. 189–196, Jan. 2009.

[39] E. Hu, Z. Zhang, L. Pan, J. Zhang, and Z. Huang, "Experimental and modeling study on ignition delay times of dimethyl ether/propane/oxygen/argon mixtures at 20 bar," *Energy and Fuels*, vol. 27, no. 7, pp. 4007–4013, 2013.

[40] S. H. Pyun, W. Ren, K. Y. Lam, D. F. Davidson, and R. K. Hanson, "Shock tube measurements of methane, ethylene and carbon monoxide time-histories in DME pyrolysis," *Combust. Flame*, vol. 160, no. 4, pp. 747–754, 2013.

[41] K. Tanoue, Y. Chado, T. Jimoto, T. Nomura, F. Shimada, and J. Hashimoto, "Effect of autoignition characteristics of fuels on knocking properties," *Int. J. Engine Res.*, vol. 17, no. 6, pp. 666–676, Aug. 2016.

[42] E. E. Dames, A. S. Rosen, B. W. Weber, C. W. Gao, C. J. Sung, and W. H. Green, "A detailed combined experimental and theoretical study on dimethyl ether/propane blended oxidation," *Combust. Flame*, vol. 168, pp. 310–330, 2016.

[43] S. S. Goldsborough, S. Hochgreb, G. Vanhove, M. S. Wooldridge, H. J. Curran, and C. J. Sung, "Advances in rapid compression machine studies of low- and intermediate-temperature autoignition phenomena," *Prog. Energy Combust. Sci.*, vol. 63, pp. 1–78, 2017.

[44] R. M. R. Higgin and A. Williams, "A shock-tube investigation of the ignition of lean methane and n-butane mixtures with oxygen," *Symp. Combust.*, vol. 12, no. 1, pp. 579–590, 1969.

[45] C. S. Eubank, M. J. Rabinowitz, W. C. Gardiner, and R. E. Zellner, “Shock-initiated ignition of natural gas-Air mixtures,” *Symp. Combust.*, vol. 18, no. 1, pp. 1767–1774, 1981.

[46] J. M. Zellner, R., Niemitz, K.J., Warnatz, J., Gardiner Jr., W.C., Eubank, C.S., Simmie, “Hydrocarbon Induced Acceleration of Ignition of Methane-Air Ignition,” *Flames, Lasers React. Syst.*, pp. 252–272, Jan. 1983.

[47] M. Carlier, C. Corre, R. Minetti, J.-F. F. Pauwels, M. Ribaucour, and L.-R. R. Sochet, “Autoignition of butane: A burner and a rapid compression machine study,” *Symp. Combust.*, vol. 23, no. 1, pp. 1753–1758, Jan. 1991.

[48] W. J. Pitz, R. D. Wilk, C. K. Westbrook, and N. P. Cernansky, “The oxidation of N-butane at low and intermediate temperatures: An experimental and modeling study.” 10-Mar-1988.

[49] S. Gersen, A. V. Mokhov, J. H. Darmeveil, and H. B. Levinsky, “Ignition properties of n-butane and iso-butane in a rapid compression machine,” *Combust. Flame*, vol. 157, no. 2, pp. 240–245, 2010.

[50] D. Healy *et al.*, “n-Butane: Ignition delay measurements at high pressure and detailed chemical kinetic simulations,” *Combust. Flame*, vol. 157, no. 8, pp. 1526–1539, 2010.

[51] D. Healy *et al.*, “Isobutane ignition delay time measurements at high pressure and detailed chemical kinetic simulations,” *Combust. Flame*, vol. 157, no. 8, pp. 1540–1551, 2010.

[52] A. Burcat, K. Scheller, and A. Lifshitz, “Shock-tube investigation of comparative ignition delay times for C1-C5alkanes,” *Combust. Flame*, vol. 16, no. 1, pp. 29–33, 1971.

[53] J. Franck, J. F. Griffiths, and W. Nimmo, “The control of spontaneous ignition under rapid compression,” *Symp. Combust.*, vol. 21, no. 1, pp. 447–454, 1988.

[54] F. F. Gabano, J.D., Kageyama, T., “Experimental Study of N-Butane Autoignition in a Rapid Compression Machine,” in *Dynamics of Deflagrations and Reactive Systems: Flames*, Washington DC: American Institute of Aeronautics and Astronautics, 1991, pp. 407–417.

[55] J. F. Griffiths, P. a. Halford-Maw, and D. J. Rose, “Fundamental features of hydrocarbon autoignition in a rapid compression machine,” *Combust. Flame*, vol. 95, no. 3, pp. 291–306, Nov. 1993.

[56] D. C. Horning, D. F. Davidson, and R. K. Hanson, “Study of the High-Temperature Autoignition of n-Alkane/O/Ar Mixtures,” *J. Propuls. Power*, vol. 18, no. 2, pp. 363–371, 2002.

[57] H. Kim, Y. Lim, K. Min, and D. Lee, “Investigation of autoignition of propane and n-butane blends using a rapid compression machine,” *KSME Int. J.*, vol. 16, no. 8, pp. 1127–1134, 2002.

[58] S. Kojima and T. Suzuoki, “Autoignition-delay measurement over lean to rich mixtures of n-butane/air under swirl conditions,” *Combust. Flame*, vol. 92, no. 3, pp. 254–265, 1993.

[59] R. Minetfi, “Autoignition Delays of a Series of Linear and Branched Chain Alkanes in the Intermediate Range of Temperature.pdf.” 1997.

[60] V. A. Davies, “Autoignition Study of Ethanol and Heptane in a Rapid Compression Machine,” 2015.

[61] J. Li, A. Kazakov, and F. L. Dryer, “Ethanol Pyrolysis Experiments in a Variable Pressure Flow Reactor,” *Int. J. Chem. Kinet.*, vol. 33, pp. 859–867, 2001.

[62] F. M. Haas, M. Chaos, and F. L. Dryer, “Low and intermediate temperature oxidation of ethanol and ethanol-PRF blends: An experimental and modeling study,” *Combust. Flame*, vol. 156, no. 12, pp. 2346–2350, 2009.

[63] J. Li, A. Kazakov, and F. L. Dryer, “Experimental and numerical studies of ethanol decomposition reactions,” *J. Phys. Chem. A*, vol. 108, no. 38, pp. 7671–7680, 2004.

[64] A. Frassoldati, A. Cuoci, T. Faravelli, and E. Ranzi, “Kinetic modeling of the oxidation of ethanol and gasoline surrogate mixtures,” *Combust. Sci. Technol.*, vol. 182, no. 7, pp. 653–667, 2010.

[65] F. N. Egolfopoulos, D. X. Du, and C. K. Law, “A study on ethanol oxidation kinetics in laminar premixed flames, flow reactors, and shock tubes,” *Symp. Combust.*, vol. 24, no. 1, pp. 833–841, 1992.

[66] Ö. L. Gülder, “Laminar burning velocities of methanol, ethanol and isooctane-air mixtures,” *Symp. Combust.*, vol. 19, no. 1, pp. 275–281, 1982.

[67] T. S. Kasper, P. Oßwald, M. Kamphus, and K. Kohse-Höinghaus, “Ethanol flame structure investigated by molecular beam mass spectrometry,” *Combust. Flame*, vol.

150, no. 3, pp. 220–231, 2007.

[68] J. Liang, G. Li, Z. Zhang, Z. Xiong, F. Dong, and R. Yang, “Experimental and Numerical Studies on Laminar Premixed Flames of Ethanol–Water–Air Mixtures,” *Energy & Fuels*, vol. 28, no. 7, pp. 4754–4761, 2014.

[69] P. Saxena, “Numerical and Experimental Studies of Ethanol Flames and Autoignition Theory for Higher Alkanes,” *Dissertation*, 2007.

[70] L. R. Cancino, M. Fikri, A. A. M. Oliveira, and C. Schulz, “Measurement and chemical kinetics modeling of shock-induced ignition of ethanol-air mixtures,” *Energy and Fuels*, vol. 24, no. 5, pp. 2830–2840, 2010.

[71] R. X. F. Changyoul, Lee, Stijn Vranckx, Karl A. Heufer, Sergey V. Khomik, Yasir Uygun, Herbert Olivier *et al.*, “On the Chemical Kinetics of Ethanol Oxidation: Shock Tube, Rapid Compression Machine and Detailed Modeling Study,” *Zeitschrift für Phys. Chemie*, vol. 226, no. 1, pp. 1–28, 2012.

[72] H. J. Curran, M. P. Dunphy, J. M. Simmie, C. K. Westbrook, and W. J. Pitz, “Shock tube ignition of ethanol, isobutene and MTBE: Experiments and modeling,” *Symp. Combust.*, vol. 24, no. 1, pp. 769–776, 1992.

[73] M. P. Dunphy, P. M. Patterson, and J. M. Simmie, “High-temperature oxidation of ethanol. Part 2.-Kinetic modelling,” *J. Chem. Soc.{,} Faraday Trans.*, vol. 87, no. 16, pp. 2549–2559, 1991.

[74] K. A. Heufer and H. Olivier, “Determination of ignition delay times of different hydrocarbons in a new high pressure shock tube,” *Shock Waves*, vol. 20, no. 4, pp.

307–316, 2010.

[75] J. Lee, Daeyup, Simone, Hochgreb, Keck, “Autoignition of Alcohols and Ethers in a Rapid Compression Engine,” *SAE Tech. Pap.*, 1993.

[76] C. Lee *et al.*, “On the Chemical Kinetics of Ethanol Oxidation: Shock Tube, Rapid Compression Machine and Detailed Modeling Study,” *Zeitschrift für Phys. Chemie*, vol. 226, no. 1, pp. 1–28, Jan. 2012.

[77] G. Mittal, S. M. Burke, V. A. Davies, B. Parajuli, W. K. Metcalfe, and H. J. Curran, “Autoignition of ethanol in a rapid compression machine,” *Combust. Flame*, vol. 161, no. 5, pp. 1164–1171, 2014.

[78] C. L. Barraza-Botet, S. W. Wagnon, and M. S. Wooldridge, “Combustion chemistry of ethanol: Ignition and speciation studies in a rapid compression facility,” *J. Phys. Chem. A*, vol. 120, no. 38, pp. 7408–7418, 2016.

[79] S. Dooley, A. Heufer, A. Farooq, G. Vanhove, and S. Goldsborough, “2 nd Rapid Compression Machine Characterisation Initiative Standard Data Collection for RCMs,” pp. 1–10.

[80] H. Wu and M. Ihme, “Effects of flow-field and mixture inhomogeneities on the ignition dynamics in continuous flow reactors,” *Combust. Flame*, vol. 161, no. 9, pp. 2317–2326, 2014.

[81] F. L. Dryer, F. M. Haas, J. Santner, T. I. Farouk, and M. Chaos, “Interpreting chemical kinetics from complex reaction e advection e diffusion systems : Modeling of fl ow reactors and related experiments,” *Prog. Energy Combust. Sci.*, pp. 1–21,

2014.

[82] O. Herbinet, D. Guillaume, O. Herbinet, D. Guillaume, J. R. Fr, and M. John, *Cleaner Combustion - Jet Stirred Reactors*. London: Springer London, 2013.

[83] R. K. Hanson and D. F. Davidson, "Recent advances in laser absorption and shock tube methods for studies of combustion chemistry," *Prog. Energy Combust. Sci.*, vol. 44, pp. 103–114, Oct. 2014.

[84] J. Würmel, E. J. Silke, H. J. Curran, M. S. Ó Conaire, and J. M. Simmie, "The effect of diluent gases on ignition delay times in the shock tube and in the rapid compression machine," *Combust. Flame*, vol. 151, no. 1–2, pp. 289–302, Oct. 2007.

[85] V. Guillaume, "100 years of compression : A brief history of Rapid Compression Machines," 2012.

[86] K. P. Grogan, S. Scott Goldsborough, and M. Ihme, "Ignition regimes in rapid compression machines," *Combust. Flame*, vol. 162, no. 8, pp. 3071–3080, 2015.

[87] K. H. Tran, P. Guibert, C. Morin, J. Bonnety, S. Pounkin, and G. Legros, "Temperature measurements in a rapid compression machine using anisole planar laser-induced fluorescence," *Combust. Flame*, vol. 000, no. 10, pp. 1–11, 2015.

[88] P. Guibert, A. Keromnes, and G. Legros, "An Experimental Investigation of the Turbulence Effect on the Combustion Propagation in a Rapid Compression Machine," *Flow, Turbul. Combust.*, vol. 84, no. 1, pp. 79–95, May 2009.

[89] C.-J. Sung and H. J. Curran, "Using rapid compression machines for chemical kinetics studies," *Prog. Energy amd Combust. Sci.*, vol. 44, 2014.

[90] J. F. Griffiths, Q. Jiao, W. Kordylewski, M. Schreiber, J. Meyer, and K. F. Knoche, "Experimental and numerical studies of ditertiary butyl peroxide combustion at high pressures in a rapid compression machine," *Combust. Flame*, vol. 93, no. 3, pp. 303–315, May 1993.

[91] D. Lee and S. Hochgreb, "Rapid Compression Machines: Heat Transfer and Suppression of Corner Vortex," *Combust. Flame*, vol. 114, no. 3–4, pp. 531–545, Aug. 1998.

[92] J. Wurmel and J. Simmie, "CFD studies of a twin-piston rapid compression machine," *Combust. Flame*, vol. 141, no. 4, pp. 417–430, Jun. 2005.

[93] G. Mittal and C.-J. Sung, "Aerodynamics inside a rapid compression machine," *Combust. Flame*, vol. 145, no. 1–2, pp. 160–180, Apr. 2006.

[94] J. Bunnell and J. A. Bunnell, "Autoignition of Methyl Pentanoate at Low to Intermediate Temperatures and Elevated Pressures in a Rapid Compression Machine Autoignition of Methyl Pentanoate at Low to Intermediate Temperatures and Elevated Pressures in a Rapid Compression Machine - THESI," 2015.

[95] K. Chen and G. a Karim, "Evaluation of the instantaneous unsteady heat transfer in a rapid compression-expansion machine," *Proc. Inst. Mech. Eng. Part A J. Power Energy*, vol. 212, no. 5, pp. 351–362, Jan. 1998.

[96] M. Ihme, "On the role of turbulence and compositional fluctuations in rapid compression machines: Autoignition of syngas mixtures," *Combust. Flame*, vol. 159, no. 4, pp. 1592–1604, Apr. 2012.

[97] J. F. Griffiths, Q. Jiao, M. Schreiber, J. Meyer, and K. F. Knoche, “Development of Thermokinetic Models for Autoignition in a CFD Code: Experimental Validation and Application of the Results to Rapid Compression Studies,” *Combust. Inst.*, vol. 24, pp. 1809–1815, 1992.

[98] P. Park and J. C. Keck, “Rapid Compression Machine Measurements of Ignition Delays for Primary Reference Fuels International Congress and Exposition,” *SAE Pap.*, p. 900027, 1990.

[99] S. Schlatter, B. Schneider, Y. Wright, and K. Boulouchos, “Experimental Study of Ignition and Combustion Characteristics of a Diesel Pilot Spray in a Lean Premixed Methane/Air Charge using a Rapid Compression Expansion Machine,” Apr. 2012.

[100] S. M. Gallagher, H. J. Curran, W. K. Metcalfe, D. Healy, J. M. Simmie, and G. Bourque, “A rapid compression machine study of the oxidation of propane in the negative temperature coefficient regime,” *Combust. Flame*, vol. 153, no. 1–2, pp. 316–333, Apr. 2008.

[101] G. Mittal and C.-J. Sung, “A Rapid Compression Machine for Chemical Kinetics Studies at Elevated Pressures and Temperatures,” *Combust. Sci. Technol.*, vol. 179, no. 3, pp. 497–530, Mar. 2007.

[102] L. Brett, J. Macnamara, P. Musch, and J. . Simmie, “Simulation of methane autoignition in a rapid compression machine with creviced pistons,” *Combust. Flame*, vol. 124, no. 1–2, pp. 326–329, Jan. 2001.

[103] C. Allen, G. Mittal, C.-J. Sung, E. Toulson, and T. Lee, “An aerosol rapid compression machine for studying energetic-nanoparticle-enhanced combustion of

liquid fuels," *Proc. Combust. Inst.*, vol. 33, no. 2, pp. 3367–3374, Jan. 2011.

[104] S. S. Goldsborough, "A Crevice Blow-by Model for a Rapid Compression Expansion Machine Used for Chemical Kinetic (HCCI) Studies," in *SAE International*, 2007, pp. 776–790.

[105] G. Mittal, M. P. Raju, and A. Bhari, "A numerical assessment of the novel concept of crevice containment in a rapid compression machine," *Combust. Flame*, vol. 158, no. 12, pp. 2420–2427, Dec. 2011.

[106] G. Mittal and M. Chomier, "Effect of crevice mass transfer in a rapid compression machine," *Combust. Flame*, vol. 161, no. 2, pp. 398–404, 2014.

[107] S. S. Goldsborough and C. J. Potokar, "The Influence of Crevice Flows and Blow-By on the Charge Motion and Temperature Profiles Within a Rapid Compression Expansion Machine Used for Chemical Kinetic (HCCI) Studies," 2007, no. 724, pp. 776–790.

[108] J. Clarkson, J. F. Griffiths, J. P. MacNamara, and B. J. Whitaker, "Temperature fields during the development of combustion in a rapid compression machine," *Combust. Flame*, vol. 125, no. 3, pp. 1162–1175, 2001.

[109] G. Mittal and A. Bhari, "A rapid compression machine with crevice containment," *Combust. Flame*, vol. 160, no. 12, pp. 2975–2981, Dec. 2013.

[110] P. R. Ganji, R. N. Singh, V. R. K. Raju, and S. Srinivasa Rao, "Design of piston bowl geometry for better combustion in direct-injection compression ignition engine," *Sadhana - Acad. Proc. Eng. Sci.*, vol. 43, no. 6, pp. 1–9, 2018.

[111] B. V. V. S. U. Prasad, C. S. Sharma, T. N. C. Anand, and R. V. Ravikrishna, “High swirl-inducing piston bowls in small diesel engines for emission reduction,” *Appl. Energy*, vol. 88, no. 7, pp. 2355–2367, 2011.

[112] C. Yin, Z. Zhang, Y. Sun, T. Sun, and R. Zhang, “Effect of the piston top contour on the tumble flow and combustion features of a GDI engine with a CMCV: A CFD study,” *Eng. Appl. Comput. Fluid Mech.*, vol. 10, no. 1, pp. 311–329, 2016.

[113] F. A. Baby, Xavier, “Investigation of the In-Cylinder Tumble: Motion In a Multi-Valve Engine: Effect of the Piston Shape,” *SAE Int.*, 1997.

[114] T. Saito, Y. Daisho, N. Uchida, and N. Ikeya, “Effects of Combustion Chamber Geometry on Diesel Combustion,” 1986.

[115] J. Song, C. Yao, Y. Liu, and Z. Jiang, “Investigation On Flow Field In Simplified Piston Bowls for Di Diesel Engine,” *Eng. Appl. Comput. Fluid Mech.*, vol. 2, no. 3, pp. 354–365, 2008.

[116] D. K. Soni and R. Gupta, “Numerical analysis of flow dynamics for two piston bowl designs at different spray angles,” *J. Clean. Prod.*, vol. 149, pp. 723–734, 2017.

[117] S. Subramaniyam, V. Ganesan, P. S. Rao, and S. Sampath, “Turbulent flow inside the cylinder of a Diesel engine - an experimental investigation using hot wire anemometer,” *Exp. Fluids*, vol. 9, no. 3, pp. 167–174, 1990.

[118] B. R. Ramesh Bapu, L. Saravanakumar, and B. Durga Prasad, “Effects of combustion chamber geometry on combustion characteristics of a DI diesel engine fueled with calophyllum inophyllum methyl ester,” *J. Energy Inst.*, vol. 90, no. 1,

pp. 82–100, 2017.

[119] A. R. Gnana Sagaya Raj, J. M. Mallikarjuna, and V. Ganesan, “Energy efficient piston configuration for effective air motion – A CFD study,” *Appl. Energy*, vol. 102, no. 102, pp. 347–354, Feb. 2013.

[120] P. R. Ganji, R. N. Singh, V. R. K. Raju, and S. Srinivasa Rao, “Design of piston bowl geometry for better combustion in direct-injection compression ignition engine,” *Sadhana - Acad. Proc. Eng. Sci.*, vol. 43, no. 6, pp. 1–9, 2018.

[121] A. A. Reese, R.A., Vick, R.K., Amer, “Impact of Tumble on Combustion in SI Engines: Correlation between Flow and Engine Experiments,” *SAE Int.*, vol. 116, pp. 1120–1237, 2007.

[122] D. K. Dasrath, R. M. Biwalkar, S. Singh, and W. F. Northrop, “CFD Analysis of Creviced Pistons for Vortex Containment in Rapid Compression and Expansion Machines,” *Cent. States Sect. Combust. Inst.*, no. Spring Technical Meeting, pp. 1–10, 2016.

[123] G. Lucachick, A. Avenido, D. Kittelson, and W. Northrop, “Exploration of Semi-Volatile Particulate Matter Emissions from Low Temperature Combustion in a Light-Duty Diesel Engine,” *SAE Int. J. Engines*, vol. 7, no. 2, 2014.

[124] A. Tripathi, D. Dasrath, Z. Sun, W. Northrop, D. Kittelson, and K. Stelson, “Design and Control of a Controlled Trajectory Rapid Compression and Expansion Machine,” *IEEE/ASME Trans. Mechatronics*, pp. 1–1, 2019.

[125] A. Tripathi, K. Li, C. Zhang, and Z. Sun, “Modeling and control of controlled

trajectory Rapid Compression Expansion Machine," in *2016 American Control Conference (ACC)*, 2016, vol. In press, pp. 3304–3309.

[126] D. K. Dasrath, J. T. Hwang, L. J. Hunt, and W. F. Northrop, "Comparison of Fourier Transform Infrared Spectroscopy and Gas Chromatography-Mass Spectroscopy for Speciating Unburned Hydrocarbons from Diesel Low Temperature Combustion," *Cent. States Sect. Combust. Inst.*, no. Spring Technical Meeting, pp. 1–10, 2016.

[127] D. K. Dasrath, R. W. Frazee, J. T. Hwang, and W. F. Northrop, "Comparison and Optimization of Fourier Transform Infrared Spectroscopy and Gas Chromatography-Mass Spectroscopy for Speciating Unburned Hydrocarbons from Diesel Low Temperature Combustion," *SAE Tech. Pap.*, no. Cdc, pp. 1–9, 2017.

[128] S. S. Goldsborough and J. Fitzgerald, "Design and Operational Characteristics of a Novel Floating-Stroke, Free Piston Internal Combustion Reciprocating Engine," Apr. 2013.

[129] K. Kumar and C.-J. Sung, "Autoignition of methanol: Experiments and computations," *Int. J. Chem. Kinet.*, vol. 43, no. 4, pp. 175–184, Apr. 2011.

[130] J. W. Meyer and A. K. Oppenheim, "On the shock-induced ignition of explosive gases," *Symp. Combust.*, vol. 13, no. 1, pp. 1153–1164, Jan. 1971.

[131] Y. Uygun, S. Ishihara, and H. Olivier, "A high pressure ignition delay time study of 2-methylfuran and tetrahydrofuran in shock tubes," *Combust. Flame*, vol. 161, no. 10, pp. 2519–2530, 2014.

[132] D. J. Vermeer, J. W. Meyer, and A. K. Oppenheim, "Auto-ignition of hydrocarbons

behind reflected shock waves," *Combust. Flame*, vol. 18, no. 3, pp. 327–336, 1972.

[133] K. Fieweger, R. Blumenthal, and G. Adomeit, "Self-ignition of S.I. engine model fuels: A shock tube investigation at high pressure," *Combust. Flame*, vol. 109, no. 4, pp. 599–619, 1997.

[134] K. Fieweger, R. Blumenthal, and G. Adomeit, "Shock-tube investigations on the self-ignition of hydrocarbon-air mixtures at high pressures," *Symp. Combust.*, vol. 25, no. 1, pp. 1579–1585, 1994.

[135] J. C. Livengood and W. A. Leary, "Autoignition by Rapid Compression.," *Ind. Eng. Chem.*, vol. 43, no. 12, pp. 2797–2805, Dec. 1951.

[136] S. M. Walton, X. He, B. T. Zigler, and M. S. Wooldridge, "An experimental investigation of the ignition properties of hydrogen and carbon monoxide mixtures for syngas turbine applications," *Proc. Combust. Inst.*, vol. 31 II, pp. 3147–3154, 2007.

[137] A. B. Mansfield and M. S. Wooldridge, "High-pressure low-temperature ignition behavior of syngas mixtures," *Combust. Flame*, vol. 161, no. 9, pp. 2242–2251, 2014.

[138] A. B. Mansfield, M. S. Wooldridge, H. Di, and X. He, "Low-temperature ignition behavior of iso-octane," *Fuel*, vol. 139, pp. 79–86, Jan. 2015.

[139] P. A. Urtiew and A. K. Oppenheim, "Experimental Observations of the Transition to Detonation in an Explosive Gas," *Proceedings of the Royal Society of London. Series A, Mathematical and Physical Sciences*, vol. 295. Royal Society, pp. 13–28.

[140] P. Aleiferis, M. Behringer, J. Malcolm, and P. Aleiferis, “Integral Length Scales and Time Scales of Turbulence in an Optical Spark-Ignition Engine.”

[141] J. H. S. Lee, *The detonation phenomenon*. Cambridge University Press, 2008.

[142] R. Sankaran, H. G. Im, E. R. Hawkes, and J. H. Chen, “The effects of non-uniform temperature distribution on the ignition of a lean homogeneous hydrogen-air mixture,” *Proc. Combust. Inst.*, vol. 30, no. 1, pp. 875–882, 2005.

[143] J. A. Gatowski, E. N. Balles, K. M. Chun, F. E. Nelson, J. A. Ekchian, and J. B. Heywood, “Heat Release Analysis of Engine Pressure Data,” 1984.

[144] M. F. J. Brunt, H. Rai, and A. L. Emtage, “The Calculation of Heat Release Energy from Engine Cylinder Pressure Data,” 1998.

[145] K. M. CHUN and J. B. HEYWOOD, “Estimating Heat-Release and Mass-of-Mixture Burned from Spark-Ignition Engine Pressure Data,” *Combust. Sci. Technol.*, vol. 54, no. 1–6, pp. 133–143, Aug. 1987.

[146] C. D. Rakopoulos, K. A. Antonopoulos, and D. C. Rakopoulos, “Experimental heat release analysis and emissions of a HSDI diesel engine fueled with ethanol–diesel fuel blends,” *Energy*, vol. 32, no. 10, pp. 1791–1808, Oct. 2007.

[147] N. R. Banapurmath, P. G. Tewari, and R. S. Hosmath, “Performance and emission characteristics of a DI compression ignition engine operated on Honge, Jatropha and sesame oil methyl esters,” *Renew. Energy*, vol. 33, no. 9, pp. 1982–1988, Sep. 2008.

[148] J. B. Ghandhi, “Pressure and Heat Release Analysis,” in *Encyclopedia of Automotive Engineering*, Chichester, UK: John Wiley & Sons, Ltd, 2014, pp. 1–13.

[149] K. Tanaka, H. Endo, A. Imamichi, Y. Oda, Y. Takeda, and T. Shimada, “Study of Homogeneous Charge Compression Ignition Using a Rapid Compression Machine,” *SAE Tech. Pap. Ser.*, no. 724, 2001.

[150] P. C. Vena, B. Deschamps, H. Guo, G. J. Smallwood, and M. R. Johnson, “Heat release rate variations in a globally stoichiometric, stratified iso-octane/air turbulent V-flame,” *Combust. Flame*, vol. 162, no. 4, pp. 944–959, Apr. 2015.

[151] S. Shiga *et al.*, “A study of the combustion and emission characteristics of compressed-natural-gas direct-injection stratified combustion using a rapid-compression-machine,” *Combust. Flame*, vol. 129, no. 1–2, pp. 1–10, Apr. 2002.

[152] S. S. Goldsborough, J. Santner, D. Kang, A. Fridlyand, T. Rockstroh, and M. C. Jespersen, “Heat release analysis for rapid compression machines: Challenges and opportunities,” *Proc. Combust. Inst.*, Aug. 2018.

[153] M. J. Pilling, *Low-temperature combustion and autoignition*. Elsevier, 1997.

[154] U. Horn, R. Egnell, and B. Johansson, “Detailed heat release analyses with regard to combustion of RME and oxygenated fuels in an HSDI diesel engine,” *Sae*, no. 724, pp. 776–790, 2007.

[155] H. Liu, H. Zhang, Z. Shi, H. Lu, G. Zhao, and B. Yao, “Performance Characterization and Auto-Ignition Performance of a Rapid Compression Machine,” *Energies*, vol. 7, no. 9, pp. 6083–6104, Sep. 2014.

[156] S. Schlatter, B. Schneider, Y. M. Wright, and K. Boulouchos, “N-heptane micro pilot assisted methane combustion in a Rapid Compression Expansion Machine,”

Fuel, vol. 179, no. March, pp. 339–352, 2016.

[157] A. Avenido, "Measurement and Fractionation of Diesel Exhaust Hydrocarbons through Variable Temperature Controlled-Condensation and Flame Ionization Detection," 2014.

[158] J. Shao, R. Choudhary, D. F. Davidson, R. K. Hanson, S. Barak, and S. Vasu, "Ignition delay times of methane and hydrogen highly diluted in carbon dioxide at high pressures up to 300 atm," *Proc. Combust. Inst.*, vol. 37, no. 4, pp. 4555–4562, 2019.

[159] M. Ihme, Y. Sun, and R. Deiterding, "Detailed Simulations of Shock-Bifurcation and Ignition of an Argon-diluted Hydrogen/Oxygen Mixture in a Shock Tube," no. January, pp. 1–14, 2013.

[160] K. P. Grogan and M. Ihme, "Regimes describing shock boundary layer interaction and ignition in shock tubes," *Proc. Combust. Inst.*, vol. 36, no. 2, pp. 2927–2935, 2017.

[161] D. O. Lignell, J. H. Chen, and H. A. Schmutz, "Effects of Damköhler number on flame extinction and reignition in turbulent non-premixed flames using DNS," *Combust. Flame*, vol. 158, no. 5, pp. 949–963, 2011.

[162] S. H. Won, S. Dooley, F. L. Dryer, and Y. Ju, "Kinetic effects of aromatic molecular structures on diffusion flame extinction," *Proc. Combust. Inst.*, vol. 33, no. 1, pp. 1163–1170, Jan. 2011.

Appendix

Table 11: Measured FT-IR species concentrations

		CDC		LTC 1		LTC 2		LTC 3	
Compound	Chemical Formula	Average [ppm]	STD [ppm]	Average [ppm]	STD [ppm]	Average [ppm]	STD [ppm]	Average [ppm]	STD [ppm]
Methane	CH_4	3.16	0.17	39.1	1.36	64.8	1.02	99.0	1.13
Acetylene	C_2H_2	1.25	0.35	10.8	0.36	16.3	0.40	24.5	0.45
Ethylene (Ethene)	C_2H_4	6.64	0.30	65.8	1.77	99.5	1.51	164	1.94
Ethane	C_2H_6	0.00	0.00	0.00	0.00	0.00	0.00	0.00	0.00
Propylene (Propene)	C_3H_6	0.60	0.44	16.6	0.61	23.3	0.50	41.5	0.74
Propane	C_3H_8	0.00	0.00	16.5	0.80	25.6	0.91	50.1	1.38
Butadiene	C_4H_6	1.42	0.35	3.72	0.40	4.97	0.39	7.19	0.37
Acetaldehyde	C_2H_4O	3.34	0.44	37.1	0.82	50.9	0.97	87.0	1.32
THC	--	77.1	2.08	680	9.29	880	9.72	1430	16.9

Table 12: GC-MS measurement of species concentrations and retention times

Compound	Chemical Formula	Retention Time [min]	CDC		LTC 1		LTC 2		LTC 3	
			Average [ppm]	STD [ppm]	Average [ppm]	STD [ppm]	Average [ppm]	STD [ppm]	Average [ppm]	STD [ppm]
Acetylene	C_2H_2	4.58	1.44	0.60	10.3	1.11	16.8	0.58	25.0	1.04
Ethylene	C_2H_4	3.95	5.08	1.29	66.9	4.56	101	7.58	161	9.24
Ethane	C_2H_6	3.68	0.00*	0.00*	0.00*	0.00*	0.00*	0.00*	0.00*	0.00*
Propene	C_3H_6	5.72	0.800	0.430	13.7	3.48	30.2	3.28	42.3	9.04
Propane	C_3H_8	4.88	0.00*	0.00*	0.00*	0.00*	0.00*	0.00*	0.00*	0.00*
Cyclopropane	C_3H_6	5.52	0.00*	0.00*	0.00*	0.00*	0.00*	0.00*	0.00*	0.00*
Methylacetylene	C_3H_4	5.88	0.00*	0.00*	0.00*	0.00*	0.00*	0.00*	0.00*	0.00*
Butane	C_4H_{10}	6.37	0.00*	0.00*	0.00*	0.00*	0.00*	0.00*	0.00*	0.00*
Propadiene (Allene)	C_3H_4	7.35	0.00*	0.00*	0.00*	0.00*	0.00*	0.00*	0.00*	0.00*
Iso-butylene	C_4H_8	7.56	0.00*	0.00*	0.00*	0.00*	0.00*	0.00*	0.00*	0.00*
Pentane	C_5H_{12}	7.99	2.12	2.13	0.00*	0.00*	0.00*	0.00*	0.00*	0.00*
Trans-2-Pentene	C_5H_{10}	9.16	0.00*	0.00*	0.00*	0.00*	0.00*	0.00*	0.00*	0.00*
Cyclo-hexane	C_6H_{12}	9.79	0.00*	0.00*	0.00*	0.00*	0.00*	0.00*	0.00*	0.00*
1-Hexene	C_6H_{12}	10.5	0.00*	0.00*	0.00*	0.00*	0.00*	0.00*	0.00*	0.00*
Heptane	C_7H_{16}	11.3	1.96	1.04	4.88	2.75	2.31	0.67	17.9	6.39
Acetaldehyde	C_2H_4O	11.6	3.75	0.91	35.3	4.04	48.6	2.51	88.8	9.14
Benzene	C_6H_6	11.8	1.19	0.46	5.96	1.97	4.35	0.43	15.7	2.15
Iso-octane	C_8H_{18}	11.9	1.25	0.51	5.57	1.99	5.08	2.27	13.7	4.03
Toluene	C_7H_8	13.8	2.09	0.85	9.86	2.73	5.18	1.18	22.7	3.38
Ethylbenzene	C_8H_{10}	16.1	1.76	0.78	15.7	3.50	6.19	0.82	30.1	2.43
P-xylene	C_8H_{10}	16.6	2.49	1.88	21.6	2.94	9.26	0.90	32.9	2.75

* Below MS detection limit